Regulation of epithelial cytokinesis and cell-cell junctions by MgcRacGAP

by

Elaina B. Breznau

A dissertation submitted in partial fulfillment
of the requirements for the degree of
Doctor of Philosophy
(Cellular and Molecular Biology)
in the University of Michigan
2016

Dissertation Committee:

Assistant Professor Ann L. Miller, Chair
Associate Professor Gyorgyi Csankovszki
Assistant Professor Allen P. Liu
Professor Kristen J. Verhey
Professor Lois S. Weisman

DEDICATION

This dissertation is dedicated to my beautiful daughters who have inspired my academic

journey. May the pages herein guide their curiosity for the natural world and help them to

appreciate that hard work bears much fruit.

Acknowledgements

I would like to thank my advisor, Dr. Ann Miller, for providing a training atmosphere that was rich in scientific scholarship and personal growth opportunities. Dr. Miller's mentorship has shaped my path and has helped me to become a rigorous experimental scientist. A heartfelt thanks goes to my thesis committee members who have generously provided their time and expertise to help make my projects the best that they could be. I am truly grateful for the mentorship from my advisor and my committee members. I would also like to acknowledge my colleagues in the Miller Lab who have contributed to discussions, provided reagents and who made the laboratory environment and graduate school a memorable experience. The ride would not have been the same without them. I would like to thank the Cellular and Molecular Biology Graduate Program and the Molecular, Cellular, and Developmental Biology Department for providing an excellent training environment and wonderful resources for student success. Last, I would like to thank my husband, Bill Breznau, who provided the moral and emotional support necessary to complete the work described in this dissertation.

TABLE OF CONTENTS

LIST OF FIGURES

LIST OF APPENDICES

Abstract

Localized activation of Rho GTPases is essential for multiple cellular functions, including cytokinesis and formation and maintenance of cell-cell junctions. Centralspindlin, a heterotetrameric complex composed of the kinesin MKLP1 and the GTPase Activating Protein (GAP), MgcRacGAP (Mgc), is required for the proper regulation of both processes. Although Mgc is required for spatially confined RhoA-GTP at the equatorial cortex of dividing cells, the target specificity of Mgc's GAP activity, whether Mgc's GAP activity is phospho-regulated, how Mgc is stabilized at microtubule plus ends, and how Mgc functions at cell-cell junctions remained unclear. We investigated Mgc's role in the regulation of RhoA-GTP and Rac1-GTP in the intact vertebrate epithelium of *Xenopus laevis* embryos and in cultured cells using a combination of fluorescence microscopy, molecular biology, and biochemical assays. We show that Mgc's GAP activity spatially restricts accumulation of both RhoA-GTP and Rac1-GTP in epithelial cells – RhoA at the cleavage furrow and RhoA and Rac1 at cell-cell junctions. Phosphorylation at serine 386 within Mgc's GAP domain is not required for GTPase specificity, but functional Mgc GAP activity is required for successful cytokinesis. We found that Mgc is localized to the plus ends of individual equatorial astral microtubules during cytokinesis in *Xenopus* embryos, and identified a putative SxIP motif in *Xenopus* Mgc, which promotes co-localization with EB1 and microtubule plus end stability. Mutation of Mgc's SxIP motif resulted in loss of Mgc tracking on growing microtubule plus ends, abnormal astral microtubule

organization, and severe cytokinesis defects resulting from misregulated RhoA-GTP accumulation. Further, we found that Mgc localizes to adherens junctions in polarized epithelial cells via its SxIP motif and regulates adherens junction structure and integrity through modulation of RhoA signaling. Together, these results indicate that Mgc has GAP activity toward both RhoA and Rac1 at spatially distinct cellular locations, and that proper localization of Mgc is dependent upon its ability to be tethered at microtubule plus ends via the SxIP motif. Our data provide novel mechanistic insight into the regulation of Rho family GTPases in epithelial tissues, which is important for improving our understanding of signaling pathways that regulate epithelial pathologies.

Introduction

One of the most fundamental and important aspects of biological life is the ability of an organism to reproduce. This process governs the laws of Natural Selection and provides the genetic basis for species variation. Reproduction is driven by cellular growth and division; the ability of an organism to reproduce is dependent upon its ability to successfully undergo multiple rounds of cell division. Cell division occurs when the genetic material is duplicated and the cell pinches itself into two, dividing the duplicated genetic information evenly between the two resulting daughter cells.

The ability of a cell to accurately divide its genetic material is critical for life at all stages. For multi-cellular organisms, this process must occur with extremely high fidelity during embryonic development, growth to adulthood, and throughout adult life in order to maintain tissues. Defects in cell division can lead to birth defects, cell death, aneuploidy, and cancer[1,2]. Because cell division is such an important aspect of physiology and the overall ability of a species to adapt and survive, cells have evolved highly regulated mechanisms to accomplish this, with multiple redundancies and checks built into the pathway to ensure success. Many of these cellular mechanisms are conserved across species; from single-celled organisms like yeast to simple multi-cellular species like worms, all the way up the evolutionary ladder to humans.

This dissertation will delve into the molecular nature of the biochemical signaling events that occur within intact tissue during the last step of cell division – cytokinesis, by providing

novel experimental findings that shed new light on the mechanisms that control cytokinesis in space and time. The novel work described here will provide experimental evidence regarding a GTPase activating protein (GAP) for the Rho family GTPases, MgcRacGAP. In the context of a live vertebrate epithelial tissue, I have investigated the questions of Mgc GAP specificity toward GTPases, how the GAP specificity is regulated, have identified a novel function of Mgc in regulating cell-cell junctions through RhoA, and investigated Mgc's ability to bind the plus ends of microtubules (MTs) through an adaptor protein called EB1. These points will be described in detail in Chapters 1 and 2, while Appendices 1 and 2 will describe unpublished work that was a result of the studies above. I will introduce the field of cytokinesis, by first explaining the process and giving a historical overview. Then I will provide a detailed description of the proteins that regulate cytokinesis, including the focus of my work, MgcRacGAP. Next, I will explain our current knowledge regarding the function of Mgc at cell-cell junctions and the importance of studying cytokinesis within a live tissue, before ending the introduction with a description of how and why this work is significant and relevant to the field.

The mitotic phase of the cell cycle

Each cell is genetically programmed with an internal clock or cycle that controls growth and division. The cell cycle governs the cell's ability to undergo growth, rest and division, and it ensures that these processes are carried out with the appropriate timing. Cell growth and protein synthesis occur during earlier stages of the cell cycle, as well as preparation for division including DNA duplication and error checkpoints (interphase, Figure 1 A). The mitotic phase of the cell cycle occurs when the cell is ready to divide. The chromosomes condense (prophase, Figure 1 A), and MTs attach to the chromosomes and align them at the center of the cell

(prometaphase/metaphase, Figure 1 A). The cell checks to make sure that all chromosomes are

properly aligned and connected to MTs before separating the chromosomes to the poles of the

Figure 1: Cellular structures during mitosis. A) Interphase and early stages of mitosis are shown. DNA is duplicated, chromosomes are condensed and aligned at the metaphase plate ready for separation by the microtubules of the mitotic spindle. B) Events of anaphase and cytokinesis showing DNA separation, actomyosin contractile ring formation, cleavage furrow ingression and telophase; DNA (blue), MTs (green), actomyosin contractile ring (red), central spindle (yellow box).

cell (anaphase, Figure 1 B). Cytokinesis is the last stage of mitosis and is the process that

physically separates the dividing cell into two daughter cells (Figure 1 B). Telophase is the last

step in the division process and describes the abscission event that occurs to separate the

daughter cells (telophase, Figure 1B).

The precise mechanisms that control cytokinesis have been an important area of study

for over a century. We now know that cytokinesis is driven by a contractile apparatus made up

of filamentous actin (F-actin) and the molecular motor protein myosin-2. During anaphase,

when the DNA is separated toward the cell poles by the mitotic spindle, a cleavage furrow is

generated in the middle of the cell which is connected to the plasma membrane to allow the

cell to pinch in two – similar to a purse string. The resultant daughter cells will each receive a

full copy of genetic material (Figure 1 B). Our current understanding of the molecular events

that occur during cytokinesis is the culmination of over 100 years of experimental investigation.

However, the precise mechanisms employed by the cell to regulate the spatio-temporal nature of cytokinesis remain a mystery.

A historical perspective on the field of cytokinesis

Understanding the regulation that underpins cytokinesis has provided a perplexing problem for scientists due to its transient nature; the process takes only a handful of minutes to complete. Consequently, early studies resulted in many different theories to explain observable phenomenon that occur during cytokinesis. One important question that was debated for the first half of the 1900's was the origin of the furrow initiation signal. Early micromanipulation experiments carried out in insects suggested that furrowing was coupled to cell contractility and established the technique of micromanipulation for the study of cytokinesis[3]. Over the next several decades this technique was used to determine that once the cytokinetic ring is established, disruption of the mitotic spindle does not hinder furrowing[4–6]. These early studies provided important clues about how the location of the furrow was determined: the mitotic spindle position dictated where and when the cleavage furrow would form. But, whether the signal for furrow initiation came from the spindle, the chromosomes, the cell membrane, or elsewhere in the cell was still unknown. Seminal experiments conducted by Rappaport (1961) in echinoderm eggs, which he manipulated to form a torus (or doughnut) shape, provided evidence to suggest that the furrow initiation signal came from a region of overlapping astral MTs at the equatorial cortex (equatorial astral MTs, Figure 2)[7]. This was an important discovery at the time and continues to be the accepted theory to explain formation of the contractile ring.

Later in his career, Rappaport continued to publish results that pushed the field of cytokinesis forward. Several of Rappaport's key findings include: 1) the identification that the furrow forms by contraction of the cortex[8]; 2) the measurement of the amount of force the cleavage furrow could generate during cytokinesis[9]; and 3) the finding that the speed at which the furrow initiation signal moves from the spindle to the cortex is consistent with the speed of motor movement along MTs[10].

Current views on cytokinesis mechanisms

While the contributions of Rappaport and others have shaped and inspired the field of cytokinesis, many unanswered questions regarding the *molecular* regulation of cytokinesis remain. One such question is the identity of the furrow initiation signal, which is generated at the mitotic spindle and moves to the cortex, and how it is delivered to the right place at the right time. This question is at the heart of my dissertation research.

Figure 2: RhoA and the contractile ring during cytokinesis. A focused zone of active RhoA (green) forms at the cell midzone at anaphase onset. Active RhoA signals to downstream effectors to form the contractile ring (red). Different MT populations are identified (arrows); central spindle MTs form between separating chromosomes (blue); astral MTs orient toward the cell cortex.
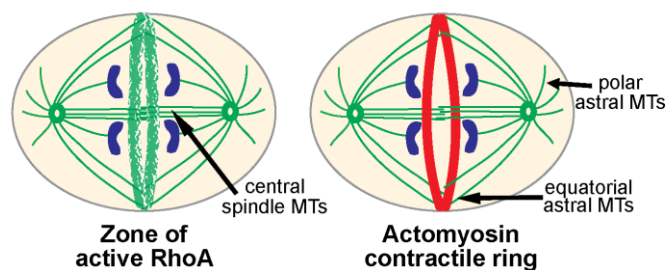
Cytokinesis represents one of several cellular events that is known to require coordination of both MTs and actin. Indeed, at anaphase onset, MTs are bundled and form a signaling platform between the separating sister chromatids – the central spindle - that specifies the location of the actomyosin contractile ring (Figure 2). The actomyosin contractile

ring, which generates the force required for ingression of the cleavage furrow[11,12], is initiated by localized activation of the small GTPase RhoA. At anaphase onset, active RhoA becomes focused in a tight band at the equatorial cell cortex to template furrowing (Figure 2)[13–15]. RhoA then functions through its effectors – formin, which promotes actin polymerization and ROCK and citron kinases, which activate myosin-2 to promote the formation of the actomyosin contractile ring at the appropriate time and place[14,16,17].

Just as Rappaport's classic torus experiment predicted that the furrow initiation signal would emanate from overlapping microtubules, it has been shown that the precise spatio-temporal activation of RhoA at the equatorial cortex is dependent upon the overlapping plus ends of the central spindle MTs at anaphase onset. The central spindle (Figure 1B and Figure 2) is a specialized MT structure composed of interdigitated MT plus ends and serves as a scaffold to recruit signaling molecules that regulate the initiation and progression of cytokinesis.

The central spindle is formed by the bundling activity of several proteins. Centralspindlin is a heterotetrameric protein complex composed of two molecules of Mitotic Kinesin Like Protein 1 (MKLP1) and two molecules of MgcRacGAP (Mgc), a GTPase Activating Protein (GAP)

Figure 3: The Centralspindlin Complex. A) Protein diagram of Mgc. B) Centralspindlin is composed of 2 molecules each of the kinesin motor, MKLP1 (blue/black) and Mgc (orange). Mgc recruits and binds the RhoA GEF, Ect2 (red). C) Centralspindlin and Ect2 localize to the central spindle and along astral MTs.
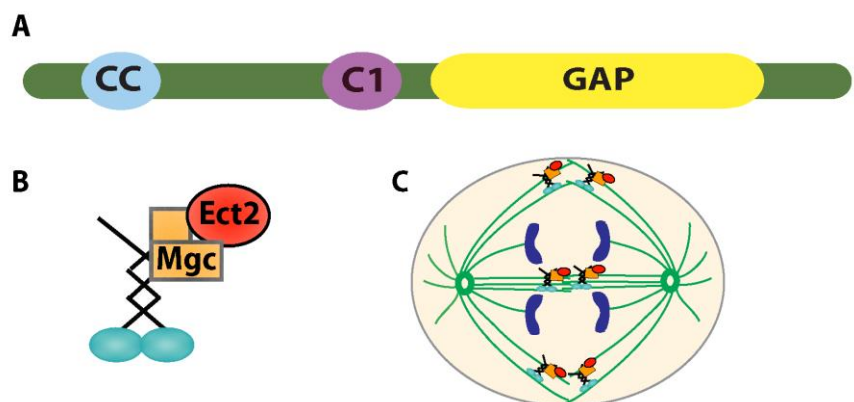
for the Rho family of small GTPases (Figure 3 A-B)[18,19]. At anaphase onset, when Cdk1/Cyclin B are degraded, an inhibitory phosphorylation on MKLP1 is relieved, which then allows Centralspindlin to bind MTs[20]. Mgc recruits the Guanine Nucleotide Exchange Factor (GEF), Ect2, which is thought to be the major RhoGEF that mediates RhoA activation during cytokinesis, and concentrates it at the equatorial cell cortex via the plus end directed motor activity of MKLP1 (Figure 3 B-C)[21–24]. Together, this work reveals a link between the central spindle and the initiation of cortical contractility at the cell equator.

While the key cytokinetic GEF for RhoA is well established (Ect2), there is currently a debate in the literature regarding the identity of the GAP for RhoA. Mgc is thought to serve this function because it localizes to the cleavage furrow region during cytokinesis, and has been shown to focus the RhoA activity zone[14,15]. However, others have shown that Mgc has GAP activity toward Rac1[25,26], and yet another report has shown that Mgc's GAP activity can be switched via phosphorylation[27]. These conflicting results highlight the need for further investigation into how Mgc regulates Rho family small GTPases, and suggests the possibility of regulation on multiple levels to control precise spatial and temporal activity of Mgc. *I will provide experimental evidence in Chapter 1 that investigates this question and concludes that Mgc acts toward both RhoA and Rac1 during vertebrate epithelial cytokinesis at spatially distinct cellular locations.*

The activity of Centralspindlin in the delivery of Ect2 to the equatorial cortex for RhoA activation presents interesting mechanistic questions. We have observed Mgc localization at both the central spindle and the equatorial cell cortex during anaphase, with both localizations being important for proper cytokinesis[15,28]. Furthermore, we have observed Mgc puncta that

decorate astral MTs and appear to make stable connections with the plus end of the MT and the cortex. These observations raise the questions of why are there two spatially distinct populations of Mgc during anaphase and how does Centralspindlin stably associate with the cell cortex throughout cytokinesis? It has been shown that Mgc contains a phospholipid binding domain that allows it to bind the cell membrane (C1 domain) and is essential for faithful separation of daughter cells during the last stage of cytokinesis, abscission[29]. Because Mgc can bind membrane and this binding is important for cytokinesis, we wanted to investigate the mechanism by which Mgc makes stable attachments to the astral MT plus ends and the cortex concomitantly. *I will provide experimental evidence in Chapter 2 that addresses the role that Mgc may have in tethering Centralspindlin to MT plus ends.* The following paragraphs will introduce in more detail each of the main protein regulators during cytokinesis.

I. Cytokinesis main players

Rho GTPases

The Rho family of small GTPases are a distinct subgroup within the Ras GTPase superfamily. Rho family proteins are distinct from other Ras-like proteins in that they have a Rho-specific insertion domain that is involved with effector binding[30]. The mammalian genome encodes 22 distinct Rho family genes, with Rho, Rac and Cdc42 being the most well characterized of the family members. There are 3 different isoforms of Rho (RhoA, RhoB, RhoC), two isoforms of Rac (Rac1 and Rac2) and one isoform of Cdc42[31]. It has been shown that each of the Rho isoforms have specific effector proteins that bind the active GTPase and carry out the cellular response, with over 30 potential effectors for Rho, Rac, and Cdc42 alone[32]. Rho

family GTPases function as binary switches by cycling between active (GTP-bound) and inactive (GDP-bound) states in order to control biochemical signaling pathways. The nucleotide binding state of Rho proteins is governed by two distinct classes of proteins: Guanine Exchange Factors (GEFs) activate the Rho signaling pathway by promoting exchange of GDP for GTP, and GTPase

Activating Proteins (GAPs) inactivate Rho signaling by stimulating the intrinsic ability of the GTPase to hydrolyze the GTP

Figure 4: The GTPase cycle. Rho family GTPases cycle between active, GTP bound states (green) and inactive, GDP bound states (grey). The GTPase can only signal to downstream effectors when GTP bound.
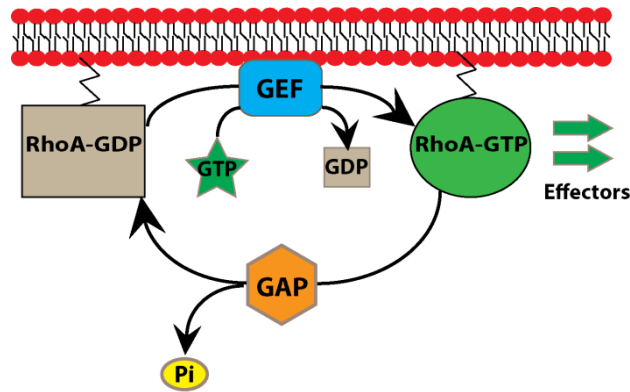
molecule to GDP (Figure 4). Rho proteins are also regulated by Guanine Disassociation Inhibitors (GDIs) that recognize and bind to the prenyl motif on the carboxy terminus; GDI binding masks the nucleotide binding site and sequesters the GTPase in the cytosol. Rho proteins all share a distinct activity domain called the Switch I and Switch II domains that undergo conformational changes upon binding by GTP/GDP[33]. These conformational changes regulate the activity cycle of the GTPase[33].

Seminal work by Ridley and Hall (1992) established Rho Family GTPases as global regulators of cytoskeleton dynamics[34]. However, Rho proteins participate in many diverse biochemical signaling pathways such as cell cycle control[35,36] gene expression[37–40], cell polarity[41,42], and cell-cell junction structure[28,43–46]. RhoA has been shown to be essential for cytokinesis; it templates the site of the contractile ring by signaling through its downstream effectors (Figure 5) to activate F-actin and myosin-2.

The canonical function of Rac1 is to control formation of lamellipodia during cell migration and to facilitate early formation of focal contacts[47,48]. Rac1 mediates formation of branched actin filaments by signaling to its effector protein, Arp2/3, which nucleates branched actin and is a driver of cell migration via dynamic branched actin formation at the leading edge[49] (Figure 5). It has been shown that Rac1 regulates cell adhesion - both cell-cell junctions and cell-substrate adhesions[26,50]. One of the main pathways through which Rac1 controls cell-cell junction adhesion occurs via co-localization of Rac1 and the adherens junction protein, E-cadherin. Rac1 is recruited to sites of E-cadherin-mediated cell adhesion at cell-cell junctions and becomes activated by the Rac1 specific GEF, P21-activated kinase (PAK)[50]. In cultured adherent cells, Rac1 participates in cell-substrate adhesion through regulation of integrin mediated adhesion complexes which anchor the cell to the substrate[51]. This pathway is important for Rac1's role during cytokinesis in cultured adherent cells. Expression of a dominant negative form of Rac1, (Rac1Q61L) abrogated the ability of HeLa cells to round up during division, resulting in cytokinesis failure[26].
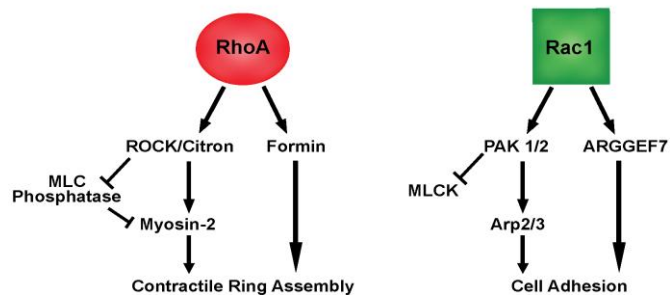
Figure 5: RhoA and Rac1 effector proteins. Active, or GTP bound RhoA and Rac1 bind to specific effector proteins that modulate the cytoskeleton. *Adapted from Jordan and Canman (2012)*[188].

The role of Rho family GTPases in controlling epithelial cell-cell junctions will be discussed later in the introduction. While it is clear that Rho proteins are master regulators of

multiple biochemical signaling pathways that rely on modulation of the cytoskeleton, there is much to be learned regarding the precise spatio-temporal mechanisms of their regulation and their role in disease.

MgcRacGAP and the Centralspindlin complex

MgcRacGAP is a Rho family GAP protein that has a coiled-coiled region at its amino terminus, a C1 domain and a conserved GAP domain (Figure 3 A). It was discovered in 1998 during a search for novel binding partners of active Rac1[52]. The researchers identified a new RhoA family GAP using a yeast 2 hybrid approach with the activated form of Rac1 as bait. A human cDNA was isolated that was found to have high sequence similarity with Rho family GAPs. To determine if their newly discovered GAP acted toward Rho GTPases, they performed an *in vitro* GTP hydrolysis assay using RhoA, Rac1, and Cdc42 as the target GTPases. Their results showed GAP activity toward Rac1 and Cdc42, but not toward RhoA. Localization studies of this protein in various human tissue found that the GAP protein strongly localized in male germ line tissue, and thus the name <u>M</u>ale <u>G</u>erm <u>C</u>ell Rac GAP or MgcRacGAP was given[52].

Since its initial discovery, much work has been done to elucidate the role of MgcRacGAP during cytokinesis. It was shown that Mgc is required for proper formation of the central spindle during cell division by a forward genetics screen carried out in the first few cell divisions of the *Caenorhabditis elegans* embryo[18]. This work provided *in vivo* evidence that the localization of Mgc and its binding partner, MKLP1 were interdependent and were both necessary for proper formation of the central spindle, formation of the cleavage furrow, and for overall cytokinesis success[18]. Therefore the name 'Centralspindlin complex' was given to MKLP1

and Mgc due to their interdependent localization to the central spindle. Follow-up work showed that Mgc and MKLP directly bind to each other both *in vivo* and *in vitro,* and form a stoichiometric 2:2 heterotetramer[19]. Binding of Mgc and MKLP1 occurs through the amino-terminal coiled-coil domain of Mgc and the 85-amino acid linker region of MKLP1, between the motor domain and MKLP1's coiled-coil domain[19,20]. The heterotetramer is formed through interaction of each protein's coiled-coil region.

Centralspindlin can form higher-order clusters along the central spindle to facilitate MT bundling and movement of the complex along MTs. To achieve this, MKLP1 generates sliding forces on the central spindle MTs by sliding along a MT while maintaining attachment to other MTs via its motor domain[19,53]. This is regulated by phosphorylation of MKLP1 on S710 which allows for binding of the 14-3-3 protein and sequestration of Centralspindlin in the cytosol[54]. An anaphase-specific phosphorylation by Aurora B kinase occurs at S708 on MKLP1, which antagonizes 14-3-3 binding. This activity along with loss of Cdk1 phosphorylation allows Centralspindlin to localize on spindle MTs and form clusters[54]. MKLP1 has an oligomerization domain that allows Centralspindlin to form higher-order clusters. These clusters have been shown to be highly processive toward the plus end of single MT tracks when compared to the Centralspindlin dimer alone, which is non-processive, in *in vitro* motility assays[55].

Unpublished live microscopy data from our lab suggests that Mgc can be stably tethered at the plus ends of individual MTs at the equatorial cortex during cytokinesis. This is consistent with a fixed imaging study showing that MKLP1 is localized at the plus ends of equatorial astral MTs during cytokinesis in hamster kidney cells[23]. However, this stable MT plus end localization is not consistent with the normal kinetics of kinesin motor mobility along MTs. Generally a

kinesin motor will use the power from ATP hydrolysis to move along the MT, but there is not a

known mechanism that describes stability of motor proteins on MT ends. Our observations of

stabilized Centralspindlin on MT plus ends led us to hypothesize that tethering of

Centralspindlin to equatorial astral MTs may be mediated by End Binding Protein 1 (EB1), a MT

Figure 6: EB1 is a MT plus tip tracking protein. A) EB1 binds the 'GTP-cap' on MT plus ends. B) Conserved EB1 binding motif and the c-terminal amino acid sequence of Mgc. C) Our working hypothesis of how Mgc may bind EB1 to facilitate tethering of Centralspindlin to MT plus ends.
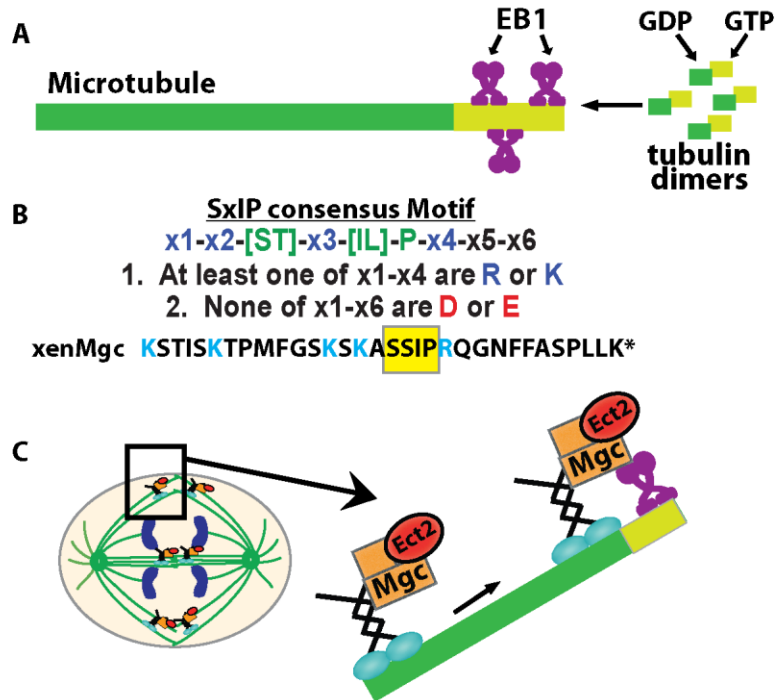
plus end tracking protein (Figure 6 A). EB1 is responsible for most intracellular plus end tracking

by recruiting other plus tip binding proteins (+TIPs) to the polymerizing MT end[56]. It has been

shown that EB family proteins facilitate MT stability and dynamics and provide a means of

attachment to MTs for proteins that do not contain MT-binding domains[57–59]. A conserved EB1

binding motif (SxIP) was recently discovered and found to be highly specific for EB binding and

MT plus tip tracking[56,57,59,60] (Figure 6 B). Proteins that contain an SxIP motif bind to the carboxy

terminus of EB1 via the EB1 homology domain. The interaction requires specific amino acid and

charge distribution, as the EB homology domain contains a binding pocket that is highly

electronegative[61]. We have found a putative SxIP motif on the carboxy terminus of Mgc, which

we hypothesize may interact with EB1 on MT plus ends in order to facilitate the stability of Centralspindlin there (Figure 6 B-C).

The RhoA GEF, Ect2

The Centralspindlin complex recruits the RhoA GEF Ect2 to the central spindle and focuses it at the equatorial cortex at anaphase onset. Ect2, or Epithelial Transforming Protein 2, is a RhoA-specific GEF that contains tandem BRCT domains on its amino terminus, a plekstrin homology domain for membrane binding, and a highly conserved Dbl-homology domain that mediates GEF activity[62]. Ect2 exists in two confirmations: an auto-inhibited form that is regulated by internal binding between the BRCT domain and the carboxy terminus which masks the GEF activity site and binding to RhoA; and an active conformation where the GEF site can bind to RhoA[62]. Ect2 can bind to Centralspindlin directly. The amino terminus of Mgc is phosphorylated by Polo-Like-Kinase 1 (PLK1) which provides a binding site for Ect2[63,64]. It has been suggested that Mgc binding may function in the activation of Ect2 to help block the auto-inhibitory intermolecular binding and thereby facilitate GEF activity toward RhoA. Importantly, when PLK1 is inhibited, Ect2 does not localize to the central spindle, and RhoA is not efficiently activated, resulting in failed cytokinesis[65]. Because Centralspindlin is required for efficient RhoA activation during cytokinesis, and Ect2 is a RhoA GEF that is also important for RhoA activation, this suggests a mechanism by which Ect2 and Centralspindlin function cooperatively to regulate RhoA activation and successful cell division. It is now accepted that RhoA activation at the cell cortex during cytokinesis is achieved by precise delivery of Ect2 to the equatorial cell cortex via directed motility of Centralspindlin and Ect2 along astral MTs (Figure 3 B-C). Astral MTs form a region of overlap at the equatorial cell cortex that coincides with the location of contractile ring

14

formation (Figure 2)[7,8]. Therefore, it is thought that Centralspindlin and Ect2 together could make up the Rappaport furrow initiation signal, since they are at the right place at the right time to control cytokinesis.

II. Rho GTPase Flux

Recent work from our lab suggests that Mgc's GAP activity plays a vital role in controlling the focused region of RhoA activation. In order for active RhoA to become focused at the equatorial cell cortex there must be precise tuning that regulates its active and inactive states at different regions along the ingressing cleavage furrow. Our lab has proposed that this cycling is cooperatively regulated by the GEF activity of Ect2 and the GAP activity of Mgc, and has named this process Rho GTPase Flux[15]. The GTPase Flux model predicts the GAP activity of Mgc would function throughout cytokinesis to prevent the spread of active RhoA to other sites along the cell cortex, thus providing a mechanism for focusing the RhoA activity zone to the precise spatial location required to dictate cleavage furrow ingression between segregating sister chromatid[14,15]. Evidence to support this model was provided using *Xenopus* embryos in which endogenous Mgc was knocked down and replaced with a truncated version of Mgc that lacked the GAP domain or with a Mgc point mutation that abrogated GAP activity (MgcR384A)[15]. Perturbation of Mgc's GAP activity resulted in 1) a broader and more intense region of active RhoA at the equatorial cortex during cytokinesis, 2) RhoA accumulated in ectopic regions along the cortex, and 3) significant increases in cytokinesis failure. To test the model further, constitutively active RhoA was expressed in the embryos and found to exhibit similar localization to the MgcGAP dead mutant embryos. Interpretation of these results suggest that Mgc's GAP activity is necessary to down regulate RhoA signaling to prevent ectopic

RhoA activation. Further evidence that shows how the cytokinetic zone of RhoA is locally activated and de-activated in response to spindle cues came from experiments in echinoderm eggs where spindle position was shifted[67]. These experiments illustrated that active RhoA was quickly lost when the spindle was moved and became re-established at the new spindle location. Collectively, these data provide compelling evidence to suggest that the GAP activity of Mgc is directly involved in maintaining a focused band of equatorial active RhoA to ensure successful cell division.

III. Controversy regarding the specificity of Mgc's GAP activity

The specificity of Mgc's GAP activity toward RhoA and Rac1 during cytokinesis is controversial. There are two lines of thought in the field, one that supports the idea of Mgc functioning as a RhoA GAP, the other that supports Mgc as a Rac1 GAP.

To address this controversy, we must first look at the current evidence from the literature. Previous work from our lab described above[15,68] provides evidence for Mgc's GAP activity toward RhoA. Work from other groups has also shown that Mgc's GAP activity is essential for proper RhoA regulation[27,69]. However, there is also a body of evidence to suggest that Mgc has GAP activity toward Rac1 and/or Cdc42[18,26,52,70]. As an example of this, it was shown in *C. elegans* embryos using a temperature-sensitive allele of Mgc that abrogated GAP activity, that the mutant Mgc caused defects in contractile ring formation[70]. To determine which GTPase Mgc's GAP activity acted upon, they reasonsed that removal of the target GTPase in the Mgc mutant background with contractile ring defects should rescue the defect. Indeed, they found that RNAi against Rac1, but not RhoA, rescued the cytokinesis defect and thus they concluded that Mgc was a Rac1 GAP. However, this study did not take into account the

possibility that Mgc's GAP domain may be required for GTPase Flux, to cycle RhoA during cytokinesis, nor did they mention that knockdown of RhoA – an essential component for formation of the contractile ring – would by itself abolish the ability of the contractile ring to form. An *in vitro* phosphorylation study using purified full length Mgc treated with purified Aurora B kinase, showed Mgc had GAP activity toward Rac1[26]. However, an important caveat to this study is that it was not conducted in a physiological context; Mgc, RhoA and Rac1 were purified and thus isolated from cellular regulatory mechanisms such as protein-protein interactions and membrane insertion (for RhoA and Rac1), which can be important for GAP specificity. Therefore, the physiological activity of the GAP domain was not established.

It was reported in 2003 that Aurora B phosphorylation of Mgc's isolated GAP domain at S386 could switch the specificity of Mgc's GAP domain from Rac1 to RhoA *in vitro*[27]. This group showed that overexpression of an Mgc non-phosphorylatable mutant (MgcS386A) caused cytokinesis defects, but not a phosphomimetic mutant (MgcS386D). These results suggested that MgcS386 is a phospho-switch that could regulate Mgc's GAP specificity. More recently, another group used an *in vivo* approach to knockdown endogenous Mgc with siRNA and replace with an MgcS386A or MgcS386D mutant. They did not observe a difference in GAP activity toward Rac1 between the mutants, but this study only looked at the effects of Mgc on Rac1 and did not fully investigate the effects of the phosphorylation mutation on localization and activation of RhoA[26].

Therefore, it was unclear whether phosphorylation at S386 could control the specificity of Mgc's GAP activity allowing for two populations of Mgc in the cell that are spatially regulated; one with GAP activity toward Rac1 and the other with GAP activity toward RhoA.

One possibility that could explain these conflicting conclusions is that there could be two distinct populations of Mgc in the cell during cytokinesis; one population that is centered on the equatorial cortex and the central spindle and the other population that is at the cell poles, possibly controlling cell-cell junctions or cell-substrate adhesions. Each population could have distinct functions during cytokinesis that could be controlled by various regulatory mechanisms, including phosphorylation. Our lab also addressed the question of whether MgcS386 conferred a phosphorylation switch for Mgc's GAP activity. We found that an MgcS386A mutant was similar to control cells during cell division and in the localization of active RhoA and Rac1, but that an MgcS386E mutant had severe cytokinesis and cell-cell junction defects.[28] This work is described in detail within Chapter 1 of this dissertation.

Another factor that might explain the conflicting results of Mgc's GAP activity is that many of the relevant studies were conducted in different systems: singled celled embryos, flat adherent cultured cells, or live developing vertebrate embryos. Because Mgc is a Rho GAP, and Rho GTPases regulate the cytoskeleton to allow for cell-cell and cell-substrate adhesion, the differences in the adhesive environment between the experimental systems could have strong effects on how Rho family GTPases and their effectors function.

IV. Epithelial cell-cell junctions

Epithelial tissues are polarized groups of cells that are tightly connected to their neighboring cells in order to form a restrictive barrier to protect underlying organs and tissues (Figure 7). Epithelial tissues are the building blocks of many organs; they line blood vessels and almost all major structures in the body. The importance of epithelial tissue in maintance of

18
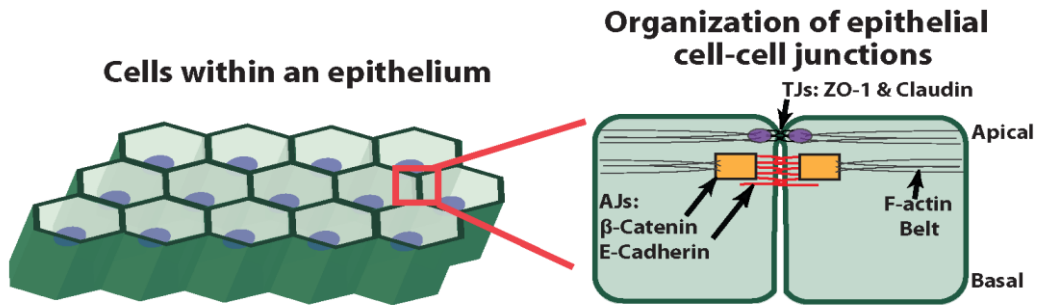
Figure 7: Epithelial cell-cell junction structure. Cells within an epithelium make tight contacts with neighboring cells. Cell-cell junctions are composed of different proteins linked to an apical ring of F-actin.

adult structures is paramount and may hold the key to elucidating the mechanisms that underly tumorogensis, as 80-90% of all human tumors are derived from epithelial tissue. It is surprising, then, that very little is known about how epithelial tissues are regulated, and less is known about how cell division occurs within the epithelium.

Cell-cell junctions provide adhesion between epithelial cells and function as a barrier between the cells. Additionally cell-cell junctions comprise an important cellular signaling location where multiple biochemical signaling events are orchestrated[46]. For the purpose of this work, I will focus on the role of Rho proteins in regulation of the two most apical junction types; 1) tight junctions, the most apical junction, which form very tight contacts with neighboring cells and function as a barrier so that solutes cannot cross the junction, and 2) adherens junctions, are basal to tight junctions and function as the main sites of cell-cell adhesion. (Figure 7). Both junction types are linked to an apical actomyosin ring that regulates short and long range tension across the epithelium (Figure 7).

Rho signaling provides the cytoskeletal framework for cell-cell junction structure and function by regulating the formation and tension of the apical actomyosin belt (Figure 7). RhoA

and Rac1 also regulate cell-cell junction structure and integrity by modulating the location of several key junctional proteins. Multiple GEFs and GAPs localize to cell-cell junctions and directly bind to junctional proteins in order to control Rho family activity at these sites[28,46,71,72]. Gaining a better understanding of the structure and integrity of cell-cell junctions and the regulatory role of Rho proteins there is an important area of study for understanding epithelial biology in both normal and diseased tissue.

Cell division within epithelial tissue

Cytokinesis employs an actomyosin based contractile ring that provides the constrictive force that pinches the dividing cell into two daughter cells. This process requires considerable cell shape changes, which are mediated by the cytoskeleton. For cultured cells that undergo division, the cell must first release their adhesive contacts to the substrate in order for the cell to undergo cleavage during cytokinesis (Figure 8 A). This is refered to as 'cell rounding' and is a common phenotype of dividing cultured cells. In fact, a synchronization method based on the cell rounding phenomena has been established where one can shake off rounded up mitotic

Figure 8: Cytokinesis in different cell adhesion environments. A) Cells that adhere to a basement membrane and cells in culture have tight adhesions to the underlying substrate. These adhesions must be released before cell division. Cell rounding occurs in order for the cell to undergo cytokinesis. B) Cells within an epithelium experience cell-cell adhesions to neighboring cells. These adhesions must be maintained throughout cytokinesis to uphold the barrier function of the tissue. DNA (blue), MTs and RhoA activity zone (green).
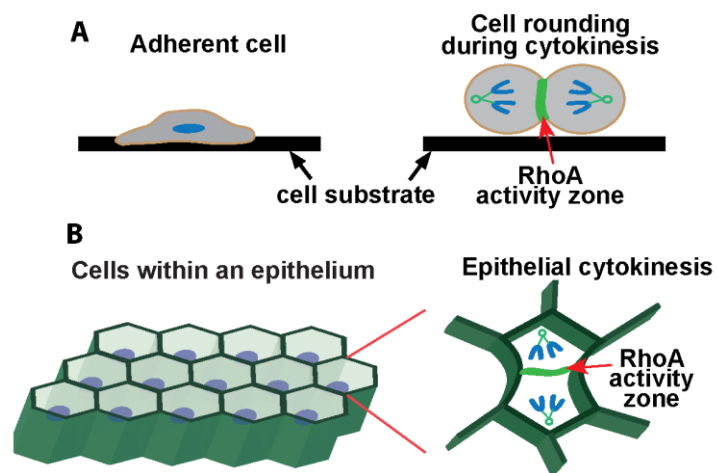
cells in order to obtain a population enriched in M-phase cells. This method is called mitotic shake-off[73].

Cells within an epithelial tissue are also adherent cells but they experience adhesions along the basolateral surface instead of along the ventral surface (Figure 8 B). The most apical cell-cell junctions, TJs and AJs, are both connected to the actin cytoskeleton through cytoplasmic proteins that bind to transmembrane junction proteins and actin. This linkage to the actin cytoskeleton plays an imporant physiological role in maintaining short and long range tension across the epithelial tissue (Figure 7). The tension is maintained through the concerted action of an apical actomyosin belt that behaves very similar to the actomyosin contractile ring during cytokinesis. The apical actomyosin belt must be precisely regulated to control tension between neighboring cells and collectively across the tissue to withstand such processes as tissue morphogenesis during development and maintain adult tissue homeostasis[74,75].

Epithelial tissue undergoes expansion through the combination of cell growth and cell division. Dividing epithelial cells have a unique problem to deal with during cytokinesis; while their cultured cell counterparts round up and release their substrate adhesions during division, epithelial cells cannot do this. They must maintain tight cell-cell junction adhesive contacts in order to uphold the tissue integrity and the barrier function of the epithelium. Cells within an epithelium must contend with regulating both of the actomyosin contractile rings; the cytokinetic contractile ring and the apical actomyosin belt at cell-cell junctions. Very little is known about the regulation of these two strucutres during epithelial tissue cytokinesis, nor if the regulation of the contractile rings is coupled. It is surprising that there is such limited knowledge in the literature regarding these processes, as this is a similar environment to the

21

tissues in our bodies where most of our cells undergo cytokinesis. Hence, studying these

questions is certainly physiologically relevant and at the leading edge of the field of cytokinesis

research.

Due to the similar structure of the contractile rings during cytokinesis and at cell-cell

junctions, it is perhaps not surprising that recent studies have uncovered a dual role for several

proteins that regulate both of these contractile arrays[28,45,46,72]. Indeed, it is generally accepted

that Rho family GTPases control cytoskeletal rearrangements at cell-cell junctions, but recent

studies (described in detail below) have now provided evidence that Centralspindlin and Ect2

regulate GTPase activity at cell-cell junctions. *I will describe novel mechanisms by which Mgc*

regulates RhoA during cytokinesis and RhoA and Rac1 at cell-cell junctions during Xenopus

epithelial cell cytokinesis in Chapter 1 [28]. *Further, in Chapter 2, I will provide a novel mechanism*

by which Centalspindlin is precisely delivered to both the equatorial cortex during cytokinesis

and to cell-cell junctions in order to regulate RhoA and Rac1 signaling.

MgcRacGAP at cell-cell junctions

Throughout the cytokinesis literature it is well accepted that Mgc is part of the

Centralspindlin complex, whose activity is tightly regulated spatio-temporally by anaphase

specific phosphorylation events. It has also been observed by numerous groups that both Mgc

and MKLP1 localize to the nucleus during interphase. This has lead to the common conclusion

that Mgc functions primarily during Mitosis when the nuclear envelope has been broken down,

and is sequestered in the nucleus during interphase. This model was challenged recently by

three papers (including my own) that show Mgc localizes at the cell-cell junctions of polarized epithelial cells in interphase[28,46,72].

Alpha Yap's lab reported that Mgc localized to adherens junctions in cultured MCF-7 cells (human epithelial cancer cell line) and that its localization was dependent upon MT delivery and the adherens junction protein α-catenin[46]. They showed that both MKLP1 and Ect2 also exhibited junctional localization and that Centralspindlin was important for regulating RhoA signaling and activation of Myosin-2 to maintain junction integrity[46]. Sandra Citi's group independantly found that Mgc localized to the tight junctions and adherens junctions of polarized MDCK cells (canine kidney epithelial cells)[72]. They showed that Mgc co-localized with Cingulin, a tight junction protein, and Paracingluin, a tight and adherens junction protein. Their study concluded that Mgc directly interacts with both Cingulin and Paracingulin at tight junctions to control the structure and integrity of the junction, presumably through downregulating Rac1 activation. Collectively, these studies have provided the first experimental evidence of Centralspindlin functioning to control RhoA and Rac1 activation extra-mitotically, and shed light on how a conserved protein complex can serve similar functions in different cellular processes. *I will discuss experiments in Chapter 1 of this dissertation that build on the story of Mgc's actvity at cell-cell junctions. I will describe how we made the novel discovery that Mgc regulates the structure and integrity of adherens junction, but not tight junctions, specifically through downregulating RhoA signalling.*

V. *Xenopus laevis* as a model system

Our lab uses the embryos of *Xenopus laevis*, the African clawed frog, as a model system to study cytokinesis. Several characteristics that make this an ideal model system for cell
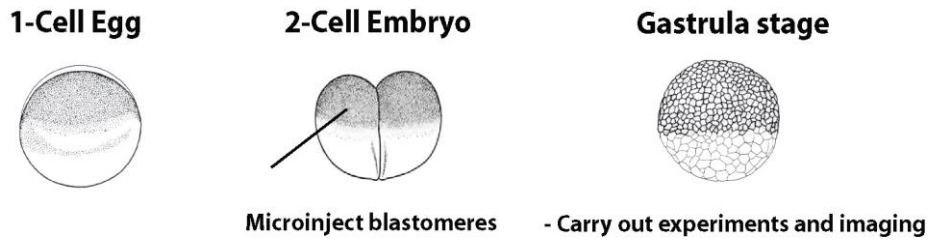
Figure 9: *Xenopus* embryo microinjection strategy.

division research are as follows. 1) *Xenopus* embryos are large (~1.2 mm in diameter) which allows for ease of handling and microinjection, 2) they divide synchronously until the mid-blastula stage, then continue to divide frequently thereafter, 3) the embryos develop externally which allows for detailed study of cell division using fluorescent confocal microscopy, and 4) the dividing cell is part of an intact epithelium, where the cells are in their natural environment and cell-cell signaling can occur unperturbed. These characteristics allow us to explore the molecular behavior of cytokinesis in the context of a live developing vertebrate epithelium, which is very similar to the environment of human cells in the body. Morpholino knockdown of endogenous protein and replacement with WT or mutant mRNAs can be achieved by direct microinjection into individual cells at the 2-8 cell stage (Figure 9).

VI. Significance

The research described in this dissertation is *significant* to human health because it provides mechanistic data regarding function and regulation of Mgc that relates to current clinical cancer studies involving Mgc in human carcinomas and v-Src-induced cellular transformation[76,77]. The data described here are also *significant* to basic cell biology, as the function of Mgc and the Centralspindlin complex are not fully understood. Although several key functions of Centralspindlin during cytokinesis have been characterized, no approaches to date

have unequivocally defined the target of Mgc's GAP activity. Chapter 1 describes a novel

approach I employed to address this gap in our knowledge about the target of Mgc's GAP

activity and reveals new information about how Mgc regulates cell-cell junctions. Chapter 2 will

seek to define the mechanism by which Centralspindlin is targeted to the equatorial cell cortex

during early cytokinesis and to cell-cell junctions during interphase. The data described here are

a collection of novel hypothesis driven experimental approaches designed to improve our

understanding of the molecular mechanisms of Centralspindlin signaling and dynamics during

epithelial cytokinesis.

Chapter 1

MgcRacGAP restricts active RhoA at the cytokinetic furrow and both RhoA and Rac1 at cell-

cell junctions in epithelial cells

This chapter describes work that was published in *Molecular Biology of the Cell.*

Breznau, E. B., Semack, A. C., Higashi, T. & Miller, A. L. MgcRacGAP restricts active RhoA at the cytokinetic furrow and both RhoA and Rac1 at cell-cell junctions in epithelial cells. *Mol. Biol. Cell* **26,** 2439–55 (2015).

Contributions to this work are as follows:

Breznau, E.B.: Contributed intellectually and to experimental design, executed all experiments except Supplemental Figure S1.5, data analysis and presentation, and manuscript preparation.

Semack, A.C.: Contributed intellectually and executed experiments described in Supplemental Figure S1.5, edited manuscript.

Higashi, T.: Contributed intellectually and provided reagents, edited manuscript.

Miller, A.L.: Contributed intellectually and to experimental design, data analysis and presentation, and manuscript preparation, as well as provided the lab space and funding for the project.

I. Abstract

Localized activation of Rho GTPases is essential for multiple cellular functions, including

cytokinesis and formation and maintenance of cell-cell junctions. Although MgcRacGAP (Mgc) is

required for spatially confined RhoA-GTP at the equatorial cortex of dividing cells, both the

target specificity of Mgc's GAP activity and the involvement of phosphorylation of Mgc at serine

386 are controversial. Additionally, Mgc's function at cell-cell junctions remains unclear. Here, using gastrula-stage *Xenopus laevis* embryos as a model system, we examine Mgc's role in regulating localized RhoA-GTP and Rac1-GTP in the intact vertebrate epithelium. We show that Mgc's GAP activity spatially restricts accumulation of both RhoA-GTP and Rac1-GTP in epithelial cells – RhoA at the cleavage furrow and RhoA and Rac1 at cell-cell junctions. Phosphorylation at serine 386 does not switch the specificity of Mgc's GAP activity and is not required for successful cytokinesis. Furthermore, Mgc regulates adherens junction but not tight junction structure, and the ability to regulate adherens junctions is dependent on GAP activity and signaling via the RhoA pathway. Together, these results indicate that Mgc's GAP activity down-regulates the active populations of RhoA and Rac1 at localized regions of epithelial cells, and is necessary for successful cytokinesis and cell-cell junction structure.

II. Introduction

The fundamental importance of cytokinesis, the last step of cell division, is evident throughout life. Cytokinesis drives development and helps maintain adult tissues, while cytokinesis failure can promote birth defects, tumor formation, and tumor cell invasion[1,2,78]. Therefore, the mechanisms that regulate cytokinesis must be tightly regulated in space and time to ensure successful cell division[79]. An actomyosin-based contractile ring, which is templated by a microtubule-dependent equatorial zone of active RhoA (RhoA-GTP)[67], generates the force required to pinch a dividing cell in two. Specific guanine nucleotide exchange factors (GEFs) locally activate Rho GTPases (including RhoA, Rac1, and Cdc42) by driving them into the active GTP-bound state. GTPase activating proteins (GAPs) inactivate Rho GTPases by promoting GTP hydrolysis. The balance of local GEFs and GAPs precisely regulates the proper

spatial and temporal activation of Rho GTPases. Disruption of this tight regulation leads to severe cellular consequences. For example, misregulation of localized RhoA activity can lead to cytokinesis failure[15].

Centralspindlin, a complex of the kinesin MKLP1 (also called KIF23 in humans, ZEN-4 in *C. elegans,* and Pavarotti in *Drosophila*) and the GAP MgcRacGAP (Mgc; also called RACGAP1 in humans, CYK-4 in *C. elegans*, and RacGAP50C or tumbleweed in *Drosophila*), is a critical regulator of cytokinesis[18,19]. Centralspindlin accumulates on the scaffold of overlapping antiparallel microtubules that is formed at the cell equator, and contributes to bundling of the central spindle microtubules[18,80]. Centralspindlin recruits and concentrates the GEF Ect2 at the cell equator, where it locally activates RhoA[21–23].

The role of Ect2's GEF activity in activating RhoA at the equatorial cortex is well established; however, the target of Mgc's GAP activity remains controversial. For example, *in vitro* analysis of Mgc from *C. elegans* showed relatively low RhoA GAP activity and high Rac1 and Cdc42 GAP activity; however, based on RNAi results indicating that Rac1 and Cdc42 were not required for cytokinesis in *C. elegans*, it was proposed that Mgc functions to inactivate RhoA *in vivo* [18]. Consistent with this notion, we previously found that in the large blastomeres of early *Xenopus* embryos (Nieuwkoop and Faber stage 7-8) Mgc's GAP activity is important to mediate "GTPase flux", the rapid cycling of RhoA between the GTP- and GDP-bound forms in order to maintain a focused RhoA activity zone[14,15]. However, others have concluded that Mgc's GAP activity is directed toward Rac1 or Cdc42[18,26,52,70], or indirectly contributes to activation of RhoA[69]. Additionally, two studies reported that in specific cell types, Mgc's GAP activity is not required at all for cell division[81,82]. Further complicating matters, work in HeLa

cells reported that Aurora B phosphorylation of serine 386 (*Xenopus* numbering is used throughout; this residue is S387 in human) in Mgc's GAP domain could convert the *in vitro* specificity of Mgc's GAP activity from Rac1/Cdc42 to RhoA [27]. In contrast, recent work found that both recombinant Mgc protein and native Centralspindlin complexes immunoprecipitated from HeLa cells exhibited Rac1/Cdc42 GAP activity rather than RhoA GAP activity, and that GAP activity was not modulated by phosphorylation at S386[26]. These researchers also showed that Mgc is important for limiting equatorial Rac1 activity and cell-substrate adhesion at the division site in adherent cultured cells[26]. While there are varying results in the literature regarding MgcRacGAP's GAP specificity, the cellular context that gives rise to these results should be considered, and may provide an explanation for the differing conclusions.

Unlike adherent cultured cells, epithelial cells do not make strong cell-substrate adhesions. Instead, they exhibit apicobasal polarity and make adhesive cell-cell junctions, which must be maintained and remodeled during cytokinesis. In this cellular context, precise spatiotemporal regulation of RhoA GTPase activity is required both at the division site and for establishment and maintenance of cell-cell junctions[43,82–85]. Notably, the Centralspindlin complex was recently implicated in regulating cell-cell junctions[46,72]. In cultured epithelial cells, Mgc is localized not only at the central spindle but also at cell junctions[46,71,72]. Furthermore, Mgc appears to play a role in regulating junctional Rho GTPase signaling as well as the structure and function of cell-cell junctions[46,72]. However, it is unclear whether Mgc's GAP activity acts on RhoA and/or Rac1 at junctions or whether Mgc's GAP activity is required for regulating adherens junction (AJ) and/or tight junction (TJ) structure.

Here, we investigate the effects of perturbing Mgc's GAP activity during cytokinesis in *Xenopus laevis* embryonic epithelial cells (all experiments were done in gastrula-stage, Nieuwkoop and Faber stage 10-11, embryos unless otherwise stated). This approach allows us to monitor the *in vivo* dynamics of active populations of RhoA or Rac1 during cytokinesis and at cell-cell junctions by live imaging in a polarized intact epithelium. In experiments where endogenous Mgc was knocked down and replaced with wild type (WT) or mutant Mgc expressed at near endogenous levels, we test whether phosphorylation of Mgc serine 386 is required for successful cytokinesis. We show that phosphorylation at S386 is not required for cytokinesis *in vivo*; in fact, a phosphomimetic mutation of this residue phenocopies GAP dead Mgc. Using fluorescent probes for active RhoA and Rac1, we determine how Mgc's GAP activity regulates localized accumulation of RhoA-GTP, Rac1-GTP, and F-actin at the division site and at cell-cell junctions. We find that Mgc's GAP activity spatially restricts RhoA-GTP at the cleavage furrow and both RhoA-GTP and Rac1-GTP at junctions. Finally, we examine how misregulation of Mgc's GAP activity functionally affects cell-cell junction integrity. We demonstrate that Mgc's GAP activity is required to maintain proper adherens junction structure through the RhoA signaling pathway.

III. Results

MgcRacGAP's GAP activity is required for cytokinesis in *Xenopus* epithelia, but phosphorylation at serine 386 is not.

Mgc's GAP specificity was reported to be regulated by Aurora B phosphorylation during cytokinesis in HeLa cells[27]. To test whether phosphorylation of serine 386 is required for

cytokinesis in the context of the live, polarized epithelium of *Xenopus* embryos, we generated

non-phosphorylatable (MgcS386A) or phosphomimetic (MgcS386E) point mutants of Mgc, as

well as a GAP-dead point mutant (MgcR384A; *Xenopus* numbering is used; this residue is R385

in human) in which the catalytic arginine finger was mutated to alanine (Figures 1A and S1B).

Endogenous Mgc was knocked down with a morpholino oligonucleotide (MO) that targets the

5' UTR of Mgc[15] and replaced with near endogenous levels of WT or mutant Mgc by

microinjecting mRNAs that are MO-resistant (Figures 1A-D and S1A and C). The level of knock

down in cells that were verified to contain MO based on the presence of an injection marker

(farnesylated mCherry (mChe-membrane)) was evaluated by immunofluorescence in fixed

embryos. In control embryos, endogenous Mgc was localized at the ingressing cytokinetic

furrows and midbodies as well as at cell-cell junctions (Figure 1B). Upon MO knock down, Mgc

signal was significantly reduced at both the contractile ring and cell-cell junctions (Figure 1, C

and D). Importantly, each of the Mgc mutants localized appropriately in live *Xenopus* embryos

(Figure S1D). 3xGFP-tagged WT or mutant Mgc constructs were expressed in embryos where

endogenous Mgc was knocked down. The 3xGFP-tagged Mgc constructs localized to the

equatorial cortex and ingressing furrows during cytokinesis (Figure S1D) and to cell-cell

junctions when expressed at higher levels (data not shown). Additionally, we and others have

shown previously that mutations within Mgc's GAP domain do not interfere with its ability to

interact with MKLP1 in order to form the Centralspindlin complex[15,26].

We next used the knock down and replacement approach to test the effects of the Mgc

GAP domain mutants on cytokinesis. Embryos were injected with Mgc MO alone, MO+WT,

MO+S386A, MO+S386E, or MO+R384A along with GFP-membrane (farnesylated GFP) as an

injection marker, and were fixed and stained for nuclei (Figure 1E). Embryos where Mgc was

knocked down exhibited significant cytokinesis defects; 23% of cells were binucleate, and 22%

had 3 or more nuclei (Figure 1, E and F). Cells in Mgc MO-injected embryos were also

significantly larger than cells from control embryos, another indication of cytokinesis failure

(Figure 1, E and G). Knockdown and replacement with MgcWT rescued multinucleation and cell

width to near control levels (Figure 1, E-G). If phosphorylation at serine 386 is required for

successful cytokinesis as previously reported[27], we would expect that mutation of the serine to

a non-phosphorylatable alanine would cause cytokinesis failure. However, this was not the

case. Instead, replacement with MgcS386A had nearly identical effects to replacement with

MgcWT; only a minor fraction of cells were binucleate, and the cell width was similar to cells

expressing MgcWT. In contrast, replacement with a phosphomimetic mutant (S386E) led to

significantly increased multinucleation and cell size compared to replacement with MgcWT

(Figure 1, E-G). In fact, the phenotype from replacement with MgcS386E was very similar to the

effect of replacement with the MgcR384A GAP-dead mutant (Figure 1, E-G). Both MO+S386E

and MO+R384A rescue the Mgc MO phenotype of 3 or more nuclei to an intermediate extent.

This is likely due to Mgc's GAP-independent functions including recruiting the GEF Ect2[21–23] and

bundling central spindle microtubules[19]. However, there is still a significant difference in the

number of cells with 3 or more nuclei in MO+S386E and MO+R384A embryos compared to

MO+WT embryos (p= 0.004 and 0.0012, respectively) (Figure 1F). It was initially surprising that

MgcS386E phenocopies MgcR384A. However, consistent with this result, Bastos (2009)[26]

showed that an MgcS386D mutant exhibited decreased GAP activity in *in vitro* GTP hydrolysis

assays. Furthermore, the crystal structure of the GAP domain of human Mgc demonstrates that

32

the catalytic arginine finger residue, arginine 384, is in close proximity to serine 386[86].

Therefore, the negative charge imposed by the glutamic acid in our S386E mutant may interfere

with the catalytic activity of the arginine finger, resulting in a similar GAP-dead phenotype for

both R384A and S386E. Taken together, these data support the conclusion that

phosphorylation of serine 386 within Mgc's GAP domain is not required for successful

cytokinesis in the *Xenopus* epithelium.

Disruption of MgcRacGAP's GAP activity leads to cytokinesis delay or failure.

To investigate the nature of the cytokinesis failure observed in fixed embryos, we

carried out live imaging on embryos injected with a probe for F-actin (mChe-UtrCH)[87]. In

control cells, a strong, focused band of F-actin accumulates at the contractile ring (Figure 2A).

Similar to the immunofluorescence analysis (Figure 1, E-G), live imaging revealed that 55%

(16/29) of cells in embryos injected with Mgc MO failed cytokinesis (Figure 2B). These cells

exhibited weak F-actin accumulation at the contractile ring, consistent with Mgc's essential role

in recruiting the GEF Ect2 to activate RhoA and thus actin polymerization[21,88]. Replacement

with MgcWT restored normal furrow formation and F-actin accumulation (Figure 2, A and B).

Likewise, replacement with S386A rescued the defect observed in embryos injected with MO

alone, and F-actin accumulation appeared normal, further confirming that phosphorylation at

serine 386 is not required for cytokinesis *in vivo* (Figure 2, A and B). In contrast, replacement

with either S386E or R384A resulted in cells with a high percentage of furrow regression (Figure

2, A and B). In some cases, multiple F-actin contractile rings were observed for MO, MO+S386E,

and MO+R384A cells, indicating that these cells had failed one or more rounds of cytokinesis

resulting in multipolar spindles (Figures 2B and S2A). In MO, MO+S386E, and MO+R384A cells

that did manage to complete cytokinesis successfully, we noted that the cells displayed

significant increases in the duration of cytokinesis, from the appearance of the contractile ring

to completion of furrow ingression (Figure 2, C and D). For example, in MO+R384A cells, the

duration of cytokinesis averaged 792 ± 72 s compared to 364 ± 40 s for MO+WT. One potential

explanation for this result could be that the larger cell size of the MO, MO+S386E, and

MO+R384A cells leads to longer cytokinesis duration. However, consistent with Carvalho *et al.*,

(2009)[89], linear regression analysis on cell size and cytokinesis completion time demonstrated

that cell size did not correlate with duration of cytokinesis completion (R^2 values ranged from

0.06-0.24) (Figure S2B). Taken together, our live imaging data indicates that Mgc's GAP activity

is required for successful cytokinesis as well as proper spatiotemporal regulation of F-actin

accumulation at the contractile ring.

In epithelial cells, the equatorial RhoA-GTP zone is not focused when MgcRacGAP's GAP

activity is disrupted.

Disrupting Mgc's GAP activity prevents it from down-regulating active Rho GTPases. The

cytokinesis failures and abnormal F-actin accumulation observed in MO, MO+S386E, and

MO+R384A cells could be due to aberrantly increased RhoA-GTP, as we observed previously in

the large blastomeres of the early *Xenopus* embryo[15], or abnormally increased Rac1-GTP, as

observed previously in *C. elegans* embryos and adherent HeLa cells[26,70], or a combination of

both. To examine these possibilities, we first tested the effects of the Mgc GAP domain

mutants upon dynamic RhoA activity during cytokinesis in *Xenopus* epithelial cells.

In order to visualize the active, GTP-bound, populations of RhoA during cytokinesis, we

microinjected a fluorescent probe for RhoA-GTP (GFP-rGBD, the GTPase-binding domain of Rhotekin fused to GFP)[90]. The effects on RhoA-GTP and F-actin accumulation when Mgc was knocked down and replaced with the MgcWT or the Mgc GAP domain mutants were monitored in polarized epithelial cells.

In control cells, a focused zone of active RhoA forms at the cell equator following anaphase onset, and RhoA-GTP zones are present at cell-cell boundaries of dividing and non-dividing cells, as observed previously[15,45,46,67] (Figure 3A). When Mgc was knocked down or its GAP activity was disrupted, RhoA-GTP localization was perturbed at the cytokinetic furrow (Figure 3A). RhoA-GTP accumulation was also perturbed at cell-cell junctions (Figure 3A and see Figure 5 below). Mgc MO injection resulted in a significant reduction in the intensity of RhoA-GTP at the cleavage furrow during early ingression (Figure 3, A and B). The width of the RhoA-GTP zone was also significantly reduced in Mgc MO embryos compared to control embryos, although the width of F-actin in the contractile ring was unchanged (Figure 3, C and D). This effect on active RhoA is consistent with other reports showing that depletion of Mgc reduced the amount of active RhoA at the cell equator[15,22,64,69]. Replacement with MgcWT rescued the effects of the Mgc MO, restoring the equatorial RhoA activity zone intensity and the width of RhoA-GTP and F-actin nearly to control levels (Figure 3, A-D). If phosphorylation at serine 386 were required for Mgc to exhibit GAP activity toward RhoA, we would predict that the non-phosphorylatable (S386A) mutant would cause the RhoA activity zone to increase in intensity and/or breadth. However, no significant differences were observed in RhoA-GTP or F-actin accumulation between MO+MgcWT and MO+S386A cells, providing *in vivo* evidence that the phosphorylation of serine 386 is not required for Mgc to act as a RhoA GAP (Figure 3, A-D).

In contrast, in MO+S386E and MO+R384A embryos, we observed significant increases in the intensity of RhoA-GTP at the contractile ring, the width of the RhoA activity zone, and the width of F-actin at the contractile ring (Figure 3, A-D). To confirm that the MgcR384A phenotypes observed *in vivo* were due to the loss of GAP function, not to an unexpected effect caused by the loss of positive charge from the active site of the GAP domain, we tested an alternate GAP dead mutant, R384K, which does not alter the charge of the active site (Figure S3A)[91–94]. Similar to results with the R384A mutant, cells expressing MO+R384K also fail cytokinesis (Figure S3, B and D) and exhibit significantly increased RhoA-GTP intensity at the furrow (Figure S3, C and E). Collectively, our data provide evidence that despite *in vitro* data showing that Mgc displays GAP activity primarily toward Rac1 and Cdc42[18,26,52], in an intact epithelial environment, Mgc's GAP activity restricts active RhoA and F-actin accumulation at the division site.

Disruption of MgcRacGAP's GAP activity causes increased accumulation of Rac1-GTP at cell-cell junctions.

In adherent cultured cells, Mgc is also important for limiting equatorial Rac1 activity and cell-substrate adhesion in order to achieve successful cytokinesis[26]. Genetic data support the idea that Mgc's GAP activity promotes furrow ingression by down-regulating Rac1[70,95]. Since the cellular contexts where these studies were carried out represent different adhesive environments than those experienced by dividing cells in an epithelium where cell-cell adhesion prevails, we next examined the effects of the Mgc GAP domain mutants on dynamic Rac1 activity during cytokinesis in the intact epithelium.

In order to image Rac1-GTP dynamics, we used a fluorescent probe that reports the active, GTP-bound population of Rac1 (GFP-pGBD, the GTPase-binding domain of Pak fused to GFP)[15]. *In vitro* binding studies support the use of GFP-pGBD as a reporter for Rac1 activity. First, work identifying effector pathways for RhoA, Rac1, and Cdc42 in HeLa cells showed that Pak1 bound to Rac1 but not Cdc42 in biochemical assays[26]. Second, GST-pGBD selectively pulled down Rac1 but not Cdc42 from *Xenopus* tadpole lysates[96]. We monitored the effects on Rac1-GTP and F-actin accumulation when Mgc was knocked down and replaced with the MgcWT or the Mgc GAP domain mutants in epithelial cells. In control embryos, we did not observe accumulation of Rac1-GTP intensity at the equatorial cortex when compared to neighboring cortical regions during early ingression (Figure 4, A and B). However, Rac1-GTP was observed along cell-cell junctions in interphase and dividing cells, and it appeared at the division site during later stages of cytokinesis, where it is likely associated with the formation of nascent cell-cell junctions in the wake of the furrow[97,98] (Figure 4A). Injection of Mgc MO alone resulted in no increase in Rac1-GTP at the division site (Figure 4, A and B). Likewise, replacement with MgcWT or the GAP domain mutants caused no significant changes in the Rac1-GTP intensity at the cleavage furrow (Figure 4, A and B). Notably, there was no increase in localized Rac1-GTP signal at the cleavage furrow during early ingression when Mgc's GAP activity was disrupted (Figure 4, A and B). This is in contrast to findings in isolated adherent cells, which exhibit increased Rac1 activity in Mgc GAP-dead cells, leading to abnormal cell-substrate adhesion[26], and suggests that in epithelial cells, Mgc's primary target at the division site is not Rac1.

We next analyzed active Rac1 accumulation at cell-cell junctions when Mgc's GAP domain was perturbed. In control embryos, Rac1-GTP localized at cell-cell junctions (Figure 4A). Mgc MO embryos exhibited a significant increase in the intensity of active Rac1 at cell-cell junctions, both at bicellular junctions and at vertices where three cells come together when compared with control embryos (Figure 4, A and C-E). Replacement with MgcWT or MgcS386A rescued the effects of the Mgc MO, restoring the Rac1-GTP activity to control levels at cell-cell junctions (Figure 4A and C-E). In contrast, in MO+S386E and MO+R384A embryos, there were significant increases in Rac1-GTP accumulation at cell-cell junctions, when compared with control or MgcWT embryos (Figure 4, A and C-E). Indeed, quantification demonstrated that the Rac1-GTP signal at junctions in MO, MO+S386E, and MO+R384A embryos was significantly increased in intensity and breadth (measured by full width at half max) compared with control, MO+WT, or MO+S386A embryos (Figure 4, C-E).

To demonstrate that the signal we observed with the GFP-pGBD probe in live *Xenopus* embryos was specific to Rac1-GTP not Cdc42-GTP, we co-injected the GFP-pGBD probe with a probe for the GTP-bound population of Cdc42 (mRFP, the GTPase-binding domain of N-WASP fused to mRFP)[90] (Figure S4A). We quantified the accumulation of the probes in control, MO+MgcWT and MO+R384A embryos and found that GFP-pGBD intensity at cell-cell junctions was increased by nearly 2-fold in MO+R384A cells compared to control or MO+MgcWT cells (Figure S4B). In contrast, there was no increase in mRFP-wGBD intensity in MO+R384A cells (Figure S4C). The mRFP-wGBD probe can, however, efficiently detect Cdc42-GTP when Cdc42 is activated around plasma membrane wounds, which are generated by laser irradiation in gastrula-stage embryos (Figure S4, D-F). Taken together, the negligible mRFP-wGBD signal

increase at cell-cell junctions when MgcRacGAP's GAP activity is disrupted allows us to conclude that the signal detected by the GFP-pGBD probe reflects primarily Rac1-GTP. However, we cannot rule out the possibility that the GFP-pGBD probe may detect Cdc42-GTP in some cellular contexts.

To complement the knock down and replacement findings described above, we overexpressed MgcWT or the Mgc GAP domain mutants and imaged the accumulation of Rac1-GTP and F-actin at an earlier point in development (Nieuwkoop and Faber stage 6-8) (Figure S5, A-C). We observed no difference in Rac1-GTP accumulation at junctions in MgcWT or MgcS386A overexpression cells when compared with control cells (Figure S5, A and B). However, we observed a significant increase in Rac1-GTP at bicellular junctions and cell vertices in embryos where MgcS386E or MgcR384A were overexpressed compared to control or MgcWT embryos (Figure S5, A-C). Taken together, the knock down and replacement and overexpression studies indicate that Mgc's GAP activity is required to restrict active Rac1 accumulation at cell-cell junctions in epithelial cells.

RhoA-GTP but not Rac1-GTP co-accumulates with dynamic F-actin-rich accumulations at cell-cell junctions when MgcRacGAP's GAP activity is disrupted.

We observed ectopic F-actin accumulations at cell-cell junctions when Mgc's GAP activity was disrupted (Figure 2A). These F-actin-rich accumulations are significantly increased in frequency in MO+R384A embryos compared with MO+MgcWT embryos (7 ± 1.1% MO+R384A vs. 1 ± 0.2% MO+MgcWT cells per minute displayed F-actin-rich accumulations) (Figure 5A). We sought to identify the upstream signal promoting these ectopic F-actin

accumulations. Two possible explanations are that they could be due to aberrantly increased

RhoA-GTP promoting actin polymerization through formins or that they could be due to

abnormally increased Rac1-GTP promoting actin polymerization through Arp2/3. Co-imaging of

F-actin and probes for active RhoA or active Rac1 revealed that RhoA-GTP co-accumulated with

the dynamic F-actin-rich structures (Figures 5, B-D and S6A). In contrast, Rac1-GTP does not

significantly co-accumulate with F-actin-rich junctional accumulations (Figures 5, E-G and S6B).

These results suggest that the ectopic F-actin-rich junctional accumulations in cells expressing

GAP-dead Mgc may be RhoA-dependent.

MgcRacGAP's GAP activity is required for proper adherens junction structure in the intact

epithelium.

Because disrupting Mgc's GAP activity led to misregulation of RhoA-GTP, Rac1-GTP, and

F-actin at cell-cell junctions, we next sought to investigate whether Mgc's GAP activity is

required for proper junctional structure. It was recently shown that Mgc localizes to cell-cell

junctions in cultured epithelial cells where it appears to play a role in regulating both tight

junctions (TJs) and adherens junctions (AJs)[46,72]. One study found that Mgc was recruited to AJs

by interacting with α-catenin[46]. In contrast, another study showed that Mgc was localized to

TJs via binding to cingulin, a component of TJs, and paracingulin, a component of both TJs and

AJs[72]. We examined Mgc's localization at cell-cell junctions in the intact *Xenopus* epithelium.

Mgc is enriched at the apical cell-cell junctions (Figure 1) and overlaps significantly with E-

cadherin (an AJ transmembrane protein; Figure 6A) and partially with the basal portion of ZO-1

(a TJ plaque protein; Figure 6B), indicating that Mgc may localize at the interface between the

TJ and the AJ. Mgc is also more weakly localized along the basolateral surface, partially

overlapping with lateral E-cadherin signal (Figure 6A).

It is currently uncertain whether Mgc is required for regulating TJ and/or AJ structure.

RhoA and Rac1 play important roles in regulating cell-cell junction formation, maintenance,

structure and function[43,83–85,99] Since we showed that disrupting Mgc's GAP activity leads to

misregulation of both Rac1 (Figure 4) and RhoA (Figure 5) activity at cell-cell junctions, we next

tested whether disrupting Mgc's GAP activity affects junction structure. First we examined AJs

in fixed *Xenopus* epithelial cells. β-catenin was apically enriched at AJs in controls (Figures 6, C

and D and S8A). However, in Mgc MO embryos, β-catenin was randomly localized along the

basolateral surface, and cells were often apically domed (Figure 6, C and D). Re-expression of

MgcWT efficiently rescued the β-catenin defect (Figure 6, C and D). Importantly, re-expression

of MgcR384A did not rescue, and β-catenin was concentrated at ectopic positions along the

basolateral surface rather than polarized at the AJ (Figures 6, C and D and S8B). These data

indicate that Mgc's GAP activity is required for proper AJ structure.

We demonstrated that RhoA-GTP co-accumulates with ectopic F-actin-rich structures at

cell-cell junctions when Mgc's GAP activity is disrupted (Figure 5), suggesting that these

structures might be RhoA-dependent. If the effects of Mgc on AJs were mediated through

RhoA, we would predict that co-expression of dominant negative (DN) RhoA in MO+R384A

embryos would rescue the AJ defects observed when Mgc's GAP activity is disrupted. Indeed,

we observed that co-expression of DN RhoA with MO+R384A partially rescued the AJ defect

(Figure 6, C and D), while expression of DN Rho alone led to AJ defects similar to MO or

MO+R384A treatment (Figure 6, C and D). In contrast, expression of DN Rac did not suppress

the junctional defects observed when Mgc's GAP activity was disrupted in MO+R384A embryos

(Figure S7, A and B). These results support a model where Mgc's GAP activity regulates the

structure of AJs through modulating RhoA-GTP signaling.

To further confirm the effects of Mgc's GAP activity on maintaining the structure of AJs,

we tested the effects of Mgc perturbations on E-cadherin, an AJ transmembrane protein. We

used live imaging and a mosaic injection strategy where all cells expressed E-cadherin-3xmChe,

and mosaic clones of cells expressed a lineage tracer (GFP-membrane) with or without the MO

or MO+Mgc replacement constructs. In control embryos and control regions of mosaic

embryos (yellow arrowheads), E-cadherin was enriched at the AJs with some localization

extending along the lateral membrane (Figures 6, E and F and S8E). Mgc MO embryos exhibited

a significant reduction in the intensity of E-cadherin, and this defect was rescued by expression

of MgcWT (Figure 6, E and F; red arrowheads). Importantly, MO+R384A embryos showed

defects in E-cadherin signal intensity similar to the MO embryos (Figure 6, E and F; red

arrowheads). These data, together with the β-catenin studies, indicate that Mgc's GAP activity

is important for regulating AJ structure. Our study extends previous work, which identified Mgc

as a regulator of AJs [46,100], by revealing the novel function of Mgc's GAP activity in regulating AJ

structure.

MgcRacGAP does not regulate tight junction structure in the intact epithelium.

RhoA and Rac1 also play important roles in regulating TJ structure and function[84,101].

Mgc was reported to be recruited to TJs by cingulin and paracingulin and to be involved in

regulating TJ barrier formation during junction assembly in MDCK cells during calcium switch experiments[72]. Therefore, we next examined whether disrupting Mgc affects TJ structure by analyzing effects on the TJ proteins claudin (a TJ transmembrane protein) and ZO-1 (a TJ plaque protein). Embryos were injected to generate mosaic regions where internal control cells (yellow arrowheads) are located next to cells expressing a lineage tracer (GFP-membrane) alone or with Mgc MO (red arrowheads). In control cells, claudin was concentrated at the TJ (Figures 7, A and B and S8C). In mosaic regions where Mgc was knocked down with the MO, claudin signal appeared nearly identical in intensity and apicobasal polarity to controls, even in large cells that had failed multiple rounds of cytokinesis (Figures 7, A and B and S8D). We also stained mosaic embryos for ZO-1. Again, we observed no defect in the junctional accumulation of ZO-1 in mosaic regions where the Mgc MO was delivered (Figures 7, C and D and S8F). These data suggest that Mgc is not required for proper TJ structure in the steady state intact epithelium.

IV. Discussion

We used the intact vertebrate epithelium of *Xenopus laevis* embryos to investigate Mgc's role in regulating localized Rho GTPase activity. We show that Mgc's GAP activity spatially restricts accumulation of RhoA-GTP and Rac1-GTP in epithelial cells by down-regulating active RhoA at the cytokinetic furrow and both active RhoA and Rac1 at cell-cell junctions. We demonstrate that Mgc's GAP activity is required for successful cytokinesis, but phosphorylation at serine 386 is not required. When Mgc's GAP activity was disrupted, we observed an increase in Rac1-GTP and RhoA-GTP at cell-cell junctions along with dynamic F-actin rich accumulations that colocalize with RhoA-GTP. Finally, we show that Mgc's GAP activity acts through RhoA to

43

regulate proper AJ structure, but is not required for TJ structure. Together, these results indicate that Mgc's GAP activity is necessary to down-regulate the active populations of both RhoA and Rac1 at localized regions of epithelial cells, and this is required for successful cytokinesis and cell-cell junction structure and function (Figure 8).

Phosphorylation at serine 386 does not switch the specificity of MgcRacGAP.

It was reported that the isolated GAP domain of Mgc exhibits GAP activity primarily to Rac1 and Cdc42 and that phosphorylation of S386 by Aurora B kinase confers GAP activity toward RhoA [27]. Our data provide *in vivo* evidence supporting the conclusion that phosphorylation of MgcS386 does not switch Mgc's GAP specificity and is not required for successful cytokinesis. If phosphorylation at this site was important for Mgc's GAP activity towards RhoA, a non-phosphorylatable mutant (MgcS386A) would be predicted to cause abnormally increased RhoA-GTP accumulation. However, when endogenous Mgc was knocked down and replaced with MgcS386A, the cells exhibited normal RhoA-GTP accumulation and normal cytokinesis. Additionally, our results raise the possibility that constitutive phosphorylation of S386 would disrupt cytokinesis and AJ structure, as a phosphomimetic mutant (MgcS386E) phenocopied the GAP-dead point mutant. MgcS386 is conserved in multiple species and is located two amino acids away from MgcR384, the conserved "arginine finger" residue that is essential for GAP activity (Figure S1B). Both residues reside at the interface between the GAP and the GTPase[91,102]. The placement of the serine residue with respect to the arginine finger is also conserved in some other Rho family GAPs; however, phosphorylation at this site is not required for these GAPs to bind RhoA[26]. Additionally, Bastos *et al.* demonstrated that Mgc's *in vitro* GAP specificity was not modulated by phosphorylation

at S386 for either recombinant Mgc protein or native Centralspindlin complexes immunoprecipitated from HeLa cells[26]. Our studies support and extend these findings by providing *in vivo* data characterizing the effects of mutating S386 on the localized activity of RhoA and Rac1 in the intact epithelium.

In vivo GTPase targets of MgcRacGAP's GAP activity.

Previous studies using diverse systems and approaches have led to conflicting conclusions regarding the specificity of Mgc's GAP activity toward RhoA and/or Rac1[15,26,27,69,70]. RhoA is the primary Rho GTPase required for cytokinesis[18,103,104]. Our previous work in the large cells of blastula-stage *Xenopus* embryos showed that expression of MgcR384A results in abnormally broad RhoA activity zones and failed cytokinesis, supporting a role for Mgc in negatively regulating RhoA activity[15]. Further, mathematical modeling suggested that the GAP activity required to focus the RhoA activity zone is localized at the cell equator, not globally[68]. However, *in vitro* GAP assays indicate that Mgc exhibits efficient GAP activity toward Rac1 and Cdc42 but little GAP activity toward RhoA[18,26,27,52]. Genetic studies in one-cell *C. elegans* embryos[70] and *Drosophila* imaginal discs[95] showed that Rac1 inhibition can partially suppress the effects of disrupting Mgc's GAP activity on cytokinesis. Additionally, in adherent mammalian cultured cells, Rac1 signal is reduced at the cell equator in control cells[105], but when GAP-dead Mgc is expressed, excess activated Rac1 accumulates at the cell equator, promoting increased cell-substrate adhesion, which antagonizes furrowing[26,106].

Our data supports the conclusion that in the physiologically relevant context of the intact vertebrate epithelium, Mgc can down-regulate both RhoA and Rac1 – RhoA at the

cleavage furrow and both RhoA and Rac1 at junctions. There may be a number of reasons for the conflicting findings in different experimental contexts. First, many of the key regulators of *in vivo* GAP activity are lacking in *in vitro* GAP assays including the lipid bilayer, prenylation of Rho GTPases, and Rho guanine nucleotide dissociation inhibitors (GDIs)[107–110]. For example, phospholipid binding to the C1 domain of β2-chimaerin activates its GAP activity[109], and interaction of p190RhoGAP with phospholipids can switch its substrate specificity from RhoA to Rac1[111]. Second, the co-localization of Mgc and RhoA-GTP at the cell equator may increase Mgc's efficiency as a RhoA GAP by facilitating access of Mgc to RhoA as a substrate. Third, the relative importance of different Rho GTPases and their regulators may differ in diverse cellular environments including HeLa cells, one-cell *C. elegans* embryos, poorly adherent cells, or epithelial cells. For example, cells of the gastrula-stage *Xenopus* embryo are of a similar size to HeLa cells but cell-cell junctions with their neighbors prevail rather than the strong cell-substrate adhesions prominent in HeLa cells.

Although our data are consistent with a role for Mgc's GAP activity in down-regulating both Rac1 and RhoA *in vivo*, alternative explanations warrant future study. It is possible that Mgc may act indirectly on RhoA via crosstalk of Rho GTPases. Antagonism between Rac1 and RhoA has been described[99,112]. If Mgc primarily suppresses Rac1, antagonism would result in Mgc indirectly increasing RhoA. However, our results would imply a mechanism of GTPase crosstalk that is distinct from this mechanism, as both RhoA-GTP and Rac1-GTP increase at junctions when Mgc's GAP activity is disrupted. Additional GAPs, such as p190RhoGAP[113,114] and MP-GAP[115] that act locally and/or globally could also be involved in regulating the spatiotemporal dynamics of RhoA-GTP.

MgcRacGAP's role at cell-cell junctions.

RhoA and Rac1 are important regulators of cell-cell junction assembly and integrity[43,83–85,99]. We demonstrate that, in agreement with previous findings in cultured cells[46,72], Mgc is localized to cell-cell junctions in both dividing and interphase cells in the *Xenopus* epithelium. Specifically, we find that Mgc is localized at the interface between the TJ and AJ, partially overlapping with each type of junction. Importantly, we demonstrate that Mgc's GAP activity is required for proper AJ structure. Expression of DN RhoA rescues the MgcR384A AJ phenotype, suggesting that the effect is due to unrestricted accumulation of RhoA-GTP. Interestingly, in contrast to the findings of Guillemot *et al.,* which showed that Mgc regulates the formation of the TJ barrier during TJ assembly[72], Mgc does not appear to regulate TJ structure in our system. While we cannot exclude the possibility that residual Mgc present in the Mgc knock down embryos can still support TJ structure, we think this explanation is unlikely, as the fixed staining for Mgc showed a severe knock down at the cellular level, and this same level of knock down was sufficient to disrupt AJs. One possible explanation for these conflicting findings is that Guillemot et al. used the calcium switch model to examine new junction formation, whereas we examined junctions at steady state in an intact epithelium.

In summary, studying Mgc's role in regulating localized Rho GTPase activation in *Xenopus* embryos has provided novel information about how this GAP spatially restricts the accumulation of both RhoA-GTP and Rac1-GTP in intact vertebrate epithelial cells. Our results highlight the possibility that Mgc's primary Rho GTPase target may differ depending on the adhesive environment of the cell.

V. Materials and methods

DNA constructs, mRNA preparation, and MgcRacGAP morpholino. *Xenopus* Mgc constructs including the R384A point mutant and the 3xGFP-tagged construct were described previously[15]. MgcS386A, MgcR384K, and MgcS386E mutants were generated by QuikChange (Stratagene) site-directed mutagenesis. A *Xenopus* E-cadherin construct was kindly provided by Dr. Pierre McCrea (University of Texas, MD Anderson Cancer Center). E-cadherin-3xmChe was generated by PCR amplifying the E-cadherin sequence and ligating it into the ClaI and XbaI sites in pCS2+/C-3XmChe. All constructs were confirmed by sequencing. The pCS2+/GFP-rGBD (probe for active Rho), pCS2+/GFP-pGBD (probe for active Rac), and pCS2+/mRFP-wGBD (probe for active Cdc42) probes were described previously[15,90]. The pCS2+/mChe-UtrCH (probe for F-actin)[87], pCS2+/mChe-H2B (probe for DNA)[45], pCS2+/mChe-membrane and pCS2+/GFP-membrane[45], and pCS2+/2XmChe-EMTB, (probe for microtubules)[116] were all described previously. pCS2+/DN Rho and pCS2+/DN Rac were kindly provided by Dr. Tim Gomez (University of Wisconsin-Madison). mRNAs were transcribed *in vitro* using an mMessage mMachine SP6 kit (Ambion). The Mgc 5' UTR MO, which was designed to target both alloalleles of *Xenopus* Mgc, was described previously[15].

Antibodies. The anti-*Xenopus* Mgc antibody was described previously (Miller and Bement, 2009). Other antibodies used were anti-mCherry (Abcam, Ab125096 [mouse] and Ab167453 [rabbit]), anti-GFP (Clontech, 632381 [mouse] and Invitrogen, A-6455 [rabbit]), anti-α-tubulin (DM1A, Sigma, T9026), anti-β-catenin (Abcam, Ab2365), anti-E-cadherin (DSHB, 5D3-c), anti-claudin-5 (Abcam, Ab53765; note that the anti-claudin-5 antibody may cross-react with other claudins so we have referred to it simply as "anti-claudin" in the text and figures), and anti-ZO-1

(Invitrogen, 61-7300 [Rabbit]). The mouse anti-ZO-1 antibody was a generous gift from Dr.

Masahiko Itoh (Dokkyo Medical University, Japan). Secondary antibodies used for

immunostaining were Alexa 488- or Alexa 568-conjugated anti-mouse or anti-rabbit

(Invitrogen). Secondary antibodies used for Western blotting were HRP-conjugated anti-rabbit

or anti-mouse (Promega).

***Xenopus* embryos and microinjection.** All studies conducted using *Xenopus* embryos strictly

adhere to the compliance standards of the US Department of Health and Human Services Guide

for the Care and Use of Laboratory Animals and were also approved by the University of

Michigan Committee on Use and Care of Animals. *Xenopus* embryos were collected, *in vitro*

fertilized, and de-jellied using methods described previously[15,117]. Embryos were stored at

different temperatures prior to injections to prolong the 2-cell or 4-cell stages (room temp.,

15°C or 17°C), then stored at 15°C in 0.1X MMR (Mark's Modified Ringer solution, 1X=100 mM

NaCl, 2 mM KCl, 2 mM $CaCl_2$, 1 mM $MgCl_2$, 5 mM Hepes, pH 7.4). Embryos were microinjected

as described previously (Reyes et al., 2014). For knock down and replacement experiments, all

four cells at the 4-cell stage were first injected with 5 nl of mRNA for indicated fluorescent

probes (see below); then, all four cells were injected again with 5 nl of a mixture of MO (4.5

mM needle concentration), Mgc rescue construct (0.6 µg/ml needle concentration), and a

fluorescent lineage tracer (see below), then placed at 15°C for ~24 hours until they reached

gastrulation (Nieuwkoop and Faber stage 10-11). For overexpression experiments, embryos

were injected at either the 2-cell or the 4-cell stage with 5 nl of Mgc WT or mutants (1.66 µg/ml

needle concentration) and allowed to develop to blastula-stage (Nieuwkoop and Faber stage 6-

8). Needle concentrations for other mRNAs were as follows: Mgc-3xGFPs (1 µg/ml), GFP-rGBD

(25 µg/ml), GFP-pGBD (15.6 µg/ml for gastrula, or 0.25 mg/ml for blastula imaging), mRFP-wGBD (15.6 µg/ml), mChe-membrane (10 µg/ml), GFP-membrane (10 µg/ml), mChe-H2B (20 µg/ml), mChe-UtrCH (10 µg/ml for gastrula, or 0.71 mg/ml for blastula imaging), DN RhoA (0.48 µg/ml), DN Rac1 (0.6 ug/ml), E-Cad-3xmChe (8 µg/ml).

Embryo lysates and immunoblotting. Gastrula-stage embryos (Nieuwkoop and Faber stage 10-11) were lysed as previously described[45] with the following modifications: lysis buffer volume was 2.5 µl per embryo, and PHEME lysis buffer did not include detergent. Samples were separated on 10% SDS-PAGE gels and transferred to nitrocellulose membranes. Membranes were probed with anti-Mgc (1:5000) or anti-β-tubulin (1:20,000) overnight at 4°C in 1X TBST (0.1% Tween-20), pH 5.0 with 5% non-fat dry milk. HRP-conjugated secondary antibodies were applied at 1:5000 (for Mgc) or 1:10,000 for (β-tubulin). Membranes were developed using an ECL detection kit (Pierce, 32209).

Immunostaining.

Staining for endogenous Mgc. Albino embryos were injected with mChe-membrane as a lineage tracer with or without the Mgc 5' UTR MO (4.5 mM needle concentration). Embryos were fixed at gastrulation by the trichloroacetic acid (TCA) protocol described in Le Page et al. and Reyes et al.[45,118], with the following changes: embryos were permeabilized in 1X PBST (2% Triton-X-100) for 20 min at room temperature, then blocked in PBST with 5% fetal bovine serum (Invitrogen, 10082-139) for 2-3 hours at room temperature. Primary antibodies used were anti-Mgc (1:600), anti-E-cad (1:200), anti-ZO-1 (mouse; 1:300), and anti-mChe (1:200). Embryos were stained with 10 µg/ml DAPI (Invitrogen, D1306) in PBST for 30 min at room

temperature, and mounted in Vectashield mounting medium (Vector Laboratories, H-1000).

Staining for β-catenin for Mgc knock down and replacement. Embryos were injected as described above, except the linage tracer was GFP-membrane. Embryos were fixed overnight with a paraformaldehyde/glutaraldehyde-based fixative following the protocol in Reyes et al.[45]. Primary antibodies were anti-β-catenin (1:200) and anti-GFP (1:200). Embryos were mounted in Murray's Clear for imaging.

Staining for claudin and ZO-1. Embryos were injected as described above using GFP-membrane or mChe-membrane as a lineage tracer. Embryos were fixed for 2 hours in 2% trichloroacetic acid following the protocol in Reyes et al.[45] except the secondary antibody was applied for 4 hours at room temperature. Primary antibodies were rabbit anti-ZO-1 (1:200), anti-claudin-5 (1:50), anti-GFP (1:200), or anti-mChe (1:200). Embryos were mounted in Vectashield for imaging.

Live and fixed confocal microscopy. Fluorescent confocal images were collected on an inverted Olympus Fluoview 1000 microscope equipped with a 60X supercorrected PLAPON 60XOSC objective (NA = 1.4, working distance = 0.12 mm) and FV10-ASW software. Live and fixed imaging was carried out as described previously[45].

Live cell wounding. Embryos were injected into four cells at the 4-cell stage with a probe for active Cdc42 (mRFP-wGBD) and incubated at 15°C for 20 hours (Nieuwkoop and Faber stage 9.5-10). Images were collected using an Olympus Fluoview 1000 microscope equipped with an auxiliary SIM scanner. Laser wounds were generated using the 405 nm SIM laser line at 37%

power for 300 ms through a 60x objective. Single plane movies were obtained before, during, and after the wound in order to capture the wound healing response.

Quantification and analysis.

Western blot intensity analysis: FIJI was used to quantify band intensity of each band from two independent anti-Mgc Western blots. The quantification was normalized to control Mgc levels.

Quantification of Mgc intensity in fixed cells. To measure Mgc intensity at the contractile ring, three circular ROI's (2.5 μm diameter) were placed along the cleavage furrow (in the center of the furrow and to the right and left of center) at ~ 50% ingression using Volocity. For normalization, a background ROI of the same size was placed outside the cleavage furrow in the same cell and subtracted from the averaged cleavage furrow intensity value. The intensity value for control embryos was set to one, and the intensity value for Mgc MO embryos was normalized to control. To measure Mgc intensity at cell-cell junctions, a line of 4 μm X 18 μm was drawn perpendicular to a cell-cell junction using ImageJ. The line was centered on the junction. Two lines were drawn per cell and the average intensity for each point along the line was determined. The intensity values for each cell were normalized to background intensity by averaging the first five and last five data points of the line and subtracting this value from the averaged line scans. The intensity value for control embryos was set to one, and the intensity value for Mgc MO embryos was normalized to control.

Cell width and percent multinucleation measurements. Using Volocity, the width of each cell was measured vertically and horizontally across the cell and averaged. The percent multinucleation was determined by counting the number of cells per 230 μm x 230 μm image.

The DAPI channel was used to count how many cells displayed a single nucleus, 2 nuclei, or 3 or more nuclei by scanning through the volume of the cell; only cells where nuclei could be clearly observed were included in the analysis.

Quantification of cytokinesis failure in live cells. Cytokinesis failure events were determined by observing cytokinesis in live cell movies from embryos injected with either a probe for RhoA-GTP or Rac1-GTP along with mChe-UtrCH. A cell was determined to have failed cytokinesis if the contractile ring regressed at any point during cytokinesis.

Quantification of cytokinesis duration. The duration of cleavage furrow ingression was only recorded for cells that completed cytokinesis successfully. The start of cytokinesis was defined as when the F-actin contractile ring was first visible at the equatorial cortex. The end of cytokinesis was determined by the time at which the cleavage furrow had fully ingressed and cortical F-actin signal was separated between the two daughter cells.

Quantification of RhoA-GTP or Rac1-GTP intensity at the cleavage furrow. Three separate circular ROI's (2.5 µm in diameter) were placed along the cleavage furrow (middle of zone, right and left side of zone) at ~25% ingression (early cytokinesis) using Volocity. For Rac1-GTP data analysis, the site of the cleavage furrow was determined via the F-actin channel, then intensity measurements were made of Rac1-GTP signal at the identified locations. The data was normalized by placing a background ROI of the same size at a region adjacent to the cleavage furrow for each cell. The background ROI was subtracted from the averaged cleavage furrow intensity for each cell included in the analysis.

Measurements of RhoA-GTP and F-actin zone widths. The width of each cell was measured,

then three separate measurements were taken across the width of the RhoA-GTP or F-actin

zone (middle of zone, right and left side of zone) and averaged. All measurements were made

in Volocity. The widths were normalized by calculating the ratio of the RhoA-GTP or F-actin

zone to cell width. Early cytokinesis measurements were taken at approximately 25% cleavage

furrow ingression, and late measurements were taken at approximately 75% cleavage furrow

ingression.

Rac1-GTP Intensity at cell vertices. The intensity of Rac1-GTP was measured in Volocity by

positioning a circular ROI of 13 µm diameter at cell vertices of dividing cells at 75% ingression. A

background ROI was positioned away from the cleavage furrow and cell-cell junctions. The data

were normalized to background fluorescence by subtracting the background measurement

from the cell vertices measurement for each cell.

Rac1-GTP line scans and full width at half max. A line of 4 µm X 18 µm was drawn

perpendicular to the cell-cell junctions of dividing cells during late cytokinesis using ImageJ. The

line was centered on the junction. Two lines were drawn per cell, and the average intensity for

each point along the line was determined. For dividing cells, the line was placed across cell-cell

junctions at polar regions of the cell to avoid the division site. The intensity values for each cell

were normalized to background intensity by averaging the first five and last five data points of

the line and subtracting this value from the averaged line scans. The Rac1-GTP junctional

intensity reflects the peak value of the line scan. The full width at half max was determined by

identifying the two points on the x axis (width values) that are associated with the line scan at

half of the maximum amplitude. The difference of the x values was calculated, and the full width at half max values were plotted in a scatter plot.

Quantification of F-actin, RhoA and Rac1 junctional accumulations. For kymographs, a rectangular ROI (25 µm x 10 µm) was cropped at the site of F-actin accumulations at cell-cell junctions. The cropped image was used to make montages of 20 frames (16 second time interval between frames) in ImageJ. Raw counts of F-actin accumulations were achieved by counting the number of F-actin-rich junctional accumulations that occur in a 500 s time interval in the top right quadrant of a 230 µm X 230 µm live movie. The total number of cells in the quadrant was counted for each embryo and used to determine the average percentage of F-actin-rich junctional accumulations that occur per cell per minute. Ten embryos were analyzed for each treatment group. The GTPase intensity at the site of an F-actin junctional accumulation was measured by identifying the location and timing of a junctional accumulation using the F-actin (red) channel, then active GTPase intensity was measured at the corresponding site and time in the green channel and plotted over time.

Intensity line scans of junctional proteins. Side views of fixed embryos were analyzed in ImageJ using the freehand line function with line width of 10 px. A line was drawn along the apical to basal axis of a cell-cell junction, and the corresponding intensity values were recorded. A background intensity line was drawn adjacent to each cell-cell junction. Normalization was achieved by subtracting the background intensity from the junction intensity for each cell-cell junction included in the analysis.

Statistical analysis. Unpaired Student's t-tests were used to determine statistical significance of

each group pairwise compared to either control or to MO+WT as indicated. Statistics were

calculated in GraphPad Prism software.

VI. Acknowledgements

*Department of Genetics, Cell Biology, & Development. University of Minnesota, College of Biological Science

†Department of Molecular, Cellular, and Developmental Biology, University of Michigan, Ann Arbor, MI 48109

Figure 1.1

A

MgcRacGAP

MgcS386A nonphosphorylatable

MgcS386E phosphomimetic

MgcR384A GAP dead

B

Control Dividing Cell
Internal plane   Apical plane   Apical

Mgc MO Dividing Cell
Internal plane   Apical plane   Apical

C

Mgc intensity at contractile ring (a.u.)

p<0.001
*

Control   MO

D

Mgc intensity across bicellular junctions (a.u.)

p<0.001
*

Control   MO

E

Control   MO   MO+WT

MO+S386A   MO+S386E   MO+R384A

nuclei
membrane

F

Multinucleation (%)

2 nuclei
3+ nuclei

Control   MO   MO+WT   MO+S386A   MO+S386E   MO+R384A

p-values

	MO	MO+WT	MO+S386A	MO+S386E	MO+R384A
MO, 2 nuclei	<0.0001	x	<0.0001	0.002	n.s.	n.s.
MO, 3+ nuclei	<0.0001	x	<0.0001	<0.0001	0.003	0.02
MO+WT, 2 nuclei	n.s.	<0.0001	x	n.s.	0.015	0.0008
MO+WT, 3+ nuclei	n.s.	<0.0001	x	n.s.	0.004	0.0012

G

Cell width (µm)

**   **   *
**

* = p<0.01
** = p<0.001

Control   MO   MO+WT   MO+S386A   MO+S386E   MO+R384A

58

Figure 1.1 MgcRacGAP localizes to cell-cell junctions, and Mgc MO, MO+MgcS386E, and MO+R384A cause cytokinesis defects. (A) Protein diagram of Mgc showing location of arginine 384 and serine 386 within the GAP domain as well as mutants used in this study. (B) Internal and apical plane en face views and side views of endogenous Mgc localization in fixed embryos injected with either mChe-membrane alone (top) or MO+mChe-membrane (bottom), then stained with an Mgc antibody. Red arrowheads indicate midbodies; red arrow indicates the contractile ring in control embryo; yellow arrow indicates attempted division site in MO embryo; yellow arrowheads indicate apical localization of endogenous Mgc at cell-cell junctions. Scale bars = 20 µm. (C) Normalized intensity of endogenous Mgc at the contractile ring in control or MO embryos during early ingression measured from embryos that were fixed and stained with an Mgc antibody. n = # cells, # embryos, # independent experiments: Control (10,7,4), MO (11,7,4). (D) Peak intensity determined from line scans measuring the normalized Mgc intensity across bicellular junctions. n = Control (20,5,4), MO (18,6,3). (E) Images of fixed embryos injected with MO or MO+MgcWT or GAP domain mutants. mChe-membrane marker (pseudocolored green) was used an injection marker, and embryos were stained with DAPI (pseudocolored red). Scale bars = 40 µm. (F) Quantification of the percentage of cells that display multinucleation. p-values from Student's t-tests were calculated from comparisons of MO cells with 2 nuclei or 3+ nuclei, pairwise to the respective nuclei group for each indicated construct. The same analysis was conducted for pairwise comparison of MO+WT with 2 nuclei or 3+nuclei to each indicated construct. n = Control (266,9,3), MO (184,9,6), MO+WT (275,9,6), MO+S386A (247,8,5), MO+S386E (275,7,5), MO+R384A (202,5,4). (G) Quantification of cell width. Graphed as box-and-whisker plot where whiskers represent the min and max values and the horizontal bar represents the median. n = Control (333,6,3), MO (120,9,3), MO+WT (208,8,3), MO+S386A (264,9,3), MO+S386E (207,7,3), MO+R384A (219,10,3). All error bars shown represent SEM unless otherwise noted.

Figure 1.2
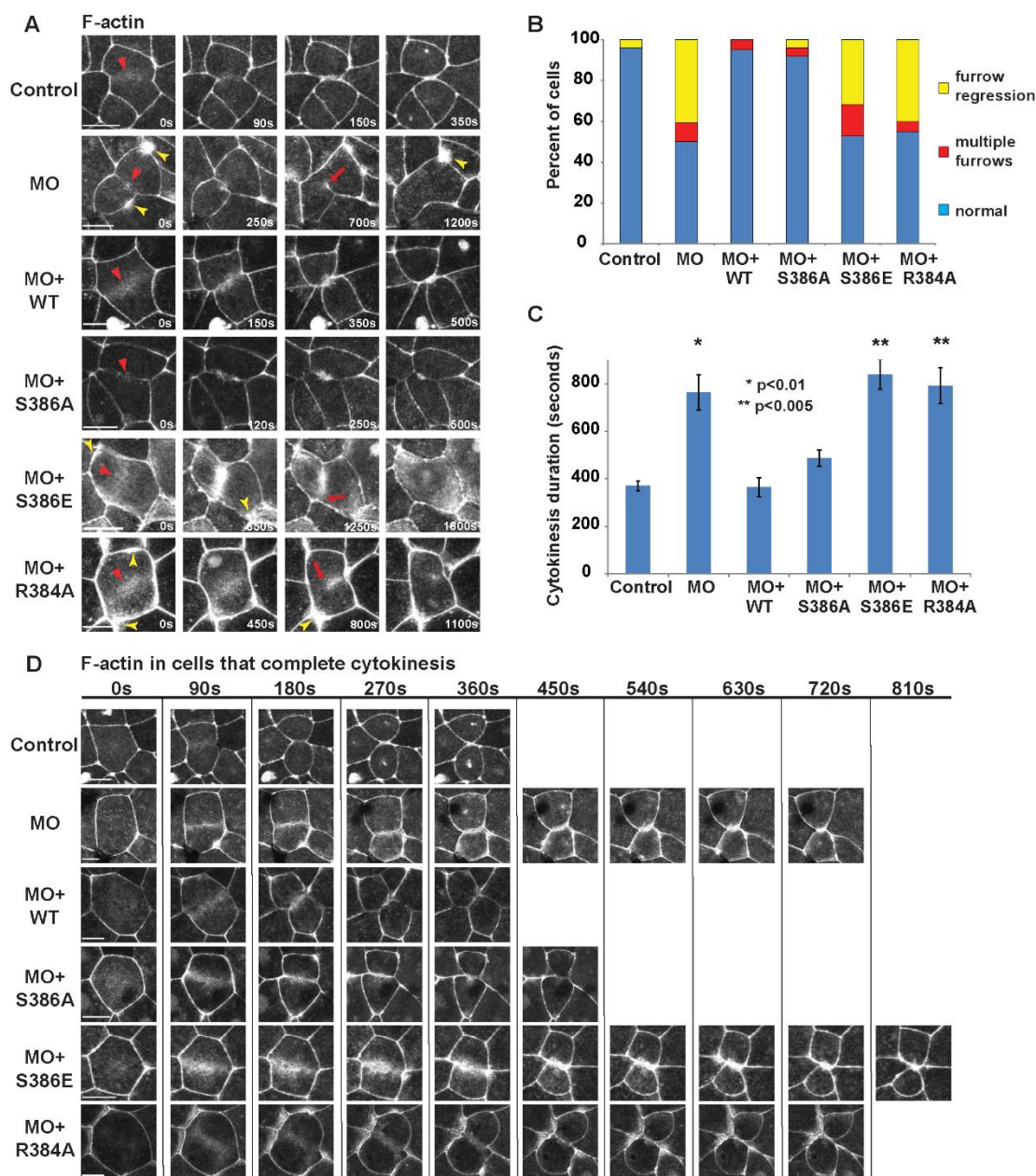
Figure 1.2 Mgc MO, MO+MgcS386E, and MO+MgcR384A cause cytokinesis failure and significant delays in cytokinesis completion *in vivo.* (A) Frames from time-lapse movies during cytokinesis. Embryos were co-injected with the indicated MO and rescue constructs along with mChe-UtrCH (F-actin probe) and mChe-H2B. Red arrowheads point to the contractile during early cytokinesis; red arrows indicate cleavage furrow regression; yellow arrowheads point to F-actin rich junctional protrusions. (B) Quantification of the outcome of cytokinesis, showing the percent of cells that complete cytokinesis normally, fail cytokinesis with cleavage furrow regression, or fail cytokinesis with formation of multiple cleavage furrows. n = # cells, # embryos, # independent experiments: Control (26,9,4), MO (29,8,4), MO+WT (20,7,4), MO+S386A (53,13,5), MO+S386E (48,12,5), MO+R384A (19,3,3). (C) Quantification of cytokinesis duration. Error bars represent SEM. P-values were calculated from pairwise comparison to MO+MgcWT. n = Control (20,7,5), MO (17,8,7), MO+WT (17,11,7), MO+S386A (22,12,5), MO+S386E (20,9,4), MO+R384A (20,9,4). (D) Frames from time-lapse movies of cells expressing mChe-UtrCH (F-actin probe) that do manage to complete cytokinesis successfully, show that the MO, MO+MgcS386E, and MO+MgcR384A cells display significantly longer cytokinesis duration compared to control or MO+MgcWT. All scale bars = 20 μm.

60
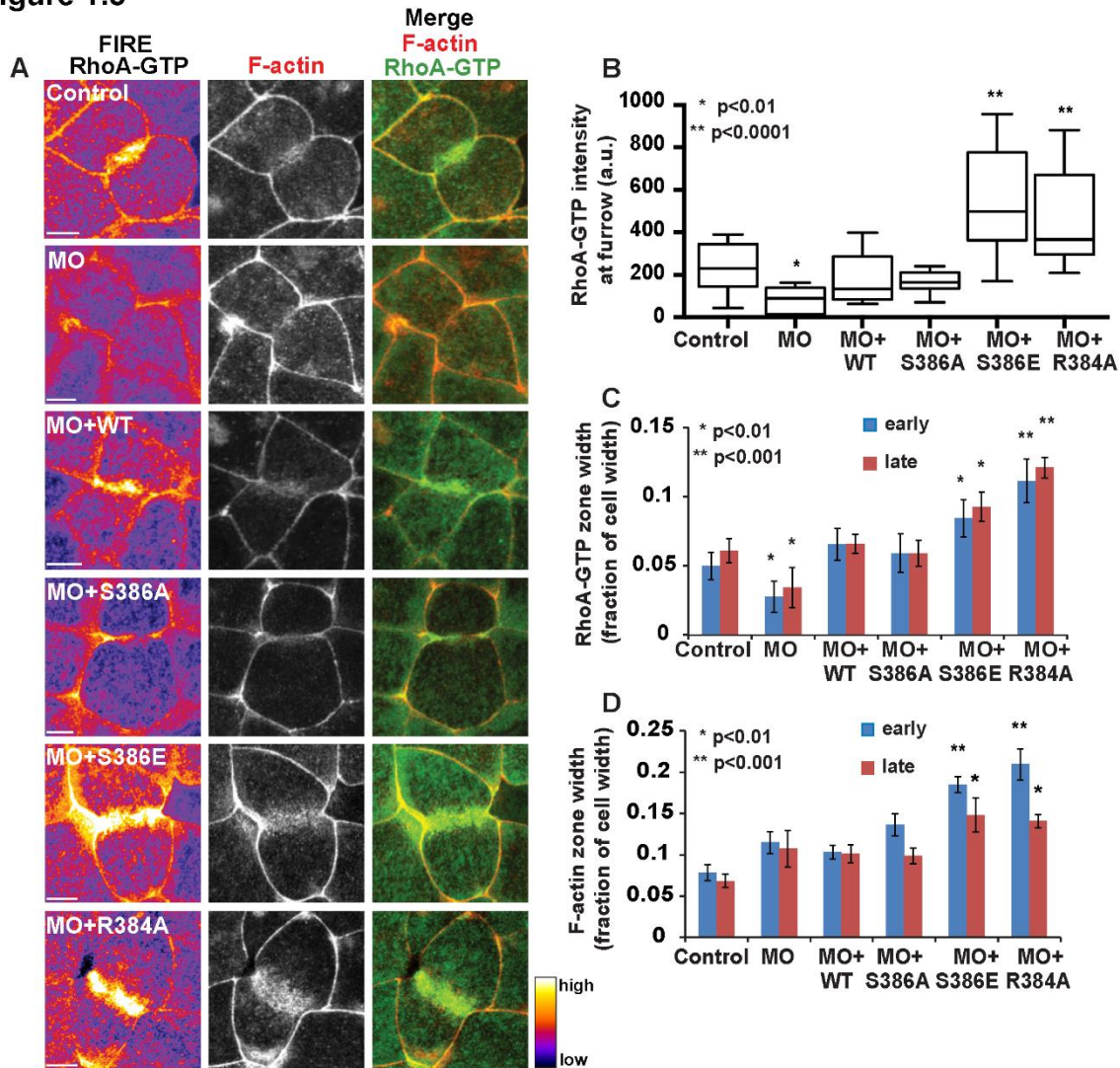
Figure 1.3

Figure 1.3 MO+MgcS386E and MO+MgcR384A embryos exhibit increased accumulation of RhoA-GTP and F-actin at the contractile ring in epithelial cells. (A) Images of cells during early cytokinesis (~25% ingression) from time-lapse movies showing the RhoA-GTP zone (GFP-rGBD), with a FIRE LUT applied to the RhoA-GTP channel, F-actin accumulation (mChe-UtrCH), and merge. Embryos were co-injected with indicated Mgc MO and rescue constructs. Scale bars = 20 μm. (B) Quantification of the normalized RhoA-GTP intensity at the cleavage furrow during early cytokinesis (~25% ingression) graphed as a box-and-whiskers plot where whiskers represent the min and max values and the horizontal bar represents the median. n = # cells, # embryos, # independent experiments: Control (14,3,2), MO (11,6,4), MO+WT (13,5,3), MO+S386A (10,6,3), MO+S386E (17,6,2), MO+R384A (18,5,3). (C) Quantification of the width of the RhoA-GTP zone as a fraction of overall cell width both early and late cytokinesis (~25% and 75% ingression, respectively). n = Control (7,4,3), MO (8,6,3), MO+WT (8,6,5), MO+S386A (11,8,3), MO+S386E (13,7,3), MO+R384A (12,5,2). (D) Quantification of the width of F-actin accumulation at the contractile ring as a fraction of overall cell width during both early and late cytokinesis (~25% and 75% ingression, respectively). n = Control (7,4,3), MO (8,6,3), MO+WT (8,6,5), MO+S386A (11,8,3), MO+S386E (13,7,3), MO+R384A (12,5,2). Error bars represent SEM unless otherwise noted. P-values were calculated from pairwise comparison to MO+MgcWT.

Figure 1.4
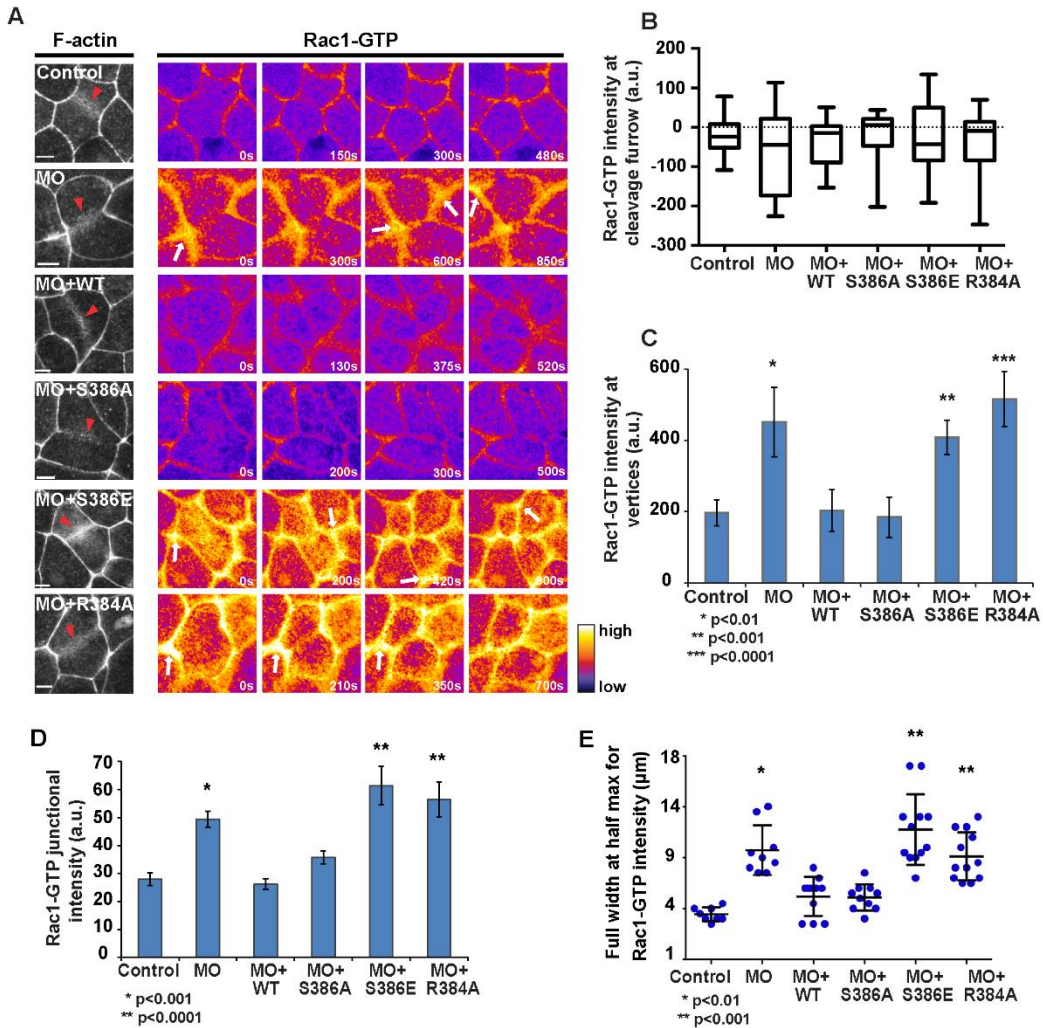
Figure 1.4 Mgc MO, MO+MgcS386E, and MO+MgcR384A embryos exhibit increased accumulation of Rac1-GTP at cell junctions. (A) Frames from time-lapse movies showing F-actin (mChe-UtrCH) at time 0s (presence of contractile ring indicates dividing cells) and Rac1-GTP in the same cells starting at time 0s and following cytokinesis over time. Red arrowheads indicate the contractile ring, and white arrows point to regions of Rac1-GTP accumulation. Scale bars = 20 µm. (B) Quantification of the normalized Rac1-GTP intensity at the cleavage furrow during early cytokinesis (~25% cleavage furrow ingression) graphed as a box-and-whiskers plot where whickers represent the min and max values and the horizontal bar represents the median. A negative value indicates that the Rac1-GTP intensity outside of the cleavage furrow is higher than at the furrow. n = # cells, # embryos, # independent experiments: Control (18,4,4), MO (10,4,4), MO+WT (12,3,3), MO+S386A (11,5,2), MO+S386E (14,5,4), MO+R384A (15,5,4). (C) Quantification of normalized Rac1-GTP intensity measured from an ROI positioned at cell vertices (tricellular junctions). n = Control (12,3,3), MO (10,4,4), MO+WT (12,4,4), MO+S386A (10,4,2), MO+S386E (22,5,3), MO+R384A (16,7,4,). (D) Quantification of the peak intensity of normalized Rac1-GTP line scans across bicellular junctions of dividing cells during early cleavage furrow ingression. Error bars represent SEM. n = Control (9,5,5), MO (10,3,3), MO+WT (11,6,5), MO+S386A (10,4,2), MO+S386E (12,5,3) MO+R384A (12,6,4). (E) Full width at half max quantification of normalized Rac1-GTP intensity line scans, to highlight the difference in breadth of the Rac1-GTP signal across bicellular junctions (see materials and methods for details). Error bars represent SEM unless otherwise noted. P-values were calculated from pairwise comparisons to MO+MgcWT

Figure 1.5
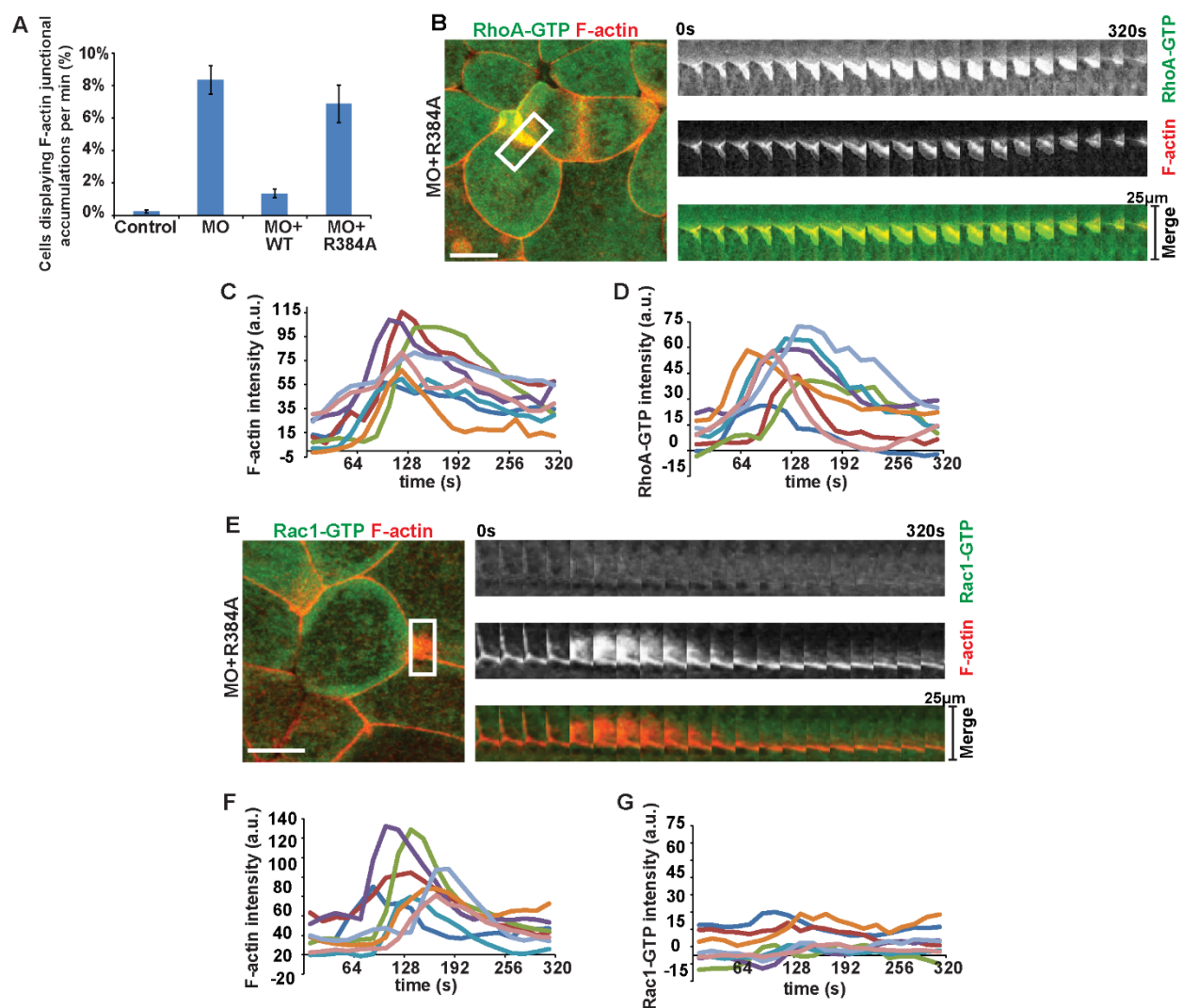
Figure 1.5 Distrupting MgcRacGAP's GAP activity results in dynamic junctional accumulations of F-actin and RhoA-GTP. (A) Quantification of the average percent of cells with F-actin junctional accumulations per minute. Error bars represent SEM. n = # cells, # embryos, # independent experiments: Control (335,10,8), MO (128,10,6), MO+WT (202,10,8), MO+R384A (163,10,4). (B) Brightest point projection images were used to generate kymographs across a junction where an F-actin accumulation occurs in MO+R384A embryos. Kymographs of RhoA-GTP (green) and F-actin (red) are shown. The white rectangle indicates the region of the kymograph. Scale bar in en face view = 10 µm. (C) Quantification of the normalized F-actin junctional accumulation intensity over time. n = # cells, # embryos, # independent experiments: (8,4,4). (D) Quantification of the normalized RhoA-GTP junctional accumulation intensity over time for the same regions quantified in C. (E) Brightest point projection images were used to generate kymographs across a junction where an F-actin accumulation occurs in MO+R384A embryos. Kymographs of Rac1-GTP (green) and F-actin (red) are shown. The white rectangle indicates the region of the kymograph. Scale bar in en face view = 10 µm. (F) Quantification of the normalized F-actin junctional accumulation intensity over time, n= (8,5,3). (G) Quantification of the normalized Rac1-GTP junctional accumulation intensity over time for the same regions quantified in G. Notice that there is not an increase in local Rac1-GTP intensity at the site of F-actin junctional accumulations.

63
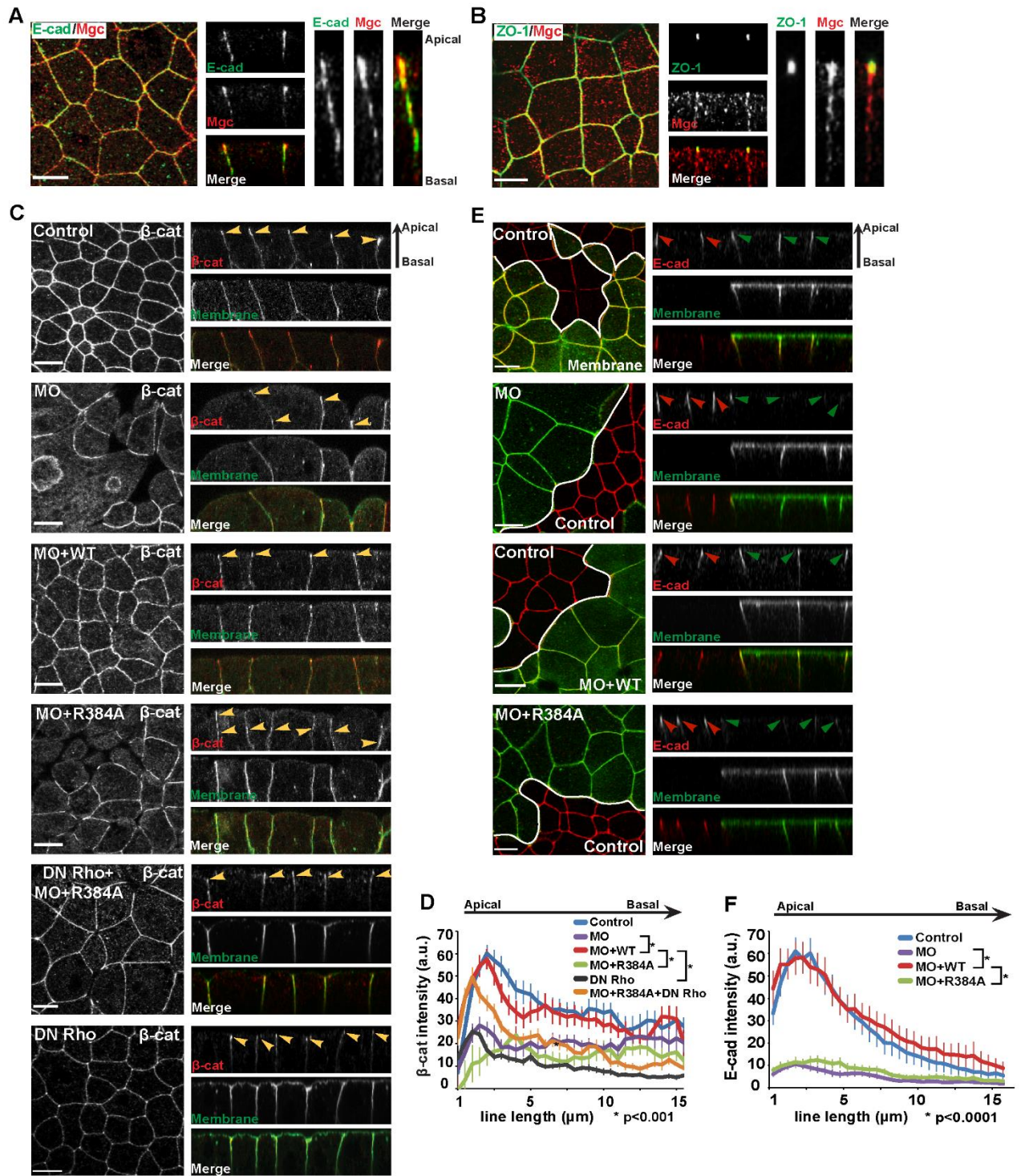
Figure 1.6

Figure 1.6 MgcRacGAP's GAP activity is required for proper AJ structure. (A-B) Fixed en face and side view images of embryos co-stained for endogenous Mgc and E-cadherin (A), or Mgc and ZO-1 (B). Side views highlight the overlapping localization (yellow) of Mgc with E-cadherin or Mgc with ZO-1. Scale bars = 20 μm. (C) Fixed en face and side view images of embryos injected with the indicated constructs (MO, MO+MgcWT, MO+R384A, or DN Rho+MO+R384A) as well as GFP-membrane as an injection marker. Embryos were fixed and co-stained for β-catenin and GFP. Yellow arrowheads indicate concentrated β-catenin localization. Scale bars = 20 μm. (D) Quantification of the normalized β-catenin intensity along the apical to basal axis of bicellular junctions. Error bars represent SEM. n = # cells, # embryos, # independent experiments: Control (20,5,3), MO (10,4,3), MO+WT (18,4,3), MO+R384A (21,5,3), MO+R384A+DN Rho (26,8,3), DN Rho (28,10,3). (E) Still images from live movies showing en face and side view images of mosaic embryos where all cells in the field of view express E-cadherin-3xmChe and only the cells expressing GFP-membrane (injection marker) contain the following: marker alone or with MO, MO+Mgc WT, or MO+R384A. Yellow arrowheads indicate E-cadherin localization in control regions, and red arrowheads indicate E-cadherin localization in regions expressing the injection marker. White lines represent separation between control region and perturbed region. Scale bars = 20 μm. (F) Quantification of the normalized E-cadherin-3XmChe intensity along the apical to basal axis of bicellular junctions. Error bars represent SEM. n = Control (21,8,2), MO (25,10,3), MO+WT (20,6,3), MO+R384A (27,9,3). Significance values were determined using a Student's t-test comapring the peak intensity value of each indicated construct to the peak value of MO+WT.

Figure 1.7
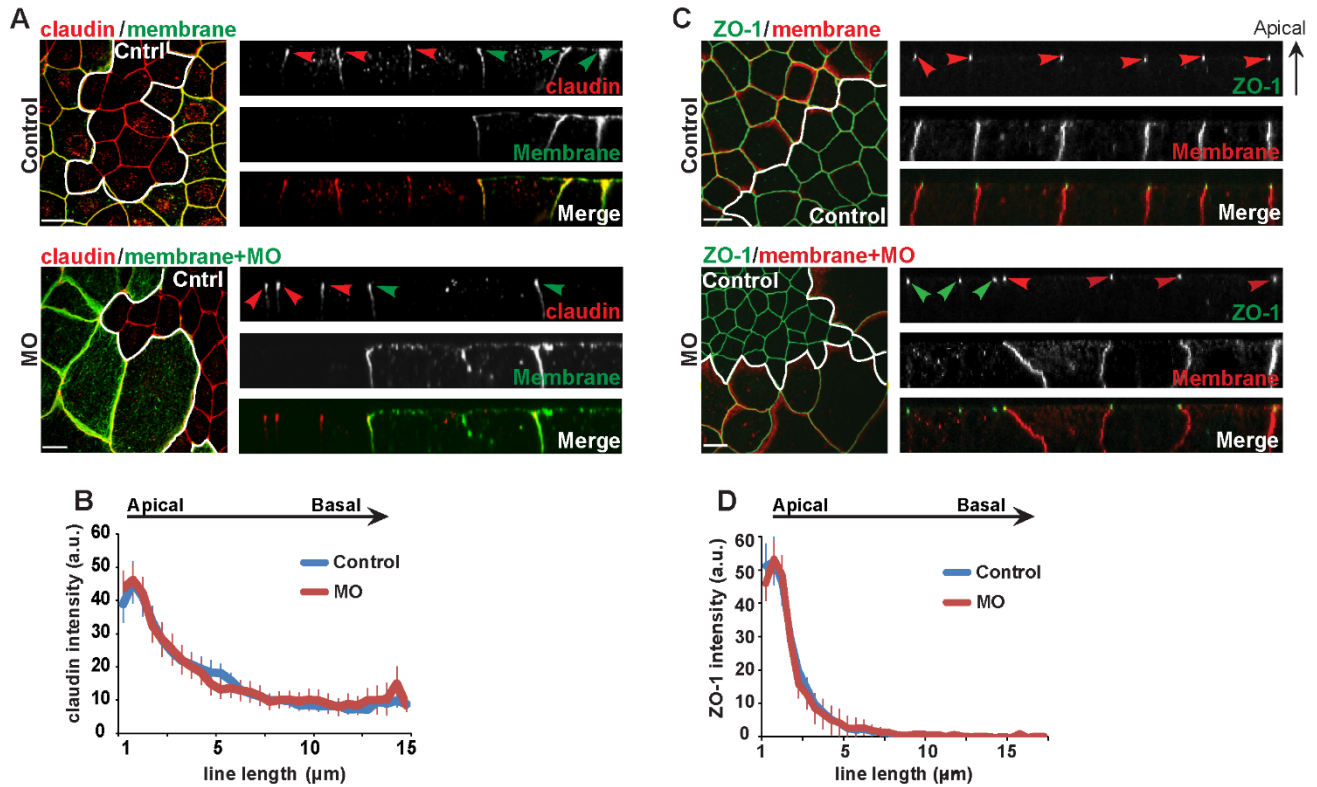
Figure 1.7 MgcRacGAP is not required for proper TJ structure. (A) Fixed en face or side view images of mosaic embryos where all cells in the field of view are stained for endogenous claudin and GFP, and the cells expressing GFP-membrane marker contain; marker alone (control) or marker + MO (MO). White lines represent separation between mosaic regions. Red arrowheads indicate claudin localization in control regions of the embryo, and green arrowheads indicate claudin localization in regions expressing the injection marker. Scale bars = 20 μm. (B) Quantification of normalized claudin intensity along the apical to basal axis of bicellular junctions. Error bars represent SEM. n= # cells, # embryos, # independent experiments: Control (16,5,3), MO (14,5,3). (C) Fixed en face or side view images of mosaic embryos where all cells in the field of view are stained for endogenous ZO-1 and mChe, and the cells expressing mChe-membrane marker contain; marker alone (control) or marker + MO (MO). White lines represent separation between mosaic regions. Green arrowheads indicate ZO-1 localization in control regions of the embryo, and red arrowheads indicate ZO-1 localization in regions expressing the injection marker. Scale bars = 20 μm. (D) Quantification of normalized ZO-1 intensity along the apical to basal axis of bicellular junctions. Error bars represent SEM. n= Control (15,6,3), MO (13,5,3).

Figure 1.8

MgcRacGAP localizes to the spindle midzone, equatorial cortex, and cell-cell junctions

MgcRacGAP spatially restricts active RhoA at the division site and both active RhoA and Rac1 at cell-cell junctions in epithelial cells

Mgc WT

Mgc GAP-dead

successful cytokinesis

cell-cell junctions intact

misregulated RhoA-GTP and Rac1-GTP, failed cytokinesis

adherens junctions disrupted

DNA
MgcRacGAP
active RhoA
active Rac1
active RhoA & Rac1

tight junction
adherens junction
apical actomyosin belt

Figure 1.8 Model of how MgcRacGAP regulates active RhoA and Rac1 in dividing epithelial cells. Mgc's GAP activity is necessary to down-regulate the active population of RhoA at the division site and both RhoA and Rac1 at cell-cell junctions in epithelial cells, and failure to do so results in defects in cytokinesis and cell-cell junctions. (Left) In dividing epithelial cells, Mgc is localized to the overlapping MTs of the spindle midzone, the equatorial cortex, and the apical surface of cell-cell junctions. (Middle) In dividing control epithelial cells, active RhoA accumulates in a focused band at the cell equator, but in Mgc GAP-dead cells, equatorial RhoA activity is not focused. Both active RhoA and Rac1 accumulate at cell-cell junctions in control cells (indicated by stripes), but when Mgc's GAP activity is disrupted, Rac1-GTP is increased at bicellular and tricellular junctions, and RhoA-GTP co-accumulates with ectopic F-actin-rich junctional structures (indicated by stars). (Right) Mgc's GAP activity is required for proper AJ structure. In Mgc GAP-dead cells, the intensity and apical polarity of AJs is disrupted. RhoA is known to regulate the apical actomyosin belt and AJ integrity. Expression of DN RhoA rescued the AJ defect in Mgc GAP-dead cells, suggesting that this defect was due to misregulated RhoA activity. Additionally, RhoA and Rac1 can exhibit crosstalk to antagonize each other (indicated by double arrow).

67
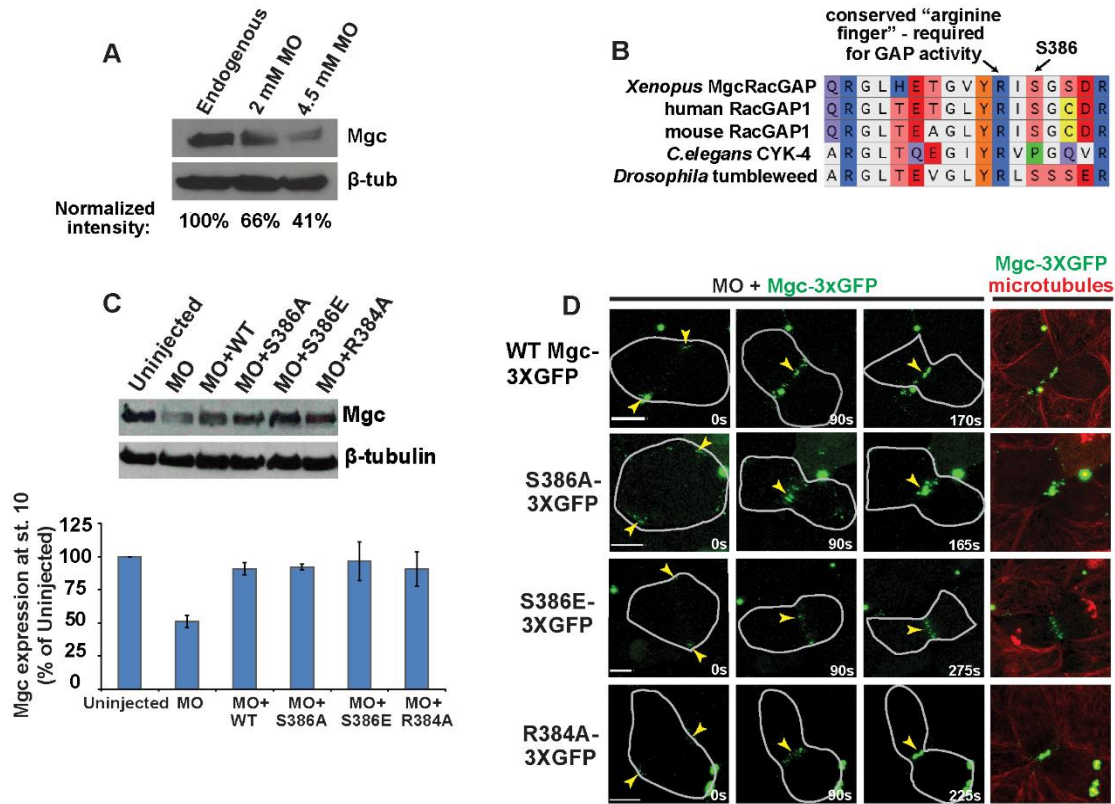
Figure S1.1

Figure S1.1 (related to Figure 1). (A) Western blot of optimized Mgc MO concentrations. Quantification of Mgc protein levels are shown as a percentage of the endogenous level. Note that while the knockdown detected by Western blotting was partial, the blots likely underestimate the level of knockdown. This is because cell lysates contain a mixture of cells that have recieved more or less MO, due to injection of the MO into the animal hemisphere of the 4 cell embryo. Where as for live and fixed epxeriments, the MO was injected with a lineage tracer and only cells that had received the full concentration of MO were imaged and analized. (B) Amino acid alignment of a portion of Mgc's GAP domain for multiple species. The arginine finger motif (R384) and serine 386 are indicated. (C) Western blot showing Mgc protein levels when Mgc was knocked down by injection with Mgc MO or knocked down and replaced with MgcWT or GAP domain mutants (top). Quantification from 3 independent Western blots (bottom). Error bars represent SEM. *Xenopus* embryo lysates were collected at gastrulation. (D) Still images from live movies showing the localization of the indicated Mgc constructs tagged with 3xGFP (green) along with microtubules (2xmChe-EMTB; red) in embryos where endogenous Mgc was knocked down with the MO. Yellow arrowheads indicate Mgc accumulations at the equatorial cortex and the midzone, and white outline shows the shape of the cell. The large accumualtions of Mgc-3xGFP are midbody remnants. Scale bars = 10 μm.

Figure S1.2

A

B

condition	R^2 value for correlation of cell size with duration of cytokinesis
control	0.1247
MO	0.0358
MO + WT	0.1609
MO + S386E	0.1523
MO + S386E	0.24
MO + R384A	0.0624
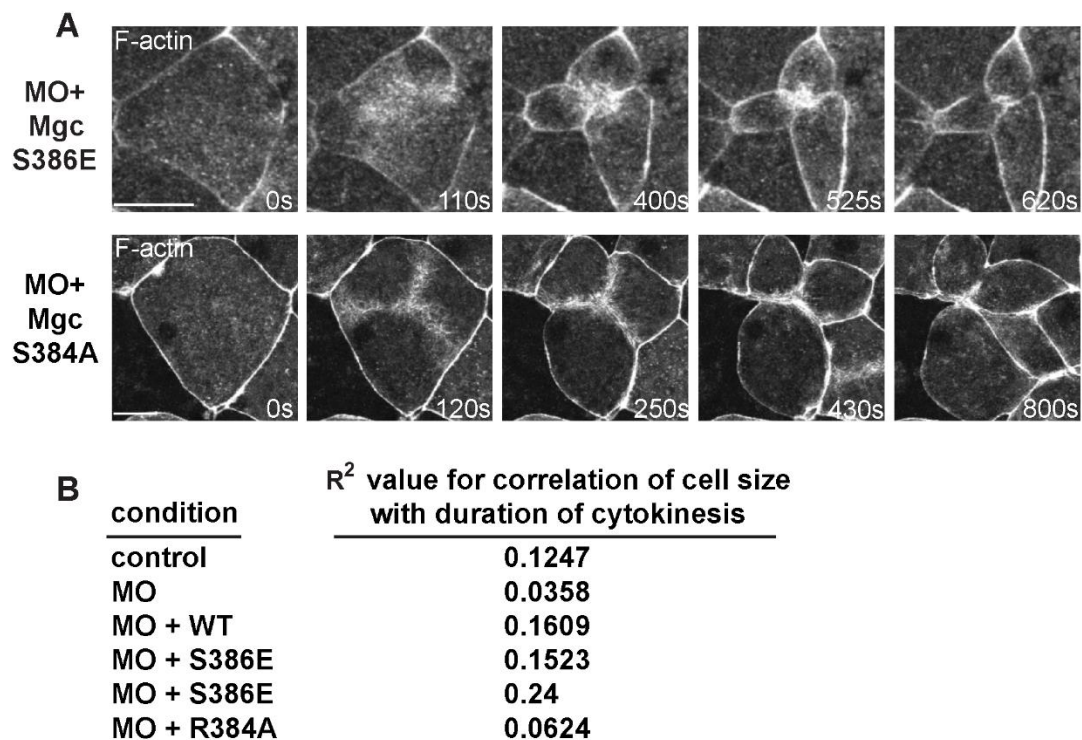
Figure S1.2 (A) Still images from live movies showing F-actin (mChe-UtrCH) in MO+S386E and MO+R384A embryos that display multiple contractile rings. Scale bars = 20 μm. (B) R^2 values from correlation analysis of cell size and duration of cytokinesis completion for the indicated conditions shows that duration of cytokinesis is not correlated with cell size.

Figure S1.3

A

MgcR384K
GAP mutant

B

F-actin/DNA
MO+R384K

C

	FIRE RhoA-GTP	F-actin	Merge F-actin RhoA-GTP

D

* = p<0.002
** = p<0.0001

E

* = p<0.01
** = p<0.0001
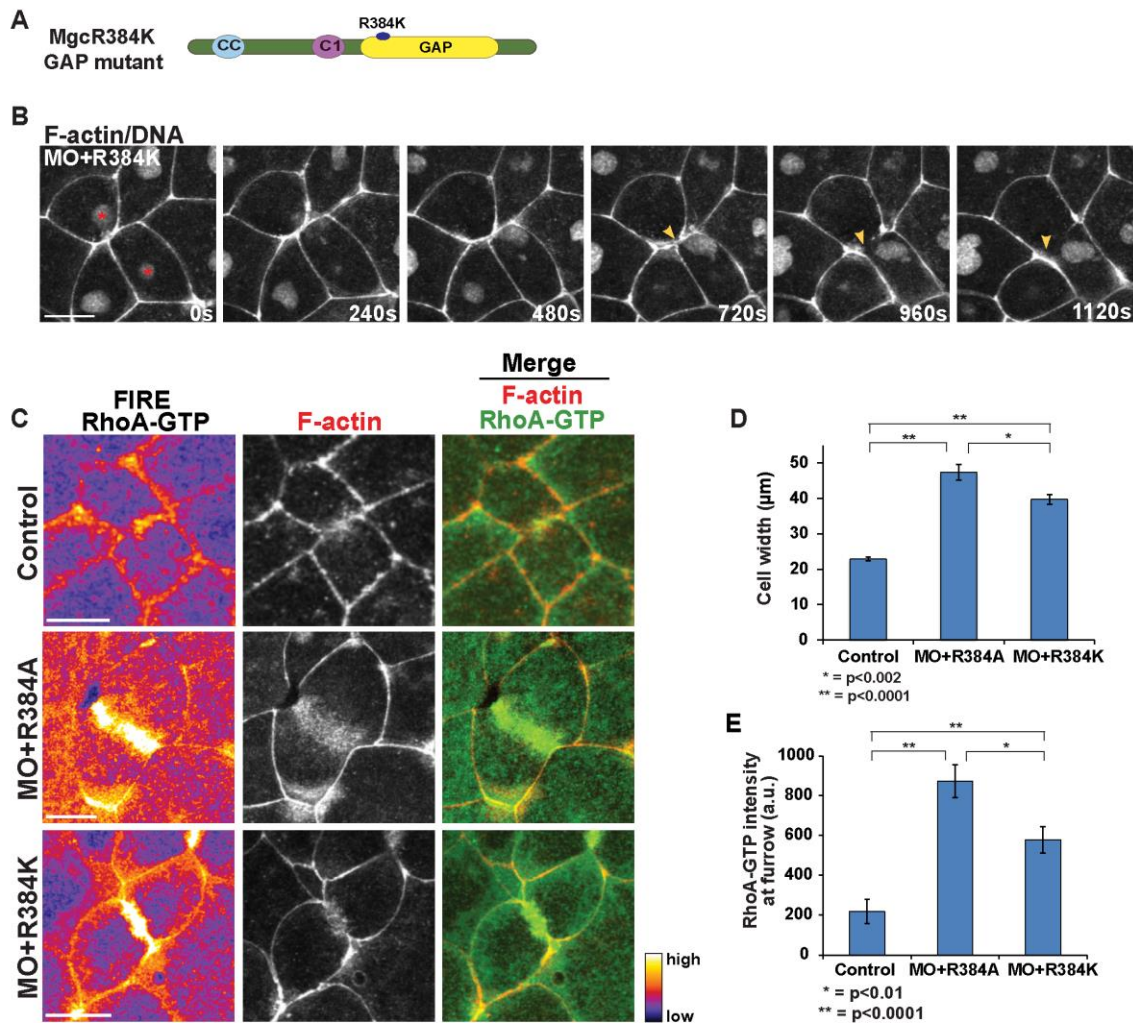
Figure S1.3 (A) Protein diagram of Mgc showing location of arginine 384 to lysine mutation within the GAP domain. (B) Still images from a time lapse movie of a MO+R384K embryo showing F-actin and DNA, where the cleavage furrow undergoes regression (yellow arrowhead). The individual nuclei are represented by red astericks in the two daughter cells prior to cleavage furrow regression in the first frame. (C) Images of cells during cytokinesis from time-lapse movies showing the RhoA-GTP zone (GFP-rGBD), with a FIRE LUT applied to the RhoA-GTP channel, F-actin accumulation (mChe-UtrCH), and merge. Embryos were co-injected with indicated Mgc MO and rescue constructs. (D) Quantification of cell width. n = # cells, # embryos, # independent experiments: Control (38,3,2), MO+R384A (39,5,2), MO+R384K (58,7,2). (E) Quantification of the normalized RhoA-GTP intensity at the cleavage furrow during cytokinesis. n = Control (10,3,2), MO+R384A (10,4,2), MO+R384K (10,4,2). All scale bars = 20 μm.
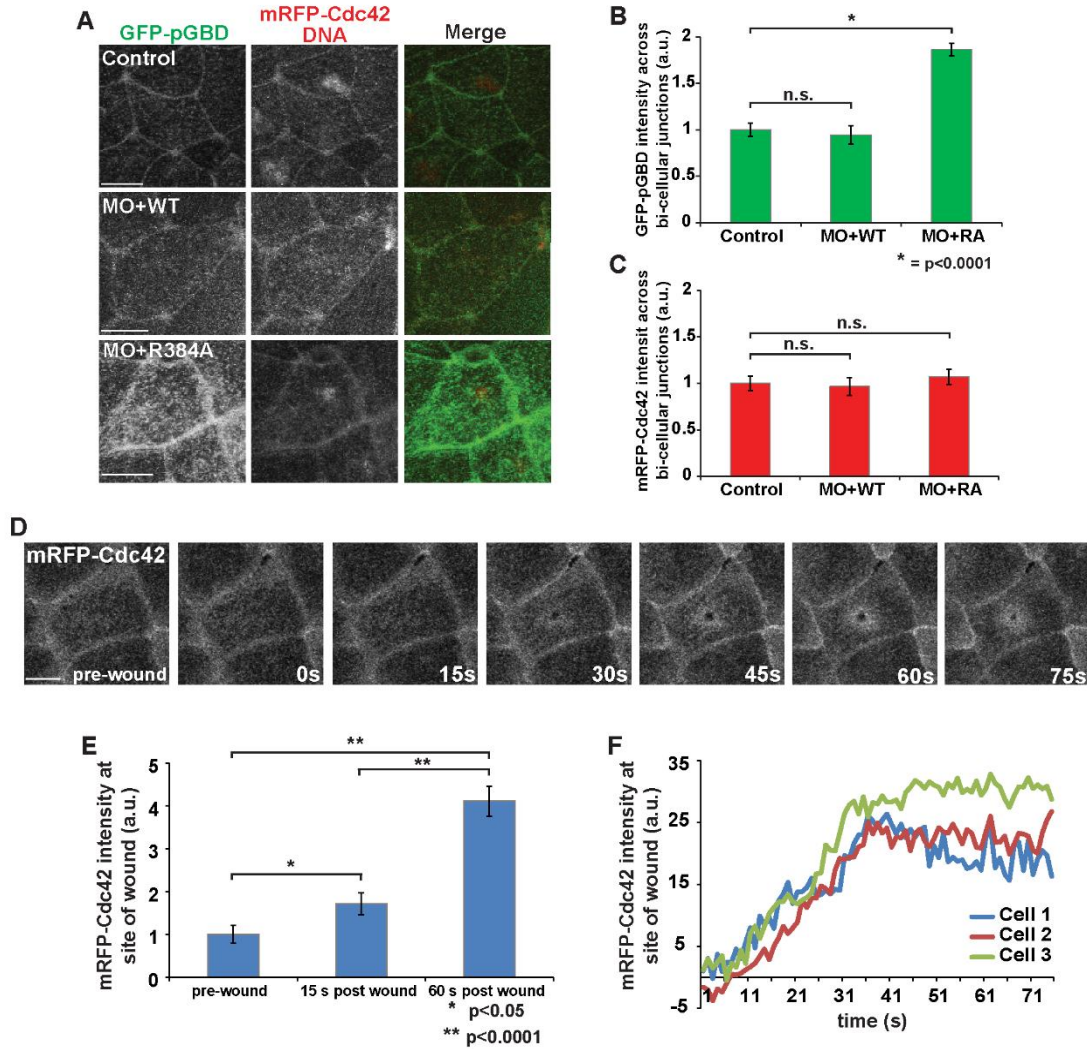
Figure S1.4

Figure S1.4 (A) To confirm that the signal we observed with the GFP-pGBD was specific to Rac1-GTP and did not detect significant levels of Cdc42-GTP, we co-injected the GFP-pGBD probe with a probe specific for the GTP-bound population of Cdc42 (mRFP-wGBD, the GTPase-binding domain of N-WASP fused to RFP) (Benink and Bement, 2005). Still images from live movies of control, MO+WT, or MO+R384A embryos (Nieuwkoop and Faber stage 10-11) injected with probes for GFP-pGBD, mRFP-wGBD, and mChe-H2B as an injection marker are shown. Scale bars = 20 μm. (B) Quantification of the normalized intensity of GFP-pGBD from line scans across bicellular junctions. Individual line scans were normalized to the background intensity of each cell. n= # cells, # embryos, # independent experiments; control (18,6,3), MO+WT (19,6,3), MO+R384A (21,8,3). (C) Quantification of the normalized intensity of mRFP-wGBD from line scans across bicellular junctions. Individual line scans were normalized to the background intensity of each cell. n= control (18,6,3), MO+WT (19,6,3), MO+R384A (21,8,3). (D) Images from a live confocal movie of control gastrula stage embryos (Nieuwkoop and Faber stage 10-11) injected with mRFP-wGBD. Embryos were wounded with a 405 nm laser for 300 μs at time 0, and accumulation of mRFP-wGBD and wound recovery was recorded over time. Scale bar = 10 μm. (E) Quantification of the normalized mRFP-wGBD intensity at the wound site for the indicated times, pre and post wounding for each indicated time n= (8,5,3). (F) Quantification of the normalized Cdc42-GTP intensity at the wound site over time. The data from three separate cells are shown. Error bars represent SEM.

Figure S1.5
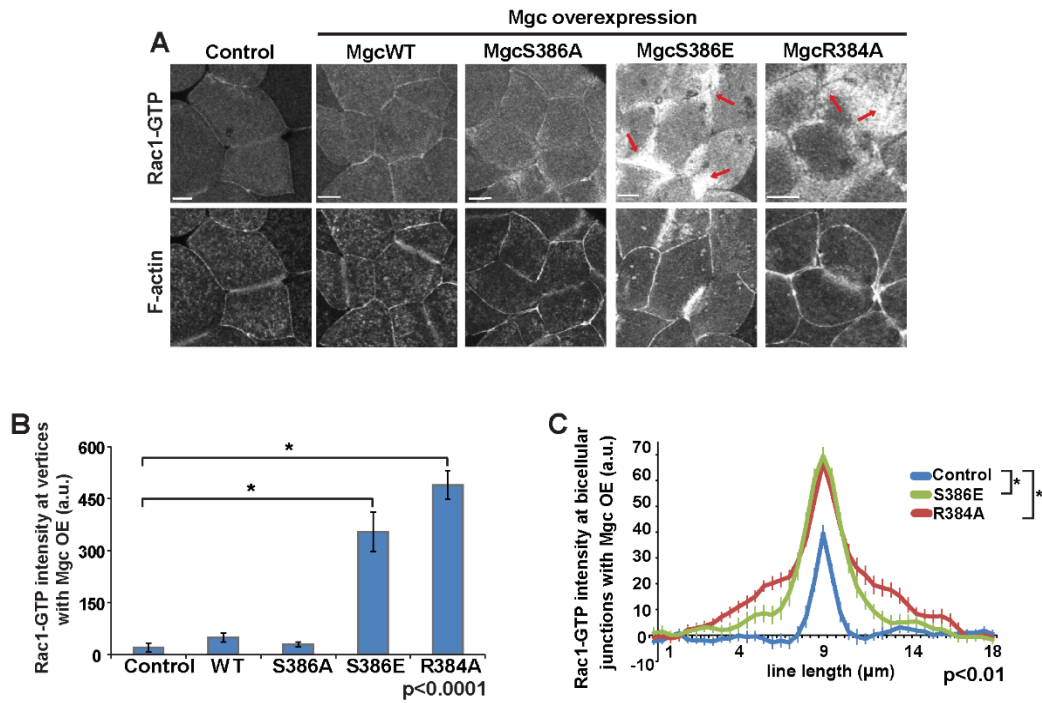
Figure S1.5 (A) Still images from live movies of control embryos or embryos overexpressing the indicated Mgc constructs at an earlier developmental stage (Nieuwkoop and Faber stage 6-8), showing the localization of Rac1-GTP(GFP-pGBD) or F-actin (mChe-UtrCH). Red arrows indicate regions of high Rac1-GTP intensity at cell vertices (regions where 3 cells meet). Scale bars = 30 μm. (B) Quantification of normalized Rac1-GTP intensity at cell vertices in dividing embryos. n = # cells, # embryos, # independent experiments: Control (28,8,4), WT (19,5,3), MgcS386A (21,5,4), MgcS386E (23,4,3), MgcR384A (24,4,3). (C) Quantification of normalized intensity line scans across bicellular junctions of Mgc overexpressing dividing cells. n= Control (17,7,6), MgcS386E (18,5,3), MgcR384A (24,4,4). Error bars represent SEM.

72

Figure S1.6

Figure S1.6 Additional examples of F-actin-rich accumulation kymographs. Brightest point projection images were used to generate kymographs across a region of a bicellular junction where an F-actin accumulation occurs for MO+R384A embryos. Kymographs of RhoA-GTP/F-actin and Rac1-GTP/F-actin are shown. The white rectangle indicates the region of the kymograph. Scale bars in en face views = 10 µm. (A) Examples of cells from two different embryos showing RhoA-GTP and F-actin in en face views and kymographs. (B) Examples of cells from two different embryos showing Rac1-GTP and F-actin in en face views and kymographs.

Figure S1.7
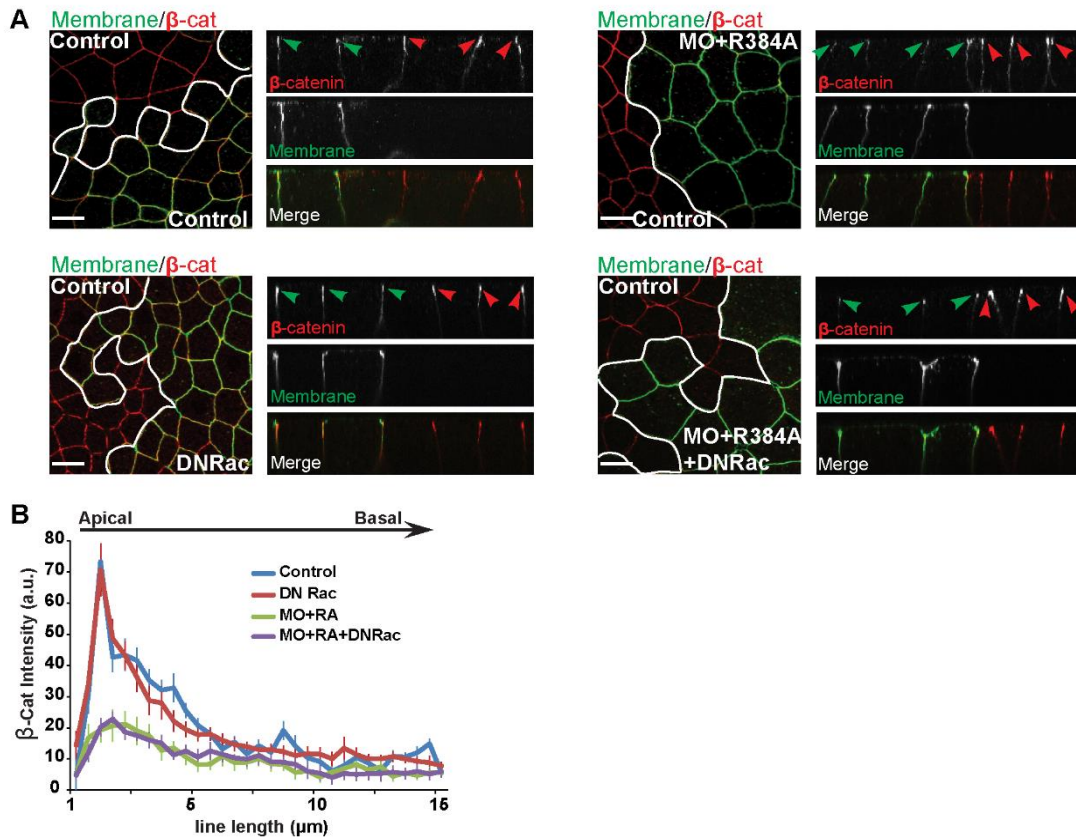
Figure S1.7 (A) Fixed en face and side view images of mosaic embryos injected with the indicated constructs (control, DN Rac, MO+R384A, or DN Rac+MO+R384A) as well as GFP-membrane as an injection marker (green). Embryos were fixed and co-stained for β-catenin and GFP. Red arrowheads indicate concentrated β-catenin localization in control regions and green arrowheads indicate β-catenin in regions that received the membrane marker and indicated construct. White lines represent separation between control region and perturbed region. Scale bars = 20 μm. (B) Quantification of the normalized β-catenin intensity along the apical to basal axis of bicellular junctions. Error bars represent SEM. n = # cells, # embryos, # independent experiments: Control (16,7,3), DN Rac (14,5,3) MO+R384A (11,4,3) MO+R384A+DNRac (15,5,3).

Figure S1.8
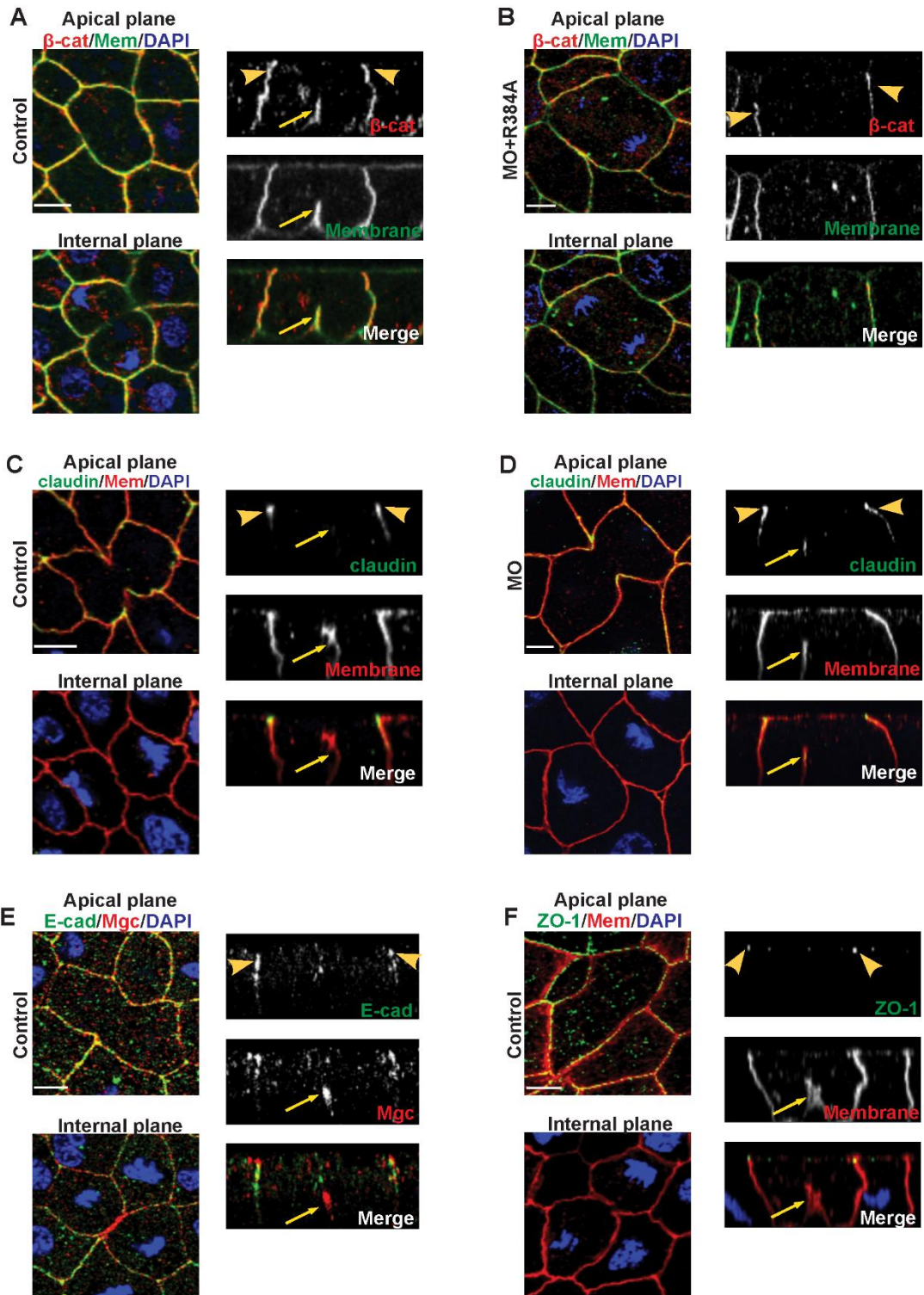
Figure S1.8 Fixed en face or side view images of dividing cells highlight the localization of the indicated junctional protein during cytokinesis. Embryos were fixed at Nieuwkoop and Faber stage 10-11. Yellow arrowheads indicate the junctional protein localization; yellow arrows indicate the contractile ring. Scale bars = 10 μm. (A) Control embryos were injected with GFP-membrane marker then fixed and co-stained for β-catenin and GFP. (B) MO+R384A embryos were co-injected with GFP-membrane as a lineage marker and fixed and co-stained for β-catenin and GFP. Note that the β-catenin localization is more lateral rather than apical for one of the junctions. (C) Control embryos were injected with mChe-membrane marker and fixed and co-stained for claudin and mChe. (D) MO embryos were co-injected with mChe-membrane as a lineage marker and fixed and co-stained for claudin and mChe. Note that the apical localization of claudin is not affected in the dividing Mgc MO treated embryos. (E) Control embryos were fixed and co-stained for E-cadherin (green) and Mgc (red). (F) Control embryos were injected with mChe-membrane marker and fixed and co-stained for ZO-1 and mChe.

Chapter 2

MgcRacGAP's SxIP motif tethers Centralspindlin to microtubule plus ends.

This chapter describes work that will be submitted for publication in Spring 2016.

Breznau, E. B., Murt, M., Blasius, L., Verhey, K.J., & Miller, A. L. MgcRacGAP's SxIP motif tethers Centralspindlin to microtubule plus ends. *Unpublished.*

Contributions to this work are as follows:

Breznau, E.B.: Contributed intellectually and to experimental design, executed all experiments except otherwise noted below, data analysis and presentation, and manuscript preparation.

Murt, M.: Contributed intellectually and experimentally to data described in Figure 2.5 D and E; Supplemental Figure S2.1. Made the MgcSxNN mutant construct desbribed in Figure 2.1E and used throughout, edited manuscript.

Blasius, L.: Contributed intellectually and experimentally to data described in Figure 2.2 and Supplemental Figure S2.2, edited manuscript.

Verhey, K.J.: Contributed intellectually and to experimental design, data analysis and data presentation for Figure 2.2 and Supplemental Figure S2.2, as well as provided all reagents, equipment and expertise for cell culture and TIRF microscopy, edited manuscript.

Miller, A.L.: Contributed intellectually and to experimental design, data analysis and presentation, and manuscript preparation, as well as provided the lab space and funding for the project. Executed experiments described in Figures 2.1 A-D.

I. Abstract

Centralspindlin, a heterotetrameric complex composed of two molecules each of Kinesin-6 (MKLP1) and MgcRacGAP (Mgc), is required for cytokinesis and structure of cell-cell junctions in animal cells. Centralspindlin directs contractile ring formation by recruiting and concentrating the GEF Ect2 at the cell equator to activate and focus the RhoA activity zone.

While MgcRacGAP is thought to be transported to microtubule plus ends via the plus-end-directed motor activity of MKLP1, how MgcRacGAP is stabilized at microtubule plus ends at the equatorial cortex is unknown. We found that Mgc is localized to the plus ends of individual equatorial astral microtubules during cytokinesis in *Xenopus* embryos. We identified a putative SxIP motif in *Xenopus* Mgc that is conserved with other SxIP motif-containing proteins that can bind EB1, a microtubule plus end tracking protein. Mutation of Mgc's SxIP motif resulted in loss of Mgc tracking with EB3 on growing microtubule plus ends, abnormal astral microtubule organization, and severe cytokinesis defects. Furthermore, Mgc's localization was redistributed from the contractile ring to the cell cortex when the SxIP motif was mutated, and RhoA and its effectors were also mislocalized. Additionally, mutation of MgcRacGAP's SxIP motif perturbed its function at adherens junctions. We propose that MgcRacGAP's SxIP motif is functionally important for its localization to the plus ends of equatorial astral microtubules in order to properly regulate Rho GTPase activity during cytokinesis as well as for its role in regulating adherens junction structure during interphase.

II. Introduction

Cytokinesis is the last step of cell division that partitions the cellular components into two daughter cells. In animal cells the position of the division plane is dictated by signals from the central spindle which are thought to be delivered by equatorial astral microtubules (MTs)[7]. At anaphase, activation of the small GTPase RhoA in a focused zone at the equatorial cortex is essential for cytokinesis[22,67]. Centralspindlin, composed of the kinesin-6 MKLP1, and the GAP protein MgcRacGAP (Mgc), accumulates on the antiparallel overlapping MTs of the central spindle[18,19,80]. Centralspindlin recruits and binds the RhoA GEF, Ect2[21,22,88], and together they

localize to the equatorial cortex to regulate the zone of active RhoA[14,15]. Mgc and Ect2 have also

been shown to regulate RhoA contractile arrays at the adherens junctions of epithelial cells[28,46].

Interestingly, the localization of Mgc and Ect2 at both locations is thought to be MT dependent,

mediated by the motor activity of MKLP1[46,54,55]. However, how Mgc is stabilized at MT plus

ends at the equatorial cortex and cell-cell junctions is unknown.

We have observed in live cells that Mgc localizes at the plus ends of non-overlapping

MTs at the equatorial cell cortex in addition to the population of Centralspindlin that is known

to bundle central spindle MTs[19]. These findings are similar to the reported localization of

Centralspindlin to astral MTs in fixed HeLa cells[23]. Equatorial astral MTs are thought to be

important for delivering the cleavage furrow-stimulating signal and may be uniquely stabilized

by an unknown mechanism, allowing them to fulfill this role[7,119–121]. The link between

equatorial astral MTs and the cortex is unknown.

EB1 is the core component of the +TIP network of proteins that binds to MT plus ends.

EB1 can autonomously recognize and track growing MT ends and acts as an adaptor to recruit

and bind other +TIP proteins[56,122]. One way EB1 recruits other proteins to MT plus ends is by

binding SxIP motifs, which are found in a diverse group of proteins[57,59]. Binding is dependent

on the SxIP motif as well as electrostatic interactions between positively charged residues that

flank the SxIP motif and negatively charged residues on EB1[57]. +TIP proteins that bind MTs

through EB1 can anchor MTs to specific cellular structures and control MT dynamics, including

those in cytokinesis[56,123]. We identified a putative SxIP motif in Mgc, and propose that this motif

is functionally important for Mgc's localization to the plus ends of equatorial astral MTs and its

MT dependent localization to cell-cell junctions for proper regulation of Rho GTPase activity.

Here we test whether Mgc's SxIP motif is required to tether Mgc to MT plus ends and whether this is functionally important for cytokinesis and/or cell-cell junction structure.

III. Results

MgcRacGAP localizes to microtubule plus ends at the equatorial cortex as cytokinesis initiates.

To test how Mgc interacts with MTs that extend toward the equatorial cell cortex during cytokinesis, we examined the localization of Mgc (Mgc-3xGFP) and a probe for MTs (2xmCherry-EMTB) in dividing gastrula stage *Xenopus* embryos (Nieuwkoop and Faber stage 10-11). Endogenous Mgc was knocked down with a morpholino oligonucleotide (MO) that targets the 5' untranslated region of Mgc[15] and was replaced with MO-resistant Mgc-3xGFP. During early anaphase, before cleavage furrow ingression initiated, Mgc-3xGFP localized in discrete puncta at the equatorial cortex near the cell membrane, then became increasingly enriched along the ingressing cleavage furrow (Figure 1 A). Mgc-3xGFP was also observed at the overlapping anti-parallel MTs of the central spindle, which are located more internally (Supplemental Figure 1). Surprisingly, Mgc-3xGFP puncta decorated individual, non-overlapping equatorial astral microtubules, and Mgc appeared to make stable contacts with both the cell cortex and the plus end of the microtubule, as evidenced by stable positioning of a bright Mgc puncta and MT bending over time (Figure 1A'). Additionally, we observed directed motility of Mgc-3xGFP, presumably along astral microtubules, as Mgc puncta coalesced and formed increasingly brighter clusters along the cleavage furrow during early cytokinesis (Figures 1 B and C). Localization of both Mgc and MKLP1 at the plus ends of individual astral MTs was previously

observed in anaphase HeLa cells[23,124], indicating this localization is not unique to *Xenopus*

embryos, but the mechanism of Mgc stability on the MT plus ends has not been investigated.

Mgc is thought to be transported to MT plus ends by the motor activity of MKLP1[55,125] and is

known to accumulate at regions of MT overlap[79]; however, how Mgc could be stabilized at MT

plus ends at the equatorial cortex is unknown.

   To determine the mechanism by which Mgc remains stabilized on microtubule plus ends,

we hypothesized that it might interact with one of several microtubule plus tip tracking

proteins (+TIPs). End Binding Protein 1 (EB1) and its family members (including EB3) are +TIPs

that autonomously track the growing plus ends of MTs via recognition of the transition state

between β-tubulin-GTP/GDP hydrolysis[56]. EB proteins are responsible for most intracellular plus

tip tracking by acting as adaptors that recruit other proteins to the polymerizing MT plus end[56].

The EB homology domain of EB1 has a hydrophobic cleft that binds other +TIP proteins through

a recently discovered conserved (S/T)x(I/L)P motif[57] (Figure 1 D). We analyzed the amino acid

sequence of *Xenopus* Mgc and identified a putative SxIP motif in Mgc's C-terminus, which also

contains other conserved sequence features of SxIP proteins including flanking basic residues

and an arginine residue at the +1 position (Figure 1 D). In order to test if Mgc's putative SxIP

motif is responsible for its stability on astral MT plus ends (Figure 1 A-B), we mutated the

isoleucine and proline residues to asparagine (MgcSxNN) (Figure 1 E). This mutation has been

shown by others to abrogate binding of SxIP proteins to the EB homology domain[57,126–129].

MgcRacGAP tracks with EB3 at growing MT plus ends.

If Mgc's putative SxIP motif indeed acts as an adaptor for EB protein binding, we reasoned

that we should observe reduced stability of Mgc at growing MT plus ends when the SxIP motif is

mutated to SxNN. To test whether Mgc tracks growing MT plus ends we co-transfected EB3

tagged with mCherry (EB3-mChe) and MgcWT-mNeon or MgcSxNN-mNeon into Cos-7 cells and

observed MT plus end tracking behavior with Total Internal Reflection Fluorescence Microscopy

(TIRF). Importantly, both MgcWT-mNeon and MgcSxNN-mNeon localized to nuclei of

interphase cells and to midbodies, suggesting that both proteins were expressed at similar

levels (Supplemental Figure 2). MgcWT-mNeon co-localized at growing MT plus ends with EB3-

mChe comets in interphase Cos-7 cells (Figure 2 A and A'). Kymograph analysis shows the tracks

of EB3-mChe at growing MT plus ends, and MgcWT-mNeon showed similar tracking behavior

(Figure 2 B). In contrast, MgcSxNN-mNeon did not co-localize with EB3-mChe comets (Figure 2

C and C') or track with EB3 at growing MT plus ends (Figure 2 D), but instead showed a more

diffuse cellular distribution. To confirm this change in distribution, we quantified the intensity

of MgcWT and MgcSxNN at EB3 comets and found that MgcSxNN intensity was significantly

reduced compared to MgcWT (Figure 2 E). We also measured the EB3-mChe run length along

MTs and found that EB3 run lengths were significantly shorter in cells expressing MgcSxNN-

mNeon compared to cells expressing MgcWT-mNeon (Figure 2 F). This indicates that disrupting

Mgc's SxIP motif has a functional effect on EB3's ability to track MTs and that MT dynamics are

changed. Finally, we measured the velocity of EB3-mChe comets and found that the velocity did

not differ between MgcWT-mNeon and MgcSxNN-mNeon (Figure 2 G). Although we were not

able to detect direct protein-protein binding between Mgc and EB via yeast 2 hybrid or

immunoprecipitation experiments, this could be due to multiple reasons including lack of key

post-translation modifications that regulate clustering of Centralspindlin or EB binding. Nonetheless, the data presented above provide solid evidence that Mgc's putative SxIP motif may mediate binding to EB proteins and provides a feasible mechanism by which Mgc can associate with MT plus ends.

MgcRacGAP's SxIP motif is necessary for proper astral microtubule structure and successful cell division.

Live imaging in dividing *Xenopus* embryos (Figure 1) and TIRF microscopy studies (Figure 2) provided evidence that Mgc may be tethered to MT plus ends. Furthermore, the TIRF data showed that perturbing Mgc's SxIP motif led to a defect in EB3 run length suggesting that, like other bona-fide +TIPs, Mgc may help to facilitate proper MT polymerization and stability[58,130,131]. Therefore, we next wanted to determine whether mutating Mgc's SxIP motif had a functional consequence on astral MT structure and on cell division itself. We co-injected MO+MgcWT or MO+MgcSxNN, along with probes for F-actin (mChe-UtrCH) and DNA (mChe-H2B) and counted multinucleate cells from images of gastrula stage *Xenopus* embryos. We found that the MO+MgcSxNN embryos exhibited a significant increase in cytokinesis defects, as the mutant embryos showed 16.7 +/- 0.11% multinucleation at 24 hours post fertilization (hpf), compared to 2.6 +/- 0.04% in MO+MgcWT (Figures 3 A and C). Additionally, the level of multinucleation in MO+MgcSxNN embryos increased at 32 hpf with 26.6 +/- 1.7% vs. 3.6 +/- 0.57% multinucleation for MO+MgcSxNN and MO+MgcWT embryos, respectively (Figure 3 B and C). Similar results were obtained when embryos were fixed at 24 hpf and stained with DAPI to quantify multinucleation (Supplemental Figure 3).

We noticed that many of the cells from MO+MgcSxNN embryos underwent asymmetric cell divisions, where the cleavage furrow formed to one side of the central axis of the cell (Figure 3 D). We quantified the percent of cells with asymmetric cell division and found a significant difference in MO+MgcSxNN vs. MO+MgcWT embryos (22.2+/-1.29% vs. 4.4 +/-0.16%, respectively). We also observed instability - that is, abnormal movements - of the metaphase spindle in cells overexpressing MgcSxNN (data not shown), which could contribute to the asymmetry of the division plane. We reasoned that if Mgc acts as a +TIP protein, then it may help facilitate metaphase spindle stability by connecting the spindle to the cortex via astral MTs; these astral MT connections to the cortex might be defective in MgcSxNN cells resulting in asymmetric divisions. To examine the morphology of astral MTs during metaphase, we injected embryos with MO+MgcWT or MO+MgcSxNN along with GFP-membrane as a lineage tracer, then fixed the embryos at 24 hpf and stained with anti-α-tubulin and anti-GFP antibodies. We compared astral MT distribution in cells by quantification of α-tubulin intensity in cytosolic regions parallel to the spindle, and along the poles (Figure 3 F). Control cells exhibit a centrally aligned spindle with strong astral MT density connecting it to the cortex (Figure 3 G). In contrast, cells injected with MO alone showed a significant decrease in astral MT density compared to control cells (Figures 3 G and H). This phenotype was rescued in MO+MgcWT cells, which exhibited astral MT density similar to controls (Figures 3 G and H). In contrast, MO+MgcSxNN cells had significantly reduced astral MT density when compared to control or MO+MgcWT cells (Figures 3 G and H). Together, these results suggest that Mgc's SxIP motif is necessary for proper astral MT structure and for successful cytokinesis, which suggests that, similar to other +TIP proteins, Mgc can help regulate proper MT polymerization and stability.

Mutation of MgcRacGAP's SxIP motif disrupts equatorial accumulation of the Centralspindlin complex and RhoA-GTP.

Because the astral MTs that point toward the equatorial cell cortex during early anaphase play an important role in regulating the formation of the cleavage furrow by providing tracks for Centralspindlin delivery to the cortex and activation of RhoA, we wanted to investigate whether accumulation of Centralspindlin at the equatorial cortex was affected when Mgc's SxIP motif was mutated. We knocked down endogenous Mgc and expressed MgcWT-3xGFP or MgcSxNN-3xGFP along with a probe for MTs (2xmChe-EMTB) and DNA (mChe-H2B), then captured movies of cells undergoing cytokinesis. MgcWT-3xGFP specifically localized to the equatorial cortex of dividing cells and became increasingly enriched at the midzone during furrow ingression (Figure 1 A and Figures 4 A-C). In contrast, MgcSxNN-3xGFP was not strongly enriched at the equatorial cortex during cytokinesis, but instead much of it was redistributed along the cell membrane (Figure 4 A-C). Quantification of the Mgc signal intensity at the contractile ring at 25% cleavage furrow ingression showed a significant decrease in MgcSxNN-3xGFP intensity compared to MgcWT-3xGFP (p<0.0001). In agreement, quantification of Mgc redistribution by measuring the intensity along the polar cell membrane at 25% ingression, showed a significant increase in MgcSxNN-3xGFP intensity compared to MgcWT-3xGFP (p=0.004). These results show that Mgc's SxIP motif is important for proper Mgc localization during cell division.

A possible explanation for the redistribution of Mgc localization is that the MgcSxNN mutation could somehow affect Mgc's ability to bind MKLP1 and form the Centralspindlin complex, which could result in mis-localization of Mgc. However, this explanation is unlikely

because the MKLP1 binding site on Mgc is near the N-terminus, and Mgc's SxIP motif is located

at the C-terminus. Nonetheless, we performed similar experiments to observe the localization

of MKLP1. We injected MO+MgcWT or MO+MgcSxNN along with MKLP1-3xGFP, and probes for

MTs and DNA. MO+MgcWT cells showed characteristic MKLP1 accumulation at the equatorial

cortex and ingressing cleavage furrow in dividing cells (Figure 4 D and E)[18,19,26]. In contrast,

MO+MgcSxNN cells showed reduced MKLP1-3xGFP accumulation at the contractile ring and a

similar redistribution to the cell membrane (Figure 4 D-F). These results suggest that Mgc's SxIP

motif may help facilitate the focused accumulation of Centralspindlin at the equatorial cortex

via association with EB1 and regulation of MT stability.

When the interaction of Mgc with EB1 is abrogated, Centralspindlin no longer remains

intensely focused at the equatorial cortex to recruit the GEF Ect2 and regulate RhoA signaling;

this could contribute to the increased cell division failure observed in MO+MgcSxNN cells. In

order to determine whether the MgcSxNN mutant affects proper RhoA signaling during

cytokinesis, we performed live imaging of embryos injected with MO+MgcWT or MO+MgcSxNN

along with a probe for active RhoA (GFP-rGBD). In MO+MgcWT cells, active RhoA accumulates

in a focused band at the equatorial cortex following anaphase onset and remains enriched at

the furrow throughout cytokinesis (Figure 4 H and I). In contrast, cells in MO+MgcSxNN

embryos show a broader, less focused accumulation of active RhoA at anaphase onset (Figure 4

H and I). The perturbation of RhoA signaling leads to furrow regression in some cells

(Supplemental Figure 4). We quantified the accumulation of active RhoA at anaphase onset

using line scans along the cell membrane and full width at half maximum (FWHM) analysis of

the breadth of RhoA-GTP signal (Figure 4 G). We reasoned that this region, where astral MTs

point to the cell cortex, might show early defects in RhoA-GTP accumulation if Mgc's SxIP motif is important for proper localized RhoA activity during cytokinesis. The FWHM analysis shows a significant increase in the breadth of active RhoA in MO+MgcSxNN compared to MO+MgcWT cells (Figure 4 H and I). These results are consistent with the redistribution of MgcSxNN away from the equatorial cortex, and suggest that Mgc's SxIP motif is important for regulating the proper localization of Centralspindlin and focusing of RhoA at the equatorial cortex during cytokinesis.

MgcRacGAP's SxIP motif is necessary for the proper regulation of RhoA effector proteins.

To better understand the downstream consequences of abnormal RhoA-GTP accumulation when Mgc's SxIP is mutated and how this may lead to cytokinesis failure, we examined proteins activated downstream of RhoA-GTP. First, we investigated the effects on F-actin, which is polymerized downstream of RhoA-GTP via formin effector proteins. Embryos were injected with MO+MgcWT or MO+MgcSxNN along with probes for F-actin (mChe-UtrCH) and DNA (mChe-H2B), and movies of dividing cells were analyzed for defects in F-actin accumulation during early anaphase. MO+MgcWT cells showed typical F-actin accumulation at the equatorial cortex of dividing cells[14,15,28]; however, MO+MgcSxNN cells exhibited a broad accumulation of F-actin. FWHM analysis of F-actin intensity at an equatorial region adjacent to the cell membrane revealed a significant increase in the breadth of F-actin accumulation in MO+MgcSxNN compared to MO+MgcWT cells (Figure 5 A-C). Second, RhoA-GTP promotes myosin II activation through its effector protein ROCK, so we overexpressed MgcWT or MgcSxNN along with a lineage tracer (mChe-membrane, not shown), then fixed and stained with anti-phospho-Myosin II (p-Myo) antibodies. In cells expressing MgcWT, p-Myo labeled a

focused band at the cleavage furrow with weak signal detected at cell-cell junctions, whereas in cells expressing MgcSxNN, p-Myo accumulated broadly at the contractile ring as well as at cell-cell junctions (Figure 5D). When quantified, we detected a significant decrease in the ratio of contractile ring/junction intensity in MgcSxNN cells vs. MgcWT cells (Figure 5E).

We also examined the localization of Anillin during cytokinesis. Anillin is a scaffolding protein that contains a Rho binding domain[13] and therefore can be considered a Rho effector and has been shown to bind Mgc and Ect2[132–134]. We expressed Anillin-3xGFP in MO+MgcWT or MO+MgcSxNN embryos and found that Anillin-3xGFP was significantly reduced at the contractile ring in MgcSxNN cells compared to MgcWT cells (Figure 5 F and G). These results are consistent with the pattern of active RhoA observed when Mgc's SxIP motif is disrupted (Figure 4 H). If RhoA forms an abnormally broader zone along the cell midzone, then it follows that downstream proteins will also exhibit a broader localization. This abnormal accumulation of the key contractile ring components, F-actin, Myosin II and Anillin likely contributes to the cytokinesis defects observed when Mgc's SxIP motif is mutated. Collectively, these data provide *in vivo* evidence that Mgc's SxIP motif plays a functional role in regulating cytokinesis by mediating the precise localization of Centralspindlin in order for proper localized RhoA activation and accumulation of downstream targets of RhoA activity.

MgcRacGAP's SxIP motif is necessary for proper adherens junction structure.

Our results in Cos-7 cells and dividing *Xenopus* embryos demonstrate that Mgc's localization is disrupted when its SxIP motif is mutated; therefore, we wanted to test if this effect is also relevant for the population of Mgc that localizes to cell-cell junctions[28,71,72]. To accomplish this, we used fixed staining coupled with a mosaic injection strategy, which results in only half of the

embryo expressing the knockdown and replacement construct (MO+MgcWT or MO+MgcSxNN) along with a lineage tracer (GFP-farnesyl), such that a direct comparison can be made to the internal control regions that did not receive the knockdown and replacement injection. The embryos were fixed at gastrula stage at which point polarized cell-cell junctions have formed, then stained with anti-GFP and anti-Mgc antibodies. Similar to our previous results[28], we found that Mgc localizes to cell-cell junctions, and is enriched at the apical surface in both the mosaic injected region and the internal control region (Figure 6 A). In contrast, MO+MgcSxNN embryos showed a significant reduction in Mgc apical junction localization compared to MO+MgcWT (Figure 6 A and B). MTs are known to regulate the junctional accumulation of Centralspindlin and its binding partner Ect2 [46]. Therefore, one explanation for the reduced localization of MgcSxNN at apical junctions is that the SxIP motif is necessary for Mgc stability and/or tethering on MT plus ends for proper delivery to the cell-cell junctions.

Because we and others have shown that Mgc contributes to cell-cell junction structure and maintenance[28,46,72], and that Mgc's GAP activity is specifically required for the proper localization of the adherens junction protein β-catenin[28], we next tested whether β-catenin was properly localized at cell-cell junctions in MO+MgcSxNN embryos. The same mosaic injection approach described above was employed, and the embryos were fixed at gastrula stage and stained with anti-GFP and anti-β-catenin antibodies. In the MO+MgcWT embryos, β-catenin was localized to the apical surface (Figures 6 C and D). In contrast, β-catenin junctional localization was significantly reduced in MO+MgcSxNN cells compared to MO+MgcWT cells (p<0.0001), and the cells often appeared apically domed, a phenotype associated with reduced cell-cell junction integrity (Figures 6 C and D). To confirm whether disrupting Mgc's SxIP motif

resulted in defective adherens junctions, or was specific to β-catenin, we performed a similar experiment to examine the localization of the trans-membrane adherens junction protein E-cadherin. E-cadherin localization was significantly reduced in Mgc MO embryos compared to control embryos (Figure 6 E and F). This defect was rescued in MO+MgcWT embryos, but was not rescued in MO+MgcSxNN embryos (Figure 6 E and F). Quantification of E-cadherin intensity along the apical to basal axis of cell-cell junctions demonstrated that both MO and MO+MgcSxNN embryos show a significant decrease in E-cadherin intensity compared to either control or MO+MgcWT embryos (Figure 6 F). Taken together, our data provide strong evidence that Mgc's SxIP motif plays an important role in regulating Mgc's localization to adherens junctions as well as the localization of adherens junction structural components themselves.

IV. Discussion

Here we have used both cultured cells and epithelial cells in intact *Xenopus laevis* embryos to investigate the mechanism and function of Mgc tethering at MT plus ends. Centralspindlin is known to accumulate at regions of MT overlap and bundle MTs[18–20,79]. Our study builds on this model suggesting that Mgc can be transported to MT plus ends, presumably via its kinesin binding partner, MKLP1. Once localized to the MT plus end, Mgc can use its SxIP motif to bind EB1 in order to be tethered at the MT plus end. We propose that this interaction is important for MT stability and for regulating the subcellular localization of Centralspindlin to functionally regulate both cytokinesis and cell-cell junction integrity (Figure 7).

We found that Mgc-3xGFP can localize to individual plus ends of MTs at the equatorial cortex during cytokinesis. To determine the mechanism by which Mgc could stably associate with these MTs at the cell cortex, we identified a putative EB1 binding motif (SxIP) on Mgc's carboxy terminus. To test whether this putative SxIP motif mediated Mgc binding to EB proteins, we mutated the site to SxNN. We used TIRF microscopy of Cos-7 cells to show that MgcWT co-localized with EB3 comets, but MgcSxNN did not. We investigated the functional effects of the MgcSxNN mutant in live *Xenopus* embryos and found significant cytokinesis defects, asymmetric cell divisions, and decreased astral MT density. To determine the mechanism by which mutating Mgc's SxIP motif causes cytokinesis defects, we investigated the localization of several key cytokinesis regulatory proteins and found that Mgc and MKLP1 showed decreased accumulation at the contractile ring coupled with redistribution to the cell cortex in MgcSxNN mutant cells. Because Centralspindlin is not properly focused at the midzone, it cannot deliver Ect2 for RhoA activation or focus the RhoA activity zone. Indeed, we observed an abnormally broad equatorial RhoA activity zone and misregulation of contractile ring proteins that are activated or recruited downstream of RhoA activity. Taken together, our results indicate that Mgc's SxIP motif is required for successful cell division in *Xenopus* embryos (Figure 7).

The effects of the MgcSxNN mutant were not restricted to M-phase. In Cos-7 cells, while a large population of Mgc was nuclear (Figure 2 A and C and Supplemental Figure 2), there was a detectable population of cytoplasmic protein, as well. This could be an artifact of overexpression in the Cos-7 cells; however, in our experiments in *Xenopus* embryos, endogenous Mgc was knocked down and replaced with MgcWT or MgcSxNN at near

endogenous levels. In interphase *Xenopus* epithelial cells, MgcWT localized to apical cell-cell junctions, while MgcSxNN showed reduced junctional localization. This suggests that Mgc's interaction with EB1 at the plus ends of MTs is required for Mgc's delivery to cell-cell junctions. Indeed, this is consistent with previous work showing that junctional localization of Centralspindlin was MT-dependent in cultured epithelial cells; the junctional localization of both Centralspindlin and its binding partner Ect2 were reduced when cells were treated with nocodazole to depolymerize MTs[71]. Because we had found previously that Mgc regulated adherens junction, but not tight junction structure[28] we focused the present study on adherens junction proteins. We compared the localization of several key adherens junction proteins and found a significant decrease in β-catenin and E-cadherin at apical junctions in MgcSxNN mutant cells. Our results demonstrate that Mgc's SxIP motif is also required for proper adherens junction structure (Figure 7).

EB1 and its homologs are the core components of the +TIP network of proteins that bind to the plus ends of microtubules. EB1 can autonomously recognize growing MT ends and recruit other +TIP proteins to growing MT ends[56,122]. Proteins recruited to MT plus ends can anchor MTs to specific cellular structures and control MT dynamics, including those during cytokinesis[56,123]. Our data has identified Mgc as a new +TIP that is tethered to EB proteins via its SxIP motif and regulates both MT dynamics and attachment to the cortex, in addition to its known functions during cytokinesis and interphase. Our data strongly support the notion that Mgc's SxIP motif directly binds to EB1 (and other EB proteins) and the SxNN mutation disrupts this binding. However, further biochemical studies will be required to determine binding conditions during different phases of the cell cycle.

MTs targeting the equatorial cortex are thought to be important for delivering the cleavage furrow-stimulating signal and may be uniquely stabilized by an unknown mechanism, allowing them to fulfill this role[7,119–121]. Our data suggest that Centralspindlin is not only localized on these individual equatorial astral MTs but may also help stabilize them. Centralspindlin is critical for delivering the furrow-inducing signal because it recruits, focuses, and may activate the GEF Ect2[21,22,69,88]. By concentrating Ect2's GEF activity at the equatorial cell cortex, Centralspindlin delivers the signal that locally stimulates cortical RhoA activity, which in turn activates formation of the contractile ring. Our *in vivo* data show that Mgc localizes strongly to the plus ends of astral MTs during anaphase and appears to tether the MTs to the cell cortex (Figure 1 A-C). This observation is consistent with a previous study in HeLa cells, which found that both MKLP1 and Mgc localize to the plus ends of astral MTs that point to the equatorial cortex during early anaphase[23].We observed a striking redistribution of Mgc localization to the cell cortex when Mgc's SxIP motif was mutated to SxNN (Figure 4 A-C). Note that we still observe a significant population of MgcSxNN at the cell equator; this is not surprising because the MgcSxNN mutant should still be able to interact with MKLP1 and bundle overlapping MTs. Further, we found that MgcWT co-localizes with EB3 comets, while an Mgc mutant with a mutated SxIP motif does not (Figure 2 A-E). These results suggest that Mgc's SxIP motif mediates binding to EB +TIP proteins. This would allow Mgc to remain tethered to the MT plus end and interact with the plasma membrane, presumably through its C1 domain[29], thus maintaining a stable attachment to the MT and the cortex.

MgcRacGAP has traditionally been thought to function primarily during M-phase to bundle the central spindle MTs[18,19,135], and regulate RhoA signaling at the cortex[15,28,68,69].

However, recent work has shown that Mgc serves a dual function in epithelial cells throughout the cell cycle. Mgc regulates the apical actomyosin belt that encircles epithelial cells by modulating Rho GTPase activity at cell-cell junctions[28,46,72]. Our previous work showed that Mgc regulates the integrity of adherens junctions, specifically by modulating RhoA activity[28]. Similarly, another study found that Centralspindlin and Ect2 localize to adherens junctions, and that Ect2 localization was dependent upon Mgc and dynamic MTs[46]. Our study builds on this work by showing that Mgc's interaction with EB proteins at MT plus ends is important for its efficient delivery to cell-cell junctions.

The ability of a cell to precisely regulate the subcellular localization of proteins that modulate Rho GTPase activity in specific cellular functions is crucial. Mgc is an important regulator of both cytokinesis and cell-cell junctions. Our work shows that Mgc's SxIP motif provides a means of efficient Centralspindlin delivery to localized sites of action at the equatorial cell cortex during cytokinesis and at apical cell-cell junctions. Key questions that remain to be answered include the binding requirements of Mgc and EB1, the precise function of Mgc as an adaptor between stable MTs and the cortex during cytokinesis, whether Mgc's binding to EB proteins may be regulated by phosphorylation in the vicinity of the SxIP motif, and whether Mgc binding to EB proteins stabilizes the dynamics of specific populations of MTs.

V. Materials and methods

DNA constructs, mRNA preparation, and MgcRacGAP morpholino. pCS2+/*Xenopus laevis* MgcRacGAP and MgcRacGAP-3XGFP were described previously[15] The MgcSxNN mutant was generated by QuikChange (Stratagene, San Diego, Ca) site-directed mutagenesis. The RhoA-

GTP probe (GFP-rGBD)[28], Anillin-3xGFP[45], MKLP1-3xGFP[15], EB3-mChe[136], pCS2+/mChe-UtrCH (probe for F-actin)[87], pCS2+/mChe-membrane and pCS2+/GFP-membrane[45], pCS2+/mChe-H2B (probe for DNA)[45] and pCS2+/2XmChe-EMTB, (probe for microtubules)[116] were all described previously. To generate the Mgc-mNeon constructs, MgcWT or MgcSxNN were cloned into the mNeonGreen vector (Allele Biotechnology, San Diego, CA) using BglII and EcoR1 restriction sites. mRNAs were transcribed *in vitro* from pCS2+-based vectors using the mMessage mMachine SP6 kit (Ambion, Waltham, MA). Antisense MOs (Gene Tools) that target the 5' UTR of *Xenopus laevis* MgcRacGAP were described previously[15].

Antibodies. A *Xenopus*-specific polyclonal MgcRacGAP antibody was described previously[15]. Other antibodies used were anti-β-catenin (Abcam, Ab2365), anti-E-cadherin (DSHB, 5D3-c), anti-GFP (clone JL-8, Clontech no. 632381 [mouse] and Invitrogen, A-6455 [rabbit]), anti-mCherry (abcam, no. Ab167453 [mouse] and Ab167453 [rabbit]), anti-α-tubulin (DM1A, Sigma no. T9026), and anti-phospho-myosin light chain (P-MLC) (Cell Signaling Technologies, no. 3671). Secondary antibodies for immunofluorescence were Alexa 488 or Alexa 568-conjugated anti-mouse or anti-rabbit (Invitrogen).

***Xenopus* embryos and microinjections.** All studies with *Xenopus laevis* embryos were conducted in compliance with the US Department of Health and Human Services Guide for the Care and Use of Laboratory Animals and were approved by the University of Michigan IACUC. *Xenopus laevis* embryos were collected, fertilized, and dejellied as described previously[28,45]. Embryos were stored at 15°C or 17°C in 0.1X MMR (1X MMR = 100 mM NaCl, 2 mM KCl, 2 mM CaCl$_2$, 1 mM MgCl$_2$, 5 mM Hepes, pH 7.4). Embryos were microinjected using a Microinject-1000 microinjector (BTX/Harvard Apparatus) with embryos in a mesh bottom dish filled with

0.1X MMR with 5% ficoll. Knock down and replacement experiments and mosaic injections were described previously[28]. For overexpression experiments, embryos were injected at either the two- or four-cell stage with 5 nl of Mgc-3xGFP (1.66 µg/ml needle concentration) and allowed to develop to blastula stage (Nieuwkoop and Faber stages 6–8). Needle concentrations for other mRNAs were as follows: Mgc-3xGFPs (1 µg/ml for gastrula), GFP-rGBD (25 µg/ml), mChe-membrane (10 µg/ml), GFP-membrane (10 µg/ml), mChe-H2B (20 µg/ml), mChe-UtrCH (10 µg/ml for gastrula, or 0.71 mg/ml for blastula imaging), Anillin-3xGFP (20ug/ml), MKLP1-3xGFP (1 ug/ml).

Immunofluorescence staining. For fixed staining, embryos at gastrula stage (Nieuwkoop and Faber stage 10-11) were fixed and stained as described previously[28]. Briefly, embryos were washed in PBS then fixed with 2% TCA in PBS for 2 h at room temperature. Embryos were bisected keeping the animal hemisphere, transferred to 0.6 ml eppindorf tubes, and permeabilized in PBS + 1-2% Triton-X-100 (PBST) for 20 min at room temperature. Embryos were then blocked with PBST + 5% fetal bovine serum (Invitrogen, no. 10082-139) for 1 h at room temperature. Embryos were incubated with primary antibodies in blocking solution overnight at 4-10°C, or for 4 hours at room temperature with gentle shaking. Embryos were washed in blocking solution (5 min, 15 min, 2 x 1 h) then incubated in secondary antibody overnight at 4°C. Embryos were washed as above, then stained with 10 µg/ml DAPI (Invitrogen, D1306) diluted in TBSN or 1XPBS for 30 min at room temperature. Embryos were mounted in Vectashield mounting medium (Vector Laboratories, H-1000) just prior to imaging. Antibody concentrations used were: anti-α-tubulin (1:50), anti-Mgc (1:600), anti-β-catenin (1:200), anti-E-cadherin (1:200), anti-phospho-myosin (1:200), anti-GFP (1:200), and anti-mChe (1:200).

Alexa conjugated secondary antibodies were used at (1:200).

For fixed staining of tubulin or P-MLC, albino embryos were injected as described above, then gastrula stage embryos (stage 10-11) were washed three times with PBS and fixed overnight at room temperature in 3.7% formaldehyde, 0.25% glutaraldehyde, 0.2% Triton-X-100 in buffer containing 80 mM K- PIPES, 5 mM EGTA and 1 mM MgCl$_2$, pH 6.8. Embryos were quenched for 6 h (tubulin staining) or 1 h (P-MLC staining) with gentle shaking at room temperature in PBS containing 100 mM sodium borohydride, rinsed once in PBS, bisected keeping the animal hemisphere, and transferred to 0.6 ml eppindorf tubes. Embryos were blocked with TBS + 10% FBS, 5% DMSO, and 0.1% NP40 for 4 h at 4°C, changing the solution 2-3 times during blocking. A volume of 450 μl of the appropriate solution was added to the tubes for this and all subsequent steps. Embryos were incubated with primary antibodies in blocking solution overnight at 4°C on a nutator, washed with blocking solution (5 min, 15 min, 2 h, overnight at 4°C), incubated with secondary antibodies in blocking solution overnight at 4°C, washed with blocking solution (5 min, 15 min, 2 h, overnight at 4°C). Embryos were stained with 10 μg/ml DAPI diluted in TBSN for 30 min at room temperature. Embryos were then dehydrated using a dilution series of TBSN:MeOH (one 10 min wash of each: TBSN:MeOH 4:1, 1:1, 1:4, then 100% MeOH), cleared with Murray's Clear (1:2 mixture of Benzyl Alcohol:Benzyl Benzoate), and mounted for imaging.

Live and fixed confocal microscopy. Images were collected on an Olympus Fluoview 1000 confocal microscope with FV10-ASW software equipped with a 60X supercorrected PLAPON 60XOSC objective (NA = 1.4, working distance = 0.12 mm). For live imaging, intact gastrula stage (Nieuwkoop and Faber stage 10-11) embryos were mounted in custom chambers that consisted of a metal slide ~0.8 mm thick with a ~0.5 cm hole in the center to which a coverslip was affixed

with a thin layer of vacuum grease (Dow Corning high vacuum grease). We use 0.17mm glass

coverslips, (Warner, 22 x 22 mm), which are of an optimized thickness for the 60X

supercorrected objective. Embryos were transferred into the chamber in 0.1XMMR, and a

second coverslip was placed over the embryos and gently pressed down and affixed with a thin

layer of vacuum grease. Fixed imaging was carried out as described previously [45].

Cell culture and transfection. COS-7 cells (monkey kidney fibroblasts) were grown in DMEM+

10% (vol/vol) FBS and 2 mM L -glutamine at 37 °C with 5% (vol/vol) CO^2. Cells were co-

transfected with 1 ug of plasmid DNA (0.5 ug of EB3-mChe and 0.5 ug of either MgcWT-mNeon

or MgcSxNN-mNeon) using Expressfect (Danville Scientific). Cells were allowed to express for

18-22 hours, then were processed for microscopy.

Total Internal Reflection Fluorescence Microscopy. Images for individual MT dynamics were

acquired using a Nikon TiE/B microscope with a 100X 1.49 NA oil immersion TIRF objective

(Nikon, Melville, NY) equipped with three 20 mW diode lasers (488 nm, 561 nm, and 640 nm)

combined into a single fiber and controlled via AOTF (Agilent, Santa Clara, CA). Images were

collected via an EMCCD detector (iXon X3 DU897, 512 × 512, 16 μm array; Andor, Belfast, UK).

For imaging in green and/or red, the microscope used a dual-band laser polychroic mirror

(ZT488/561rpc; Chroma Technology, Rockingham, VT), a dual-band sputtered emission filter

(ZET488/561m; Chroma), and a dual-band sputtered cleanup filter (ZET488/561×; Chroma), and

either a 488 nm (10-15% mW power) or 561 nm (10-15% mW power) laser was used for TIR-

based illumination. Images were acquired with 50 ms exposures, and image acquisition was

controlled by Nikon Elements software.

Quantification and analysis.

Kymograph generation and analysis: Kymographs were made in ImageJ from raw data using the Multiple Kymograph plug-in (width = 3). The segmented line tool (line width = 1) was used to trace the outline of an EB3-mChe comet in a single channel image. The line segment ROI was saved to ROI manager so the same line could be generated in the Mgc-mNeon channel. The intensity of Mgc-mNeon (Figure 2E) was determined in ImageJ. The channels were split and synchronized, then the freehand line tool was used to draw a line in the mNeon channel (10 pixels wide) that followed the EB3-mChe comet exactly. A background line (100 pixels long) was drawn on the MT lattice behind the plus end. Normalization was achieved by subtracting the background line from the mNeon intensity line. EB3-mChe run length (Figure 2F) was determined by observing EB3-mChe comets for the duration of a 30s live movie (0.103 s interval between frames). The starting frame number where an EB3 comet was first observed was subtracted from the ending frame number. Only comets that started after frame #2 were counted. EB3 velocity (Figure 2G) was determined using the ImageJ velocity measurement tool and raw data kymographs.

Percent multinucleation measurements. Using Volocity software (PerkinElmer, Waltham, MA) the percent multinucleation was determined by first counting the number of cells per 230 µm x 230 µm image. The DAPI channel was used to count how many cells displayed a single nucleus, or 2 or more nuclei by scanning through the volume of the cell; only cells where nuclei could be clearly observed were included in the analysis. The percent multinucleation was calculated as the percentage of cells that contain 2 or more nuclei.

Percent of asymmetric cell division. Live movies of cell division were analyzed using Volocity. The pole to pole length of each dividing cell was measured at the widest part of the cell perpendicular to the cleavage furrow at 50% ingression. A cell was determined to have symmetric division if the cleavage furrow was positioned within 4 μm on either side of the measured middle of the cell. Cells in which the cleavage furrow was positioned away from the center axis (more than 4 μm from either side of the middle) were considered to have asymmetric division.

Quantification of astral microtubule intensity. Astral MT intensity was measured using ImageJ. Intensity was measured from four lines and averaged; two 40x160 pixel lines were placed in the cytosol parallel to the spindle and two 40x80 pixel lines were placed in the cytosol just adjacent to the spindle poles. Another 40x80 pixel line was placed in the cytosol away from the spindle to measure background intensity. Normalization was achieved by subtracting the background intensity from the average intensity for each cell. Only metaphase cells were measured.

Quantification of Mgc-3xGFP and MKLP1-3GFP. The intensity of Mgc-3xGFP or MKLP1-3xGFP along the contractile ring at 25 % cleavage furrow ingression was determined in ImageJ by drawing a line (width 20 pixels) that encompassed the furrow from side to side, but did not contain membrane signal. The same sized line was drawn in both polar regions of the cell and the average polar value was determined. Normalization was achieved by subtraction of a background intensity line from both lines described above.

Quantification of RhoA-GTP intensity at the cleavage furrow. Live movies of dividing cells just after anaphase onset were analyzed using Volocity. Only frames where the initial appearance of

F-actin at the contractile ring was detected were used for the analysis. The intensity of RhoA-GTP at the equatorial cortex was measured by line scans of early anaphase cells; two separate 175 pixel long lines (1 pixel wide), along the cell membrane of both sides of the developing furrow, were measured for each cell. Another 175 pixel line was placed in the cytosol in the polar region of the cell to measure background intensity. Normalization was achieved by subtracting the background intensity from the average furrow intensity for each cell.

Measurements of F-actin intensity at the cleavage furrow. Live movies of dividing cells at 25 % cleavage furrow ingression were analyzed using Volocity. The width of each cell was measured, then two separate line scan measurements were taken across the width of the F-actin zone (175 pixels long x 1 pixel wide, right and left side of zone, 5-10 pixels away from the membrane) and averaged. Another 175 pixel line was placed in the cytosol in the polar region of the cell to measure background intensity. Normalization was achieved by subtracting the background intensity from the average intensity for each cell.

Full width at half max (FWHM). The RhoA-GTP and F-actin normalized line scans described above were used for the FWHM analysis (normalized for background fluorescence intensity). For each cell included in the analysis, the normalized averaged line scan was imported into ImageJ. Using the curve fitter function, a Gaussian Curve was fit to each data set. The subsequent c-value of each Gaussian were used to find the FWHM. The FWHM value of each cell was divided by the individual cell size, measured as the longest cell width perpendicular to the cleavage furrow. The size normalized FWHM values were used to plot a box and whiskers graph. Statistics were performed using the individual FWHM values.

P-myosin intensity at the Contractile Ring and Junctions of dividing cells. Images of fixed dividing cells were analyzed in FIJI. For contractile ring measurements, a 3 pixel wide line was drawn along the contractile ring and the average intensity was measured. Junctional intensity was measured by using the freehand line tool to draw a 3 pixel wide line along the junction of each half of the dividing cell, beginning and ending at both ends of the contractile ring. The average intensity of the two junction lines were averaged. A 5x5 pixel circular ROI was measured in the center of each cell as a background intensity value. Normalization was achieved by subtracting the background intensity of each cell from the contractile ring measurement of the corresponding cell. Background was also subtracted from the averaged junctional measurement. The junctional/contractile ring ratio was calculated for each condition.

Intensity line scans of junctional proteins. Side views of fixed embryos were analyzed in ImageJ using the freehand line function (line width = 10 pixels). A line was drawn along the apical to basal axis of a cell-cell junction, and the corresponding intensity values were recorded. A background intensity line was drawn adjacent to each cell-cell junction. Normalization was achieved by subtracting the background intensity from the junction intensity for each cell-cell junction included in the analysis.

Box-and-whisker plots. When data are presented as box-and-whisker plots, the whiskers represent the minimum and maximum, the top of the box represents the 75th percentile, the bottom of the box represents the 25th percentile, and the horizontal bar represents the median.

Statistical analysis. Unpaired Student's t-tests were used to determine statistical significance of each group pairwise compared to either control or to MO+WT as indicated. Statistics were calculated in GraphPad Prism software.

VI. Acknowledgements

[*]Current address: Stratos Genomics, Seattle, WA 98121

[†]Department of Cell and Developmental Biology, University of Michigan, Ann Arbor, MI 48109

[°] Department of Molecular, Cellular, and Developmental Biology, University of Michigan, Ann Arbor, MI 48109

Figure 2.1
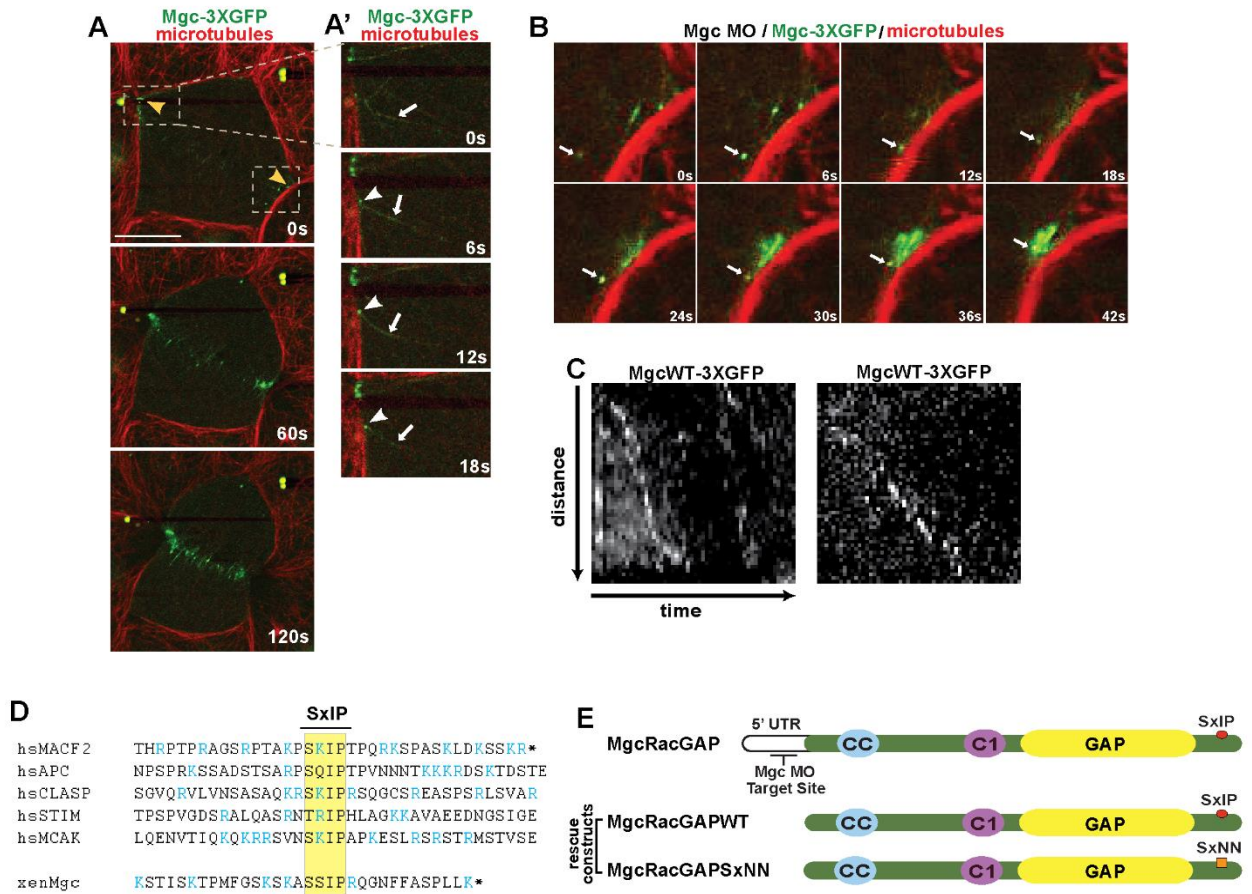
Figure 2.1 MgcRacGAP localizes to microtubule plus ends at the equatorial cortex as cytokinesis initiates. (A) Still images from time-lapse movies of *Xenopus* embryos co-injected with Mgc MO+Mgc-3xGFP and a probe for MTs (2xmChe-EMTB), showing Mgc-3xGFP (green) localization along MTs (red) at the equatorial cell cortex (yellow arrow-heads) prior to cytokinesis. The dashed boxes indicate regions that are enlarged in A' and B. The frames in A' show Mgc-3xGFP puncta decorating astral MTs (white arrow) and stabilized at MT plus tips (white arrowheads). scale = 20 μm. (B) Enlargements of the dashed box at the lower right in A. Mgc-3xGFP puncta show directed movement (white arrows), apparently along MTs (red), as they form clusters at the equatorial cell cortex. (C) Kymographs from a line drawn in the direction of Mgc-3xGFP movement illustrate directed transport of Mgc clusters over time. (D) Amino acid sequence alignment surrounding the SxIP motif (yellow box) of five known EB1-binding proteins and the carboxyl-terminus of *Xenopus* Mgc. Basic arginine (R) and lysine (K) amino acids are shown in blue. (E) Mgc domain diagram showing the knockdown and replacement strategy. Endogenous Mgc is knocked down with MOs that target the 5' UTRs, while replacement Mgc constructs do not contain the endogenous 5' UTR sequence, so they are not targeted by the MOs. The location of Mgc's putative SxIP motif and the SxNN mutant construct are indicated.

Figure 2.2
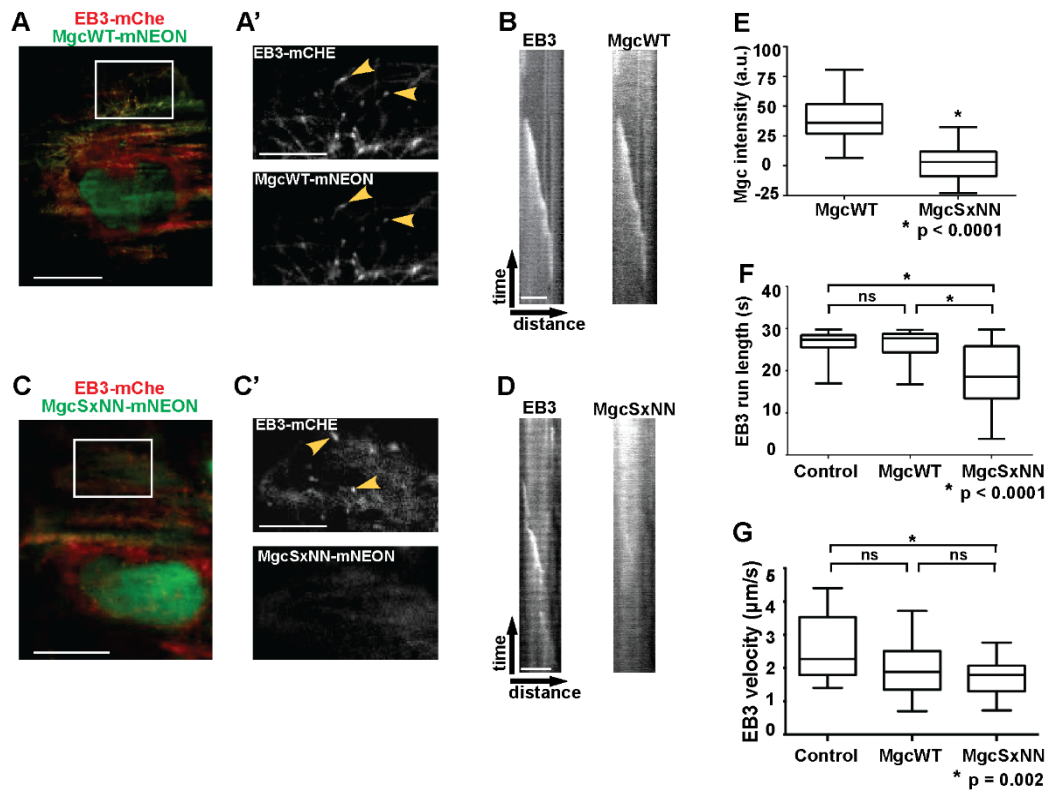
Figure 2.2 MgcRacGAP tracks with EB3 at growing microtubule plus ends. (A) TIRF microscopy image of a Cos-7 cell transfected with EB3-mChe (red) and MgcWT-mNeon (green). scale = 20 μm. (A') A zoomed in view of the boxed region from (A) showing EB3-mChe and MgcWT-mNEON accumulate on the plus tips of microtubules (yellow arrowheads). Scale = 5 μm (B) Representative kymographs traced along an EB3-mChe comet from TIRF images of Cos-7 cells co-expressing EB3-mChe and MgcWT-mNeon. Single channel kymographs are shown. The total time represented is 6.5 s, scale = 4.3 μm. (C) TIRF microscopy image of a Cos-7 cell expressing EB3-mChe (red) and MgcSxNN-mNeon (green). (C') A zoomed in view of the boxed region from (C) showing EB3-mChe comets (yellow arrowheads) and lack of corresponding signal in the MgcSxNN-mNEON cell. Scale = 5 μm (D) Representative kymographs traced along an EB3-mChe comet from TIRF images of Cos-7 cells co-expressing EB3-mChe and MgcSxNN-mNeon. Single channel kymographs are shown 6.5 s, scale = 4.3 μm. (E –G) Box and whiskers plots showing quantification of: (E) Mgc-mNeon intensity at growing MT plus ends. n = # of kymographs used in analysis, # of cells (MgcWT = 25, 9) and (MgcSxNN = 24, 8); (F) EB3-mChe run length on MT plus ends. n = # of EB3 comets analyzed, # of cells: (Control = 35, 7); (MgcWT = 50, 10); (MgcSxNN = 50, 10). (G) Velocity of EB3-mChe comets. n = # of EB3 comets, # of cells: (Control = 15, 7); (MgcWT = 17, 9); (MgcSxNN = 17, 9). All n values represent 3 independent experiments. See materials and methods for additional details regarding quantification.

Figure 2.3
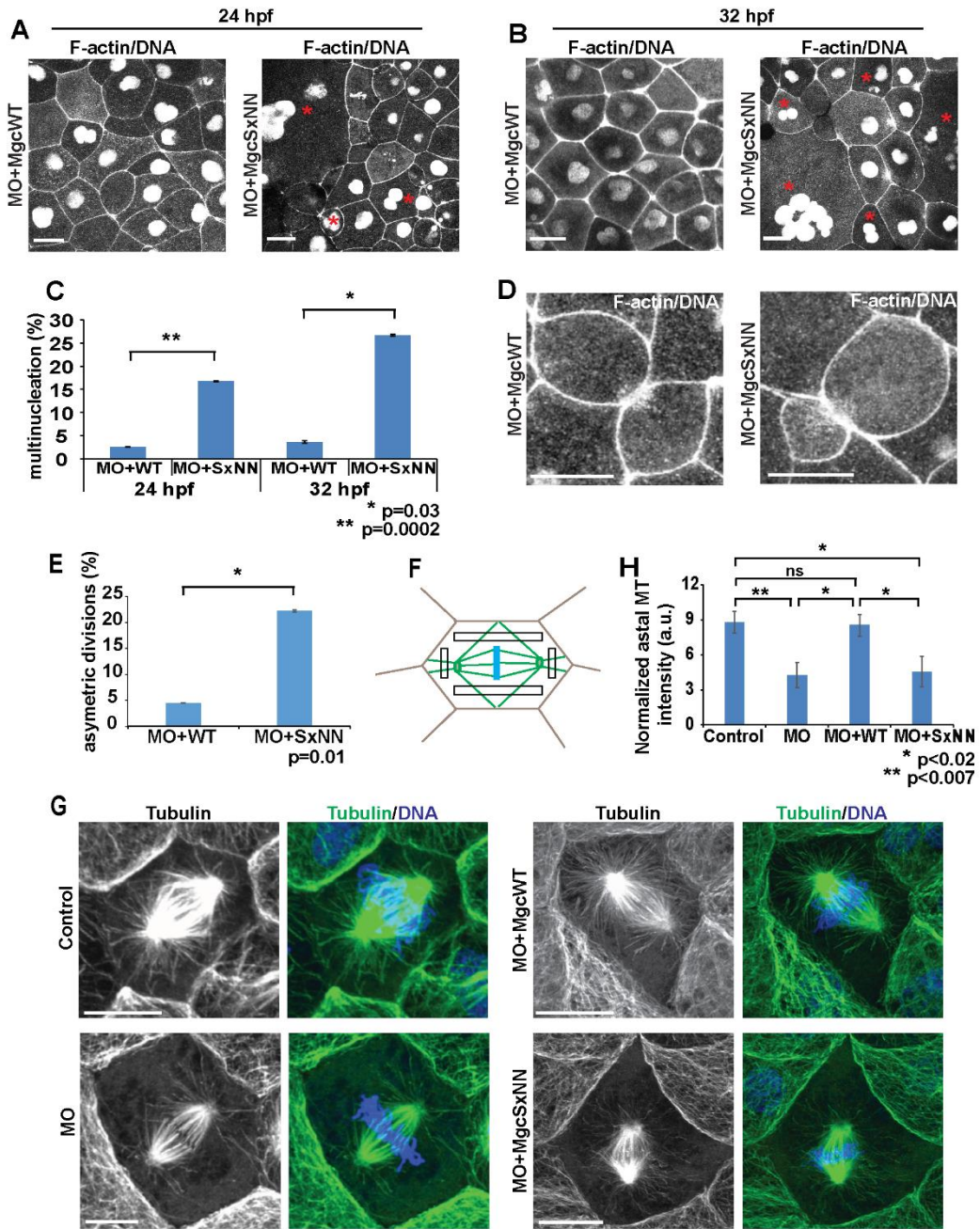
Figure 2.3 MgcRacGAP's SxIP motif is necessary for proper astral microtubule structure and successful cell division. (A) Still images from time-lapse movies of *Xenopus* embryos 24 hours post fertilization (hpf) (Nieuwkoop and Faber stage 10-11). Embryos were co-injected with Mgc MO and either MgcWT or MgcSxNN along with a probe for DNA (mChe-H2B) and a probe for F-actin (mChe-UtrCH). Red asterisks indicate multinucleate cells. (B) Still images from time-lapse movies of *Xenopus* embryos 32 hpf (Nieuwkoop and Faber stage 13-14), injected as described in (A). Red asterisks indicate multinucleate cells. (C) Quantification of the percent of multinucleate cells in MO+MgcWT or MO+MgcSxNN embryos at 24 or 32 hpf. n = # cells, # embryos, # experiments: 24 hpf: MO+MgcWT=230, 13, 5; MO+MgcSxNN=203, 12, 5; 32 hpf; MO+MgcWT=109, 3, 1; MO+MgcSxNN=60, 4, 1. (D) Still images from time-lapse movies of Xenopus embryos 24 hpf injected as in A showing symmetric (MO+MgcWT) and asymmetric (MO+MgcSxNN) divisions. (E) Quantification of the percent of asymmetric cell divisions in MO+MgcWT or MO+MgcSxNN embryos. n = # cells, # of embryos: MO+MgcWT=45, 12; MO+SxNN=63, 8. (F) Illustration of astral MT intensity quantification strategy. Intensity measurements were taken from the boxed regions and averaged for each cell (see materials and methods). (G) Images of fixed *Xenopus* embryos that were co-injected with a lineage tracer (mChe-farnesyl, not shown) along with MO alone, MO+MgcWT, or MO+MgcSxNN, then fixed at 24 hpf and stained with anti-tubulin antibodies to reveal MTs and DAPI to label DNA. (H) Quantification of astral MT intensity, normalized to cytosol background. n= # of cells, # of embryos: Control =7, 6; MO=7, 7; MO+MgcWT=7, 6; MO+MgcSxNN= 8, 6. SEM is shown. Scale bars: (A-C) = 25 μm, (D) = 10 μm. All n values represent 3 or more independent experiments unless otherwise indicated.

Figure 2.4
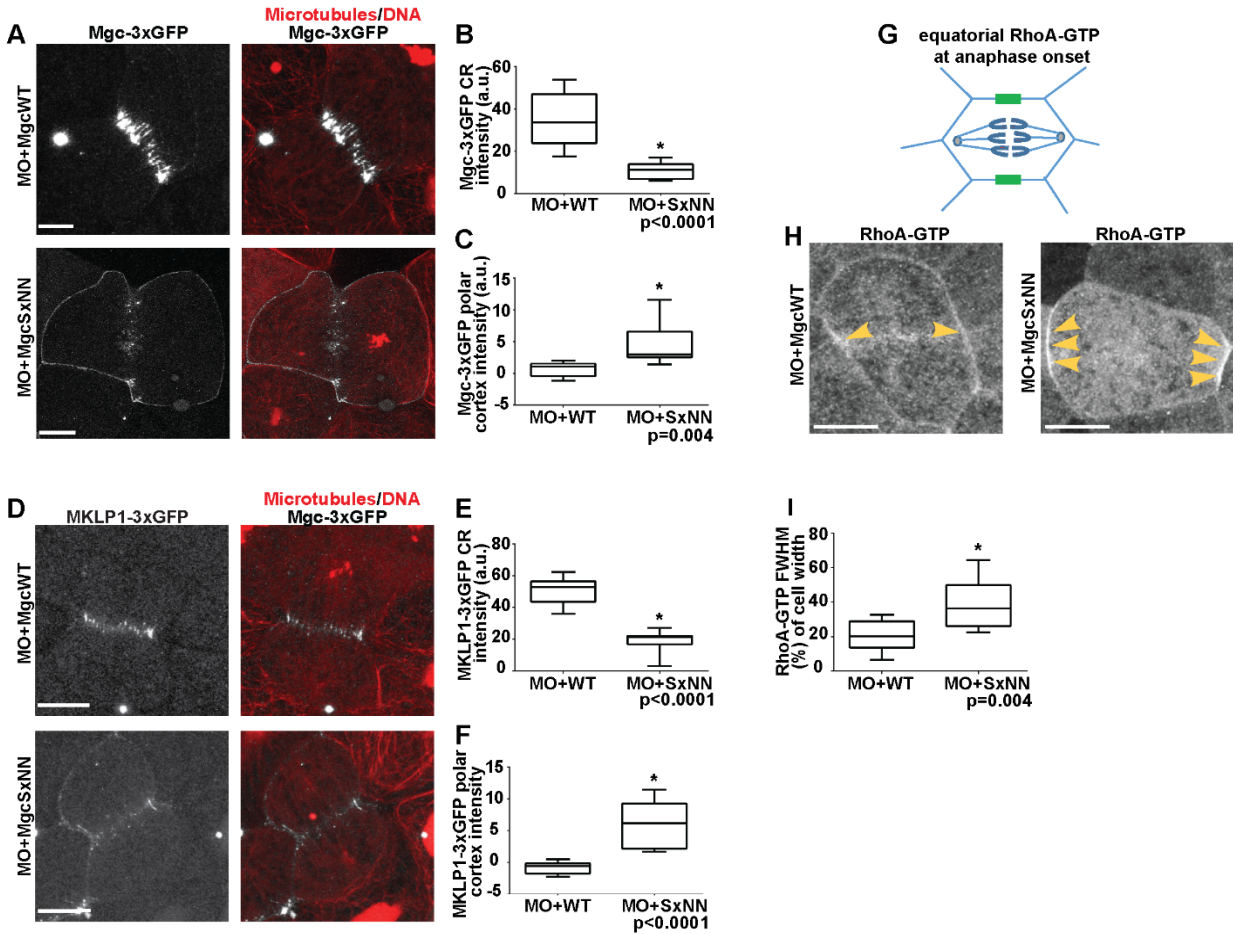
Figure 2.4 Mutation of MgcRacGAP's SxIP motif disrupts localization of the Centralspindlin complex and the equatorial accumulation of RhoA-GTP. (A) Still images from live movies of *Xenopus* embryos 24 hpf (Nieuwkoop and Faber stage 10 -11) co-injected with MO+MgcWT-3xGFP or MO+MgcSxNN-3xGFP (grey), a probe for MTs (red), and a probe for DNA (red). (B) Quantification of the normalized Mgc-3xGFP intensity across at the contractile ring. n = # cells: MO+MgcWT, 10; MO+MgcSxNN, 8. (C) Quantification of the normalized Mgc-3xGFP intensity along the polar cortex of dividing cells. n = # cells: MO+MgcWT, 9; MO+MgcSxNN, 10. (D) Still images from live movies of Xenopus embryos 24 hpf co-injected with MO+MgcWT or MO+MgcSxNN, along with MKLP1-3xGFP (grey), a probe for MTs (red), and a probe for DNA (red). (E) Quantification of the normalized MKLP1-3xGFP intensity across at the contractile ring. n = # cells: MO+MgcWT, 8; MO+MgcSxNN, 8. (F) Quantification of the normalized MKLP1-3xGFP intensity along the polar cortex of dividing cells. n = # cells: MO+MgcWT, 8; MO+MgcSxNN, 8. For B-C and E – F, quantification was done at 25% cleavage furrow ingression. (G) Quantification scheme illustration for RhoA-GTP equatorial accumulation during early anaphase. (H) Still images from time-lapse movies of Xenopus embryos 24 hpf that were co-injected with Mgc MO and either MgcWT or MgcSxNN along with a probe for active RhoA (GFP-rGBD) and a probe for DNA (mChe-H2B) as a lineage tracer. Yellow arrowheads show RhoA-GTP accumulation along equatorial cell cortex during anaphase onset. (I) Full width at half maximum (FWHM) quantification of the breadth of RhoA-GTP accumulation at the equatorial cortical membrane during early anaphase. Line scans along the RhoA-GTP signal were generated and normalized to background intensity. The FWHM value was found by fitting a Gaussian curve to the line scan data. Each FWHM value was normalized to cell size, measured as the longest cell width perpendicular to the cleavage furrow. The FWHM is graphed as a percentage of cell width. n = # cells, # embryos: MO+MgcWT=10,6; MO+MgcSxNN=9,5. Scale = 10 µm. SEM is shown. All n values represent 3 or more independent experiments.

Figure 2.5
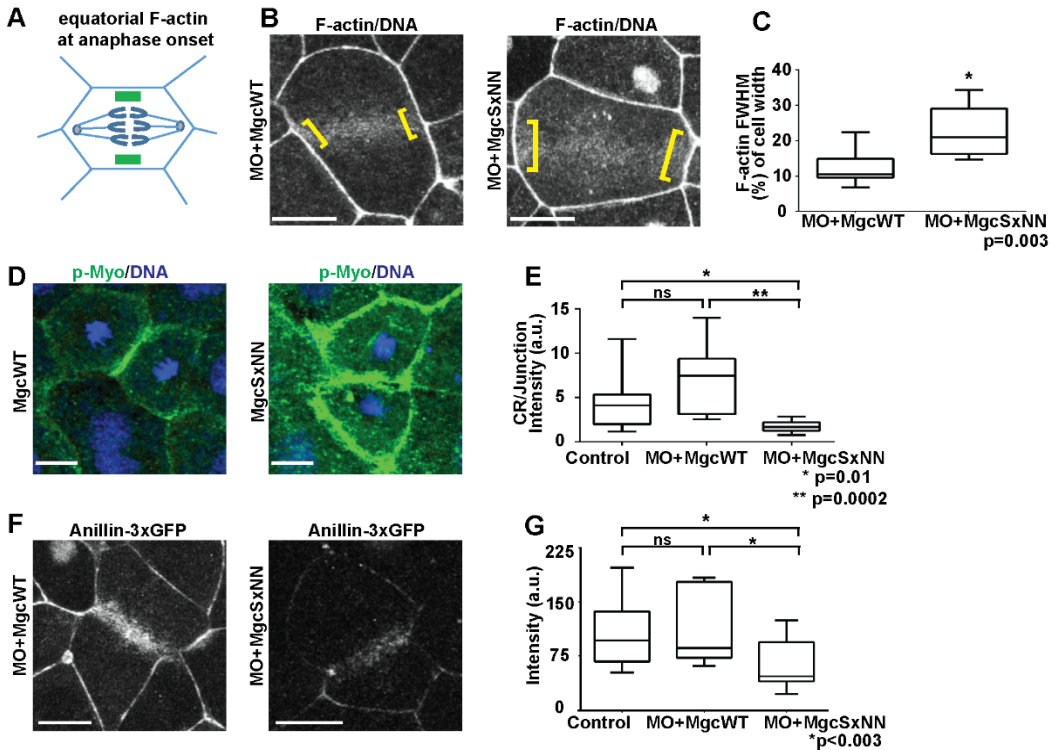
Figure 2.5 MgcRacGAP's SxIP motif is important for the proper regulation of proteins activated or recruited downstream of RhoA-GTP. (A) Quantification scheme illustration for the measurement of F-actin intensity during early anaphase. (B) Still images from live time-lapse movies of *Xenopus* embryos 24 hpf (Nieuwkoop and Faber stage 10 -11). Embryos were co-injected with Mgc MO and either MgcWT or MgcSxNN along with a probe for F-actin (mChe-UtrCH) and a probe for DNA (mChe-H2B) as a lineage tracer. Yellow brackets highlight equatorial F-actin accumulation during early anaphase. (C) Full width at half maximum (FWHM) quantification of the breadth of F-actin accumulation at the equatorial cortex during early anaphase. Line scans along the F-actin signal were generated and normalized to background intensity. The FWHM value was found by fitting a Gaussian curve to the line scan data. Each FHWM value was normalized to cell size, measured as the longest cell width perpendicular to the cleavage furrow. The FWHM is graphed as a percentage of cell width. n = # cells, # embryos: MO+MgcWT=10,6; MO+MgcSxNN=9,5. Scale = 10 μm. (D) Images of Xenopus embryos fixed at 24 hpf. Embryos were co-injected for overexpression studies with MgcWT or MgcSxNN and mChe-membrane as a lineage tracer (not shown), then fixed and stained with an anti-phospho-myosin antibody (green) and stained with DAPI (blue). (E) Quantification of the normalized ratio of phospho-myosin intensity at the contractile ring:cell-cell junction. n = # cells: Control, 8; MgcWT, 6; MgcSxNN, 11. (F) Still images from live time-lapse movies of Xenopus embryos at 24 hpf. Embryos were co-injected with MO+MgcWT or MO+MgcSxNN, Anillin-3xGFP, and a probe for DNA (mChe-H2B) as a lineage tracer. (G) Quantification of the normalized Anillin-3xGFP intensity at the contractile ring at 25 % cleavage furrow ingression. n = # cells: Control, 13; MO+MgcWT, 18; MO+MgcSxNN, 17. Scale = 10 μm. SEM is shown. All n values represent 3 or more independent experiments.

110
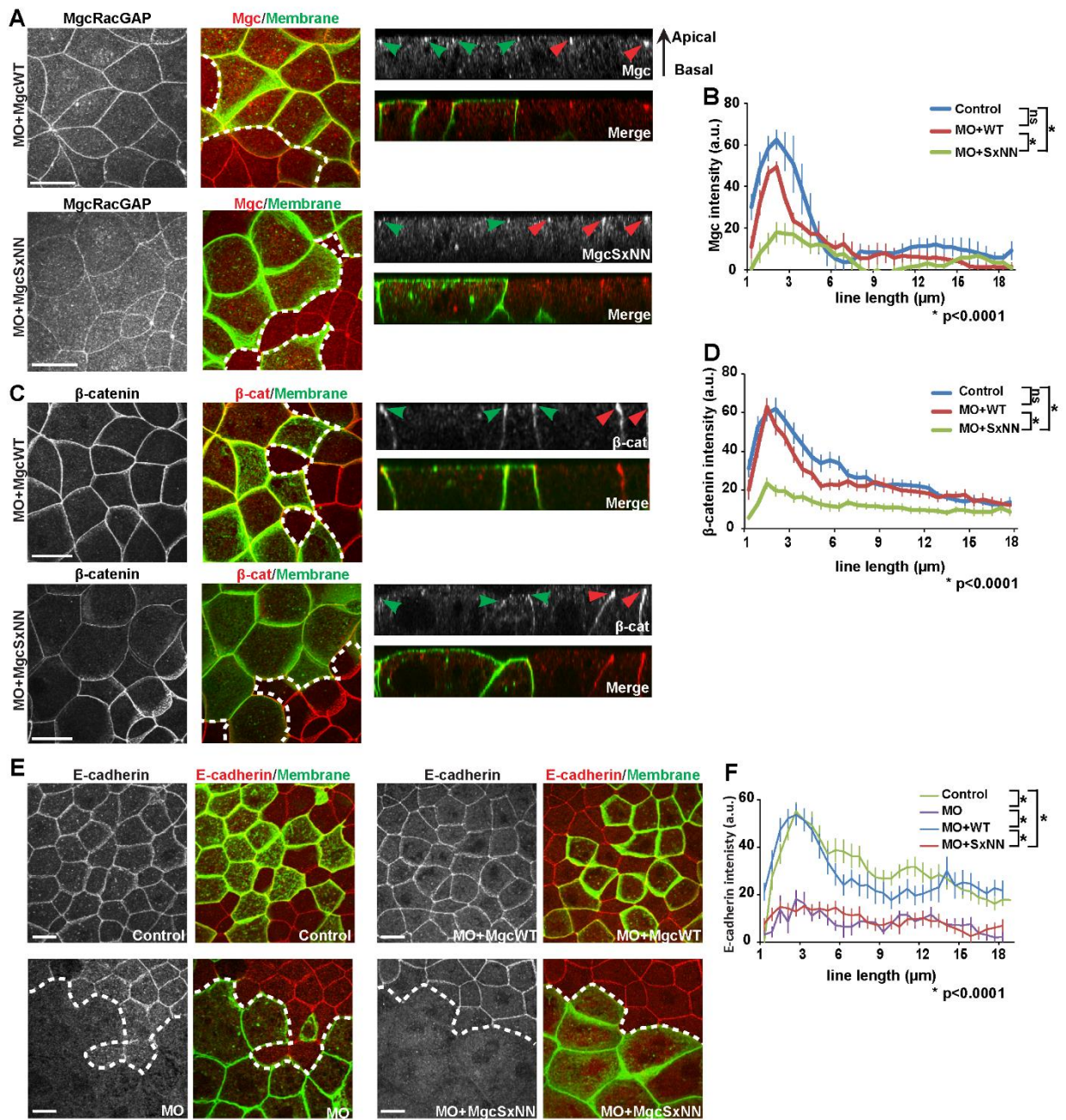
Figure 2.6

Figure 2.6 MgcRacGAP's SxIP motif is necessary for proper adherens junction structure in epithelial cells.
(A, C, E) Fixed en face (left) and side view (right) images of mosaically injected *Xenopus* embryos (Nieuwkoop and Faber stage 10-11). The mosaic injection strategy allows for ~half of the embryo to express the indicated knockdown and replacement construct along with GFP-membrane as a lineage tracer, while the other ~half of the embryo serves as an internal control and is not injected. The dotted white line in the merged en face image represents the boundary between the internal control and injected region of mosaic embryos. Antibodies against GFP and either Mgc (A), β-catenin (C), or E-cadherin (E) were applied to the embryos after fixation. Side views show the localization of the indicated protein along the apical to basal axis of cell-cell junctions (red arrows = internal control regions and green arrows = injected regions). (A) Mgc (red) and GFP-membrane (green). (B) Quantification of the normalized Mgc intensity at bicellular junctions from apical to basal. n = # cells: Control, 13; MO+MgcWT, 14; MO+MgcSxNN, 19. (C) β-catenin (red) and GFP-membrane (green). (D) Quantification of the normalized β-catenin intensity along the bicellular junctions from apical to basal. n = # cells: Control, 17; MO+MgcWT, 16; MO+MgcSxNN, 19. (E) E-cadherin (pseudo-colored red) and mChe-membrane (pseudo-colored green). (F) Quantification of the normalized E-cadherin intensity along the bicellular junctions from apical to basal. n = # cells: Control, 19; MO, 7; MO+MgcWT, 15; MO+MgcSxNN, 19. Error bars represent SEM. Scale bars = 20 μm. All n values represent 3 independent experiments.

Figure 2.7

Centralspindlin accumulation at regions of micro-tubule overlap is assisted by EB binding and results in bundled microtubules.

Centralspindlin accumulates at microtubule plus ends via tethering Mgc to EB1. This regulates Mgc's proper localiza-tion, focused RhoA activity, successful cytokinesis and proper adherens junction structure.

Cells within an epithelium

cell-cell junctions

Supplemental Figure S2.1

Mgc-3xGFP/Microtubules
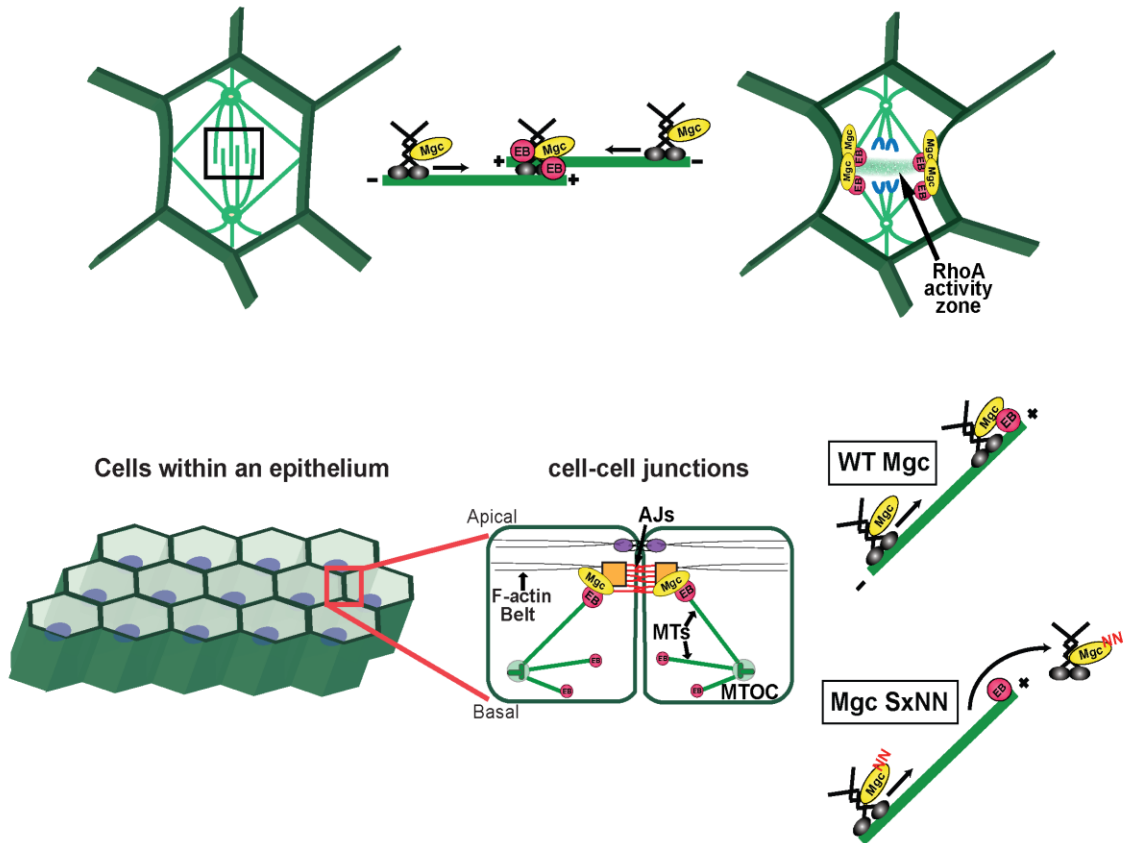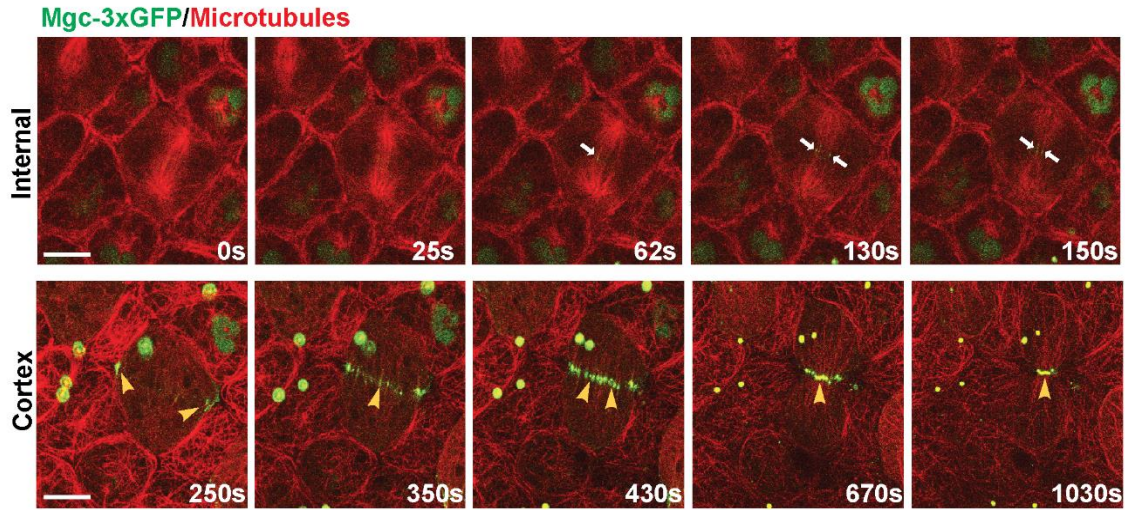
Supplemental Figure S2.1:
Still images from a time lapse movie of cells in a *Xenopus* embryo (Nieuwkoop and Faber stage 10-11) overexpressing MgcWT-3xGFP (green) and a microtubule probe (red). An internal plane (top) is shown to highlight the localization of Mgc to the central spindle (white arrows). A cortical plane (bottom) shows Mgc's anaphase localization to the equatorial cortex (yellow arrowheads). Large green puncta located away from the cell equator represent Mgc localization to midbody remnants. Scale = 40 μm.

Supplemental Figure S2.2
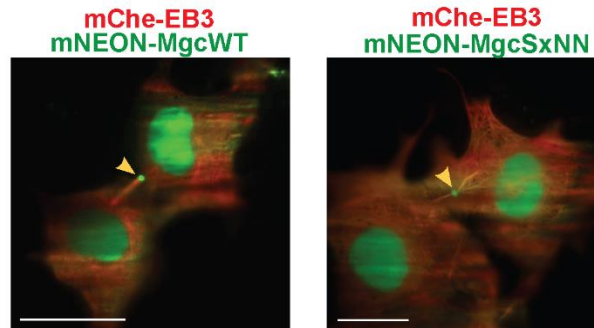
Supplemental Figure S2.2:
TIRF microscopy images of Cos-7 cells expressing mChe-EB3 (red) and MgcWT-mNeon or MgcSxNN-mNeon (green) as indicated. Yellow arrowhead points to mNeon-Mgc accumulation at the midbody in both WT and SxNN cells. Scale = 25 μm.

Supplemental Figure S2.3
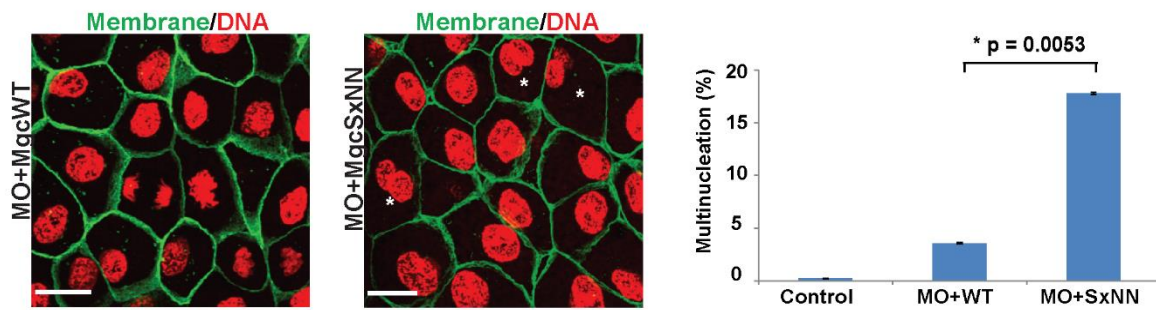
Supplemental Figure S2.3:
Images of fixed *Xenopus* embryos co-injected with MO+MgcWT or MO+MgcSxNN along with GFP-membrane as an injection marker. Embryos were fixed at 24 hpf (Nieuwkoop and Faber stage 10-11) and stained with an anti-GFP antibody (green) and DAPI (pseudo-colored red). Asterisks indicate multinucleate cells. Quantification of the percentage of cells that display multinucleation is shown. n = # cells: Control, 358; MO+MgcWT, 256; MO+MgcSxNN, 224. N values represent 3 independent experiments. SEM is shown.

Supplemental Figure S2.4
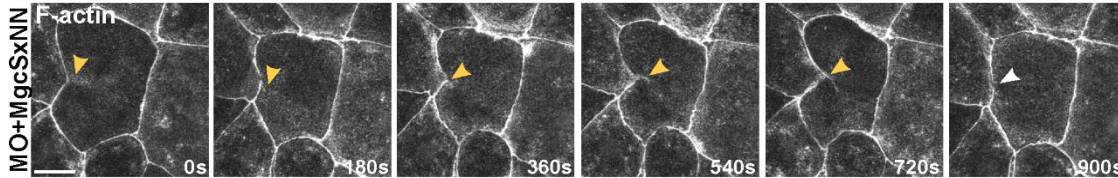
Supplemental Figure S2.4:
Frames from a time-lapse movie from of a *Xenopus* embryo (Nieuwkoop and Faber stage 10-11) co-injected with MO+MgcSxNN, a probe for F-actin (mChe-UtrCH) and a probe for DNA (mChe-H2B). The image sequence shows cleavage furrow ingression then regression in a MO+MgcSxNN embryo. Yellow arrowheads point to slow ingression of the cleavage furrow. White arrowhead points to the regressed furrow. Scale = 20 μm.

Chapter 3: Perspectives and future directions.

Much work has been done to establish the role of Centralspindlin and its GAP component, MgcRacGAP (Mgc), during cytokinesis. However, many unanswered questions remain about the regulation of Centralspindlin, specifically of Mgc's GAP activity, and the role of Mgc at cell-cell junctions. Because Mgc has dual functions during cell division and in controlling epithelial tissue homeostasis, an interesting question emerges as to what role Mgc may play in the misregulation of RhoA or Rac1 in human tumors. These issues will be discussed and speculated upon in the following pages.

I. Regulation of MgcRacGAP's GAP specificity toward RhoA and Rac1.

There have been numerous reports in the literature of Mgc's GAP activity acting toward RhoA or toward Rac1 (described in detail in the introduction)[15,18,19,26,28,69,70], but there has yet to be a unifying mechanism identified that explains the observed discrepancies. Previous work from our lab and others suggest that Mgc is important for the cycling of RhoA to maintain a focused activity zone at the equatorial cortex throughout cytokinesis[15,28,69]. Other groups have shown that Mgc is important for downregulating Rac1 during cytokinesis[26,70]. To further complicate the issue, it was shown that an anaphase specific phosphorylation event within Mgc's GAP domain (S386) switched the GAP specificity from Rac1 to RhoA[27]. However, two recent studies (including my own described in Chapter 1 of this dissertation) found that

116

phosphorylation of MgcS386 did not confer differential GAP activity and was not required for successful cytokinesis[26,28]. Nonetheless, the issue of Mgc's GAP specificity continues to be a controversial topic in the field of cytokinesis, and it is likely that more questions will arise before a definitive answer is found.

Effects of Rho GTPase compensation and RhoGDI.

Due to the complexity of the cellular environment and the precise spatio-temporal nature of Rho GTPase signaling during cell division, it is difficult to investigate GTPase regulation *in vivo*. Modulation of GTPases themselves commonly leads to detrimental effects or compensation from other GTPases, making it hard to interpret experimental results. For example, it was shown in a recent study that the three key Rho GTPases, RhoA, Rac1, and Cdc42, exhibit compensatory effects when the level of any one of them is artificially modulated through siRNA-mediated knockdown or expression of dominant negatives[107]. This study showed that siRNA knockdown of RhoA caused a proportional increase in the protein levels of both Rac1 and Cdc42. Similarly, overexpression of affinity tagged RhoA, Rac1, or Cdc42 resulted in the inability of the endogenous GTPases to bind quanine nucleotide dissociation inhibitors (GDIs)[107]. GDIs bind the prenyl moiety of GTPase proteins and sequester the inactive form in the cytosol. Additionally, they can extract GTPases from the membrane for cytosolic sequesteration[137]. Through these mechanisms, GDIs regulate the stability of the inactive pool of GTPases by protecting them from proteosomal degradation[107]. Thus, GDIs are important Rho regulators that maintain an inactive cytosolic pool of GTPase that can be quickly mobilized for participation in signaling pathways.

It is unclear whether GDIs play a role in dictating GEF and GAP specificity for Rho GTPases. Delivery of a GTPase to the membrane and release by GDI has been shown to precede GEF activation[137], and there is evidence to suggest that different GDI members can control GEF-mediated GTPase activation[138]. However, the extent to which GDIs govern GEF or GAP specificity has not been investigated. Of note, there are three members of the Rho GDI family (GDIα, β, γ), each of which has been shown to exhibit preferential binding to different Rho GTPases[139–141]. Because it has been shown in mammalian cells that the level of GDIα is roughly equivalent to the combined levels of RhoA, Rac1, and Cdc42[107], it is interesting to speculate whether different GDI homologs may have preferential activity during cytokinesis to help control which GTPase is active, and which GEFs and GAPs have access to it. To my knowledge, the effect of GDIs in regulating Mgc's ability to bind RhoA or Rac1 has not been addressed. It has been shown that RhoGDIβ can control the ability of the Rho GEF Vav to activate RhoA[138]. This presents the interesting question of whether GDIs may also play a role in dictating GAP specificity toward RhoA and Rac1. These under-appreciated interactions of GDIs with specific GTPases and GTPase regulators could be a mechanism to help explain the reported differences in Mgc GAP specificity toward GTPases, and will be an important question to address in future studies.

The subcellular localization of GTPases likely contributes to MgcRacGAP's GAP specificity.

Another factor that contributes to Mgc's GAP specificity is the sub-cellular localization of both Mgc and the Rho GTPases it regulates. Active Rho GTPases are localized on the plasma membrane via insertion of their prenyl moiety into lipid bilayer, while inactive GTPases are

sequestered in the cytosol by GDI. How does the cell regulate which part of the plasma membrane the various GTPases will populate? One plausible explanation for this is the preferential insertion of the GTPase into membrane of specific lipid composition. It has been shown that RhoA and Cdc42 localize in DAG-rich lipid zones[142], that RhoA inserts into PIP_2 rich lipid at the equatorial cortex during cytokinesis[143], and that Rac1 binds phosphatidic acid to regulate phosphatidylinositol-5-kinase[144]. Furthermore, there is evidence to suggest that both active and inactive Rac1, in complex with GDI, can bind phosphatidylinositol-5-kinase to help regulate its activity[144]. This presents an interesting question: to what extent does GDI regulate its bound Rho GTPase to insert into membrane of specific lipid composition? Further studies are required to elucidate the mechanisms of lipid preference for GTPase insertion, whether it is controlled by GDI, and how this may dictate the availability of GTPase binding for GEFs and GAPs.

RhoA and Rac1 localization during cytokinesis can vary between cell and tissue types, which has led to conflicting results regarding the specificity of Mgc's GAP activity during cytokinesis. One study showing that Mgc has GAP activity toward Rac1 during cytokinesis was conducted in cultured HeLa cells where Rac1 localizes strongly to the division site, as does RhoA and Mgc[26]. However, in *Xenopus* epithelia, active Rac1 does not localize strongly to the equatorial cortex during division[28]. These differing results must be considered in the context of the cell's adhesive surroundings. In order to undergo cell division, a cultured cell must round up to allow for constriction of the contractile ring, therefore Rac1 must be downregulated to eliminate branched actin and relieve cell-substrate adhesions[26,103]. In contrast, *Xenopus*

epithelial cells adhere tightly to one another along their baso-lateral membrane and must undergo division while maintaining cell-cell junction contacts with neighboring cells.

Another system commonly used to study Rho GTPases and their regulators during cytokinesis is the first division of the *Caenorhabditis elegans* embryo. In this system, the adhesive environment is minimal at best and RhoA activity is focused at the contractile ring (as observed by fluorescent fusion proteins of RhoA effectors[70,145]) and is required for successful cytokinesis[70]. In contrast, Rac1 is not required for cytokinesis as siRNA knockdown of Rac1 shows no apparent cell division defects[70]. Furthermore, studies during the first cell division in *C. elegans* have shown that rather than opposing RhoA activation as a GAP should, Mgc surprisingly promotes RhoA activation[69,70]. Whether this positive activity toward RhoA is direct or indirect remains unknown.

The GTPase specificity differences described in these studies could be attributed to the different forces that are experienced by the cell cortex in a cultured cell, an epithelial tissue, and a single celled embryo. It is logical to surmise that the forces being generated during cytokinesis will have a profound effect on which GTPase functions at different regions throughout the cell, because GTPases can respond to changes in force by modulating the cytoskeleton to maintain homeostasis across the cell cortex[146,147].

In *Xenopus* embryos, our lab has shown that Rac1 does not localize strongly to the division site, but instead localizes to the basolateral cell-cell junctions[28], which serve as the primary adhesive input for epithelial cells. In this context, it is not necessary to downregulate Rac1 at the contractile ring – because it does not strongly localize there. We tested whether

Mgc had GAP activity toward RhoA or Rac1 during cytokinesis by expressing an Mgc GAP-dead mutant, then observing the effects on the active population of RhoA or Rac1 *in vivo* using live cell imaging. This approach allowed us to quantify changes in Rho GTPase activity in space and time. We observed significantly increased active Rac1 accumulation at cell-cell junctions when Mgc's GAP activity was perturbed, but did not observe an effect on Rac1 at the contractile ring. We also observed significant effects on active RhoA at both cell-cell junctions and the equatorial cortex during division in the Mgc GAP-dead mutants. Our data suggest that Mgc's GAP activity acts toward both RhoA and Rac1; RhoA at the equatorial cortex during cytokinesis, and toward both RhoA and Rac1 at cell-cell junctions.

Our data in *Xenopus* embryos contributes to the field of cytokinesis by providing an example of how the adhesive environment (which affects cortical force generation), combined with the subcellular localization of RhoA and Rac1, contributes to the specificity of Mgc's GAP activity. It will be important to follow up on these results to test if and how Mgc's GAP specificity at cell-cell junctions can distinguish between RhoA and Rac1. One possible mechanism for this could be that Mgc binds to specific cell-cell junction proteins that dictate which GTPase it can act upon. Additionally, it will be important to determine whether other local GAPs are involved.

II. Other RhoA GAPs with known roles during cytokinesis and at junctions.

It is well accepted that the conserved GEF Ect2 is essential for RhoA activation during cytokinesis[22,23,46,79,148,149], but as described above, the GAP that regulates RhoA inactivation has been debated for years. While it is clear that Mgc plays a major role in RhoA regulation during

121

cytokinesis[15,28,54,68,69], there are other GAPs that have been reported to regulate RhoA during cytokinesis as well. It is quite possible that these GAPs work in concert to maintain a tightly focused zone of active RhoA at the equator while down regulating RhoA throughout the rest of the cell. Numerous groups have reported that constitutive RhoA inactivation at the cell poles is required for successful cytokinesis[79,116,150]. There are two known mechanisms that regulate RhoA inactivation away from the division site: the centrosomal aster[67,120,151] and the supposed activity of GAP proteins acting at polar regions[115]. Since the GTPase Flux model[15,68] predicts that Mgc downregulates RhoA at the furrow, there could be other GAPs that downregulate RhoA in other sub-cellular locations or that work in concert with Mgc at the furrow.

Function of MP-GAP during cytokinesis

A recent study identified a previously uncharacterized Rho GAP through a screen of 67 predicted human Rho GAPs[115]. This GAP was found to preferentially target RhoA *in vitro,* and localization studies revealed that it was sequestered in the nucleus during interphase and telophase, but was localized to the cortex from prophase through anaphase. Thus, it was named mitotic phase-GAP, or MP-GAP[115]. This study characterized the activity of MP-GAP during cytokinesis in HeLa cells and during the first division of *C. elegans* embryos and found that siRNA knockdown of MP-GAP result in failed cytokinesis (15% for MP-GAP defective vs. 0% for control) and cortical protrusions at the midzone and poles of dividing cells. The researchers tested MP-GAP's GAP specificity *in vitro* using the purified GAP domain in GTP hydrolysis assays, and *in vivo* with RhoA staining in fixed cells. Both of these experiments showed specific GAP activity toward RhoA, which was further verified in an experiment where RhoA activity was abrogated in three different ways in a MP-GAP knockdown background. If MP-GAP acted

toward RhoA *in vivo*, then artificial RhoA inactivation was predicted to rescue the abnormal

cortical protrusions observed in MP-GAP knockdown cells. All three mechanisms to inhibit RhoA

rescued the effects of MP-GAP knockdown. Collectively, this study demonstrated that MP-GAP

is essential for regulating cortical homeostasis during division and for successful cytokinesis.

Further studies are needed to better characterize MP-GAP's role during cytokinesis. I am

particularly interested in whether MP-GAP and Mgc play cooperative or redundant roles at the

equatorial cortex during cytokinesis.

Function of p190RhoGAP during cytokinesis and at cell junctions.

Another GAP that has been shown to have activity toward RhoA is p190RhoGAP. p190 is

a multi-domain protein[152] that has 2 isoforms, p190A and p190B, which are encoded on

different chromosomes[114]. A study in HeLa cells and cultured human mammary cells found that

overexpressed p190A localized to the contractile ring throughout cytokineis[114]. Several years

later, FRET bio-sensors that report active RhoA were used to show that active RhoA co-localizes

with p190 at the cell cortex during cytokinesis[153]. Overexpression studies revealed that p190A

affected the ability of HeLa cells to position the spindle and that multiple cleavage furrows form

then regress when excessive p190A is present[114]. Likewise, a dominant negative version of

p190A caused hyperactive RhoA contractility during cytokinesis, which was rescued in a dose

dependent manner by addition of WT p190A[153]. Later, another study used siRNA knockdown of

p190A to show that it was both necessary for successful cytokinesis and for proper RhoA

activity and localization of RhoA effector proteins[113]. These data are consistent with p190A

acting as a RhoA GAP during cytokinesis. While these are important findings that further our

understanding of RhoA regulation, additional work is need to elucidate the spatio-temporal

nature of p190A's GAP activity during cytokinesis. Future studies could also address whether

p190B or p190A have GAP activity toward Rac1 or Cdc42 *in vivo*, and the cellular consequences

of perturbing both Mgc's and p190A and/or p190B's GAP activity in the same cell. These studies

could help to elucidate the precise mechanism of RhoA regulation by GAP proteins during

cytokinesis.

Less is known about the activity of p190B during cytokinesis, but both p190A and p190B

have been shown to localize to cell-cell junctions[46,154,155] and control RhoA activity via Rac1-

dependent antagonsism[154]. It was shown that p190B translocates to adherens junctions upon

Rac1 activation and directly binds p120 catenin there to modulate junctional RhoA singalling[154].

Several years later, another group was the first to show that Mgc localized to adherens

junctions and that this localization was dependent on dynamic MTs[46]. This group also confirmed

that p190B localized to adherens junctions but only in the presence of nocodozole, suggesting

that dynamic MTs inhibited its localization. This was an interesting finding, given that Mgc and

its binding partner MKLP1 require dynamic MTs for junctional localization. Could Mgc influence

the localization of p190B to adherens junctions and therefore, its ability to modulate RhoA

signaling? This question was tested in an Mgc knockdown background which resulted in

increased p190B adherens junction localization, suggesting that Mgc negatively regulates

p190B's junctional localization[46]. Indeed, these results show that Mgc and dynamic MTs

negatively regulate the localization of p190B to cell-cell junctions and provide additional insight

into the molecular regulation of GTPases at junctions. Taken together, the data described

above regarding the activity of other GAPs during division and at cell-cell junctions, highlights

the complexities of RhoA regulation and eludes to the possibility that multiple GAPs may have

overlapping function to achieve proper Rho GTPase regulation.

Do RhoA GAPs have overlapping functions?

It is of the utmost importance for the cell that cytokinesis completes successfully each

and every time. So in this sense, the idea that there are several redundant GAPs that function

during cytokinesis is intuitive. Many other vital cellular processes are controlled by redundant

pathways to ensure their success and vitality. Why then would cytokinesis not be one of these?

Since precise localization of active RhoA is essential for successful cytokinesis, it is logical to

assume that there are multiple regulatory mechanisms in place so that if one of them is

disrupted, the others can compensate to ensure successful division. Evidence to support this

notion comes from multiple studies in the literature that show only a small defect in cytokinesis

completion (usually < 20%, but up to 50%) upon knockdown of important RhoA GAPs[15,18,28,69,70].

Why would knockdown of a GAP that regulates RhoA at the division site only cause some cells

to fail division? How do the other cells that have received the same mutant construct complete

division? One possible explanation is that multiple GAPs work cooperatively and/or redundantly

to properly regulate RhoA during cytokinesis. An experiment that could be done to address this

question would be to perturb the GAP activity of two or more known RhoA GAPs, for example

MgcRacGAP, MP-GAP, or p190ARhoGAP and compare the effects on cytokinesis to control cells

and cells were only one GAP at a time is perturbed. Whether this experiment answered the

question of cooperative function between RhoA GAPs or not, it would certainly help to

elucidate the finer details of RhoA GAP regulation during cytokinesis.

III. MgcRacGAP functions as a +TIP to facilitate its subcellular localization and MT dynamics.

Classic experiments performed by Rappaport (1961) established a long-standing hypothesis that a positive cue is carried from the overlapping MTs of the central spindle to the equatorial cell cortex via MTs in order to stimulate furrow ingression during cytokinesis. However, the molecular nature of this cue is still being debated. Because Centralspindlin localization to the central spindle and the equatorial cell cortex is necessary for successful cytokinesis[18], it is possible that the cytokinetic cue could be Centralspindlin itself. This became more than just a possibility after our observations that populations of Mgc-3xGFP accumulate on astral MT plus ends that point toward the equatorial cell cortex during cytokinesis and tether the MT to the cortex. We were excited about this finding, and began work to elucidate the mechanism that could control this localization. We found that Mgc contained a conserved EB1 binding motif, an SxIP motif, near its carboxy terminus. EB1 associates with the growing ends of polymerizing MTs and is responsible for most intracellular plus end tracking by acting as an adaptor that recruits other plus-end tracking proteins (+TIPs) to the polymerizing MT end[56,131]. We proceeded to carry out experiments to test the hypothesis that Mgc binds to EB1 via its SxIP motif. These experiments and results are described in detail in Chapter 2 of this dissertation, but many unanswered questions remain. For instance: is this EB tethering mechanism conserved in other organisms? What other cellular processes are regulated by the ability of Mgc's SxIP motif to tether MT ends? Do other RhoA GAPs use a similar MT tethering mechanism or tethering to other cellular structures to facilitate proper RhoA regulation? Is Centralspindlin unique among +TIP proteins because it contains a both a kinesin motor protein and an SxIP motif-containing protein, Mgc?

Similarities between MT plus end localization of Centralspindlin and the tumor suppressor, adenomatous polyposis coli (APC).

Our model of Mgc tethering to MT plus ends predicts that at anaphase onset, Mgc travels along the astral MT lattice via the motor activity of MKLP1. Then, when Centralspindlin encounters EB1 on the MT plus ends, Mgc's SxIP motif can bind EB1 and tether the complex at the MT plus end. Most other +TIPs associate only with the MT plus end and exhibit weak affinity for the MT lattice[56,59,131,156]. The only known exception to this is the +TIP and tumor suppressor, adenomatous polyposis coli (APC), which accumulates at MT plus ends via association with the kinesin associated protein KAP3[61]. The binding of APC to KAP3 allows for movement along the MT lattice via the kinesin motor Kif3B. APC, a multifunctional tumor suppressor gene that regulates many cellular processes such as chromosomal instability, β-catenin mediated transcription regulation, MT dynamics, and MT attachment to kinetochores, is commonly mutated in colon cancer[157,61]. It has been shown that APC can bind MTs directly[157] and has a carboxy terminal SxIP motif[158]. Additionally, APC carboxy terminal truncation mutants fail to accumulate at MT plus ends and show defects in MT attachments to kinetochores[157,159]. Further work revealed that APC binds the spindle assembly checkpoint protein Bub1 and MTs concomitantly[159]. The fact that APC is a +TIP protein that regulates important cellular processes due to its ability to travel along the MT lattice via a kinesin motor prior to EB1 binding, is remarkably similar to Centralspindlin. The Centralspindlin component, Mgc, has been identified (in work described in Chapter 2 of this dissertation) to be a +TIP protein and also travels along MTs via its kinesin motor binding partner before binding to EB1 via its SxIP motif. Given the similarities here, it is possible that Mgc and Centralspindlin could be important for additional

yet to be identified processes that require Rho GTPase regulation via precise subcellular localization mediated by MT transport.

Mgc function outside of cytokinesis and cell-cell junctions.

As an example of how Centralspindlin, via Mgc's SxIP motif, could serve other functions during the cell cycle, recent work has identified a role for Centralspindlin in centromere regulation[160]. It makes sense that a nuclear function for Mgc has emerged because Mgc has a nuclear localization sequence[161] and localization studies have repeatedly detected a strong population of Mgc in the nucleus during interphase. Indeed, it was shown that Mgc interacts with the essential histone variant CENP-A, which is an epigenetic marker for centromere location[160]. The researchers utilized a live cell assay which employed high resolution microscopy to reveal that Mgc co-localized with CENP-A during interphase, but not during anaphase or telophase[160]. Additionally, they found that Mgc's GAP activity and the presence of Ect2 were necessary for proper CENP-A accumulation at centromeres, and that Cdc42 was the target GTPase.

This study provided an example of non-canonical Mgc function, and is interesting when considered in light of another study that identified Cdc42 as an important factor in MT attachment to kinetochores[162]. While the assembly of the kinetochore and MT attachment is regulated by multiple interconnecting pathways, I propose that there could be a link between Mgc localization with CENP-A at centromeres and the ability of MTs to attach to the kinetochore. Could Mgc provide a link between K-fiber MTs and the centromere? This is similar to how APC regulates MT kinetochore attachment by binding simultaneously to the kinetochore

checkpoint protein, Bub1, and the plus end of the MT via its SxIP motif. The formin mDia3 can

bind Cdc42 and co-localizes with CENP-A at the kinetochore, while participating in MT

attachment[162]. Because APC and Mgc are the only +TIPs identified to date that use similar MT

lattice and +TIP localization mechanisms, and because Mgc co-localizes with other centromere

proteins that regulate MT attachment, it is plausible that Mgc may function in MT kinetochore

attachment via its SxIP motif, similar to APC.

To complement this line of thought and provide preliminary data suggesting that Mgc's

GAP activity and SxIP motif may be important for kinetochore attachment, I have observed

chromosomal bridging events in both Mgc GAP-dead mutants and in MgcSxNN mutants. These

bridges can result in chromosome breakage, which leads to aneuploidy and eventually

chromosomal instability, both of which are hallmarks of cancer. The parallels between APC

kinetochore binding and the potential of Mgc to bind kinetochores is intriguing, and certainly

warrants future investigation. If found to be true, this would add to the list of important cellular

processes that are regulated by Mgc (cytokinesis, cell-cell junctions, interaction with CENP-A),

any of which would have profound deleterious effects when misregulated and could contribute

to tumorigenesis.

IV. MgcRacGAP's potential role in tumorigenesis.

It is well established that Rho GTPases are master regulators of cell motility and

cytoskeleton-dependent responses to biochemical signals. It did not become clear until the late

1990's that Rho proteins regulated many important cellular processes, including but not limited

to: gene regulation, growth factor signaling, transcription, cell proliferation and cell

survival[32,163–166]. It is now apparent that Rho GTPases are versatile signaling molecules that can participate in numerous signaling pathways. This fact is exploited in cancer cells to confer a survival advantage. Rho proteins and their GEF and GAP regulators are commonly overexpressed or mutated in many human cancers[48,75,76,148,167–169] and have been popular targets for drug discovery programs for the past 15 years[101,170,171].

Several studies have identified mutations or aberrant expression levels of Mgc to be associated with human cancers[76,77,168]. A recent study identified the human homologue of Mgc, RacGAP1, along with 3 other proteins, as early-stage biomarkers for ovarian epithelial cancer[77]. The researchers found that patients with late stage epithelial ovarian cancer have a survival rate of only approximately 30%, whereas patients with early stage cancer have a survival rate of nearly 90%. Therefore, a reliable method for early-stage disease detection may contribute to a decrease in mortality rate. Similarly, RacGAP1 was also identified as a prognostic predictor for recurrence of Hepatocellular Carcinoma (HCC) in patients who have undergone possible curative treatment [168]. Hepatocellular Carcinoma is the most common form of human liver cancer and is the third leading cause of cancer related deaths in the world[168]. The ability to accurately identify patients at risk of HCC recurrence would allow for clinical intervention and could decrease the occurrence of mortality. A comprehensive analysis of the function of Mgc in these cancers and in healthy tissue is therefore clinically relevant. Likewise, the investigation of Mgc as a biomarker for epithelial cancer could lead to more efficient early stage detection and better treatment options for patients.

Not only is Mgc implicated in several human cancers, but it has also recently been found to play a role in cellular transformation. Doki and colleagues (2009)[76] found that increasing

levels of phosphorylation on Mgc S386 are correlated with soft agar colony formation of v-SRC-transformed NIH-3T3 cells. They showed that a phosphomimetic mutant (Mgc S386E) significantly enhances colony formation. Data from our lab reported in Chapter 1 of this dissertation show that a phosphomimetic mutant of Mgc (MgcS386E) appeared to be GAP dead, which resulted in ectopic RhoA and Rac1 activity and disrupted cytokinesis and cell-cell junction integrity in *Xenopus* epithelia. The study by Doki and colleagues concluded that v-Src induced phosphorylation of Mgc on S386 inactivates GAP activity toward Rac1, thus allowing for increased levels of Rac1-GTP to function in v-Src induced transformation[76]. Indeed, the data described in Chapter 1 of this dissertation demonstrate that MgcS386E leads to misregulated RhoA and Rac1 signaling in epithelial cells. However, we did not observe a GAP specificity switch under any of our experimental perturbations to Mgc's GAP activity[28]. Nonetheless, it is important to understand the molecular mechanisms of Centralspindlin function in order to fully understand the role that it may have in the development or progression of human carcinomas.

Important to the study of human cancers is the metastatic potential of a tumor. The ability of a cell to escape the primary tumor is largely dependent upon changes that occur in adhesions to the matrix and adhesions between cell-cell junctions[172]. Therefore understanding the molecular properties of the adhesive environment is important for our understanding of metastatic tumors. We and others have shown that defective Mgc GAP activity leads to defects in cell-cell junction structure[28,72,100]. Additionally, I found that perturbations to Mgc's GAP activity lead to cell extrusion events (see Appendix 1). The fact that Mgc regulates cell-cell junction integrity through modulating RhoA and Rac1 signaling, and that Mgc is implicated in live cell extrusion, strongly supports the idea that Mgc may regulate metastatic behavior.

Indeed, if the Mgc mutation MgcS386E confers greater transformative properties[76], and the defective GAP activity contributes both to loss of junction integrity and to increased rates of live cell extrusion, then Mgc GAP defective mutants would be the perfect storm for a metastatic pathway. With the aforementioned properties, Mgc GAP defective mutants could lead to live cell extrusion of cells that are capable of escape from the primary tumor and that have transformative properties that would confer advantage to the establishment of secondary tumors.

The data described in this dissertation highlight the importance of MgcRacGAP in regulating multiple cellular processes. While Mgc had long been considered to function only during cytokinesis, it is now clear that Mgc is an important signaling molecule in several cellular contexts and may have additional, yet to be identified functions. The studies described here illustrate the importance of cellular context when trying to elucidate GTPase regulation. If the ultimate goal of basic science is to be able to translate our findings to gain a deeper understanding of human biology, then we need to shift towards experimental design that can recapitulate cellular contexts more similar to those in human tissues. Technological advancements and the emerging use of live tissues as a model will certainly lead to new findings, and will perhaps identify other proteins that are multi-process regulators, similar to MgcRacGAP.

Appendix 1: Disruption of MgcRacGAP's GAP activity promotes cell extrusion.

Cell extrusion is the process by which a cell, either live or dying, can be removed from the tissue while maintaining constant barrier function. Cell extrusion occurs via an F-actin and myosin II contractile belt that forms in the cells adjacent to the extruded cell[75,173,174]. This actomyosin belt constricts so that the neighboring cells come closer together to squeeze the extruded cell out of the tissue. The constrictive force of the actomyosin belt continues until the neighboring cells are in close proximity to each other and new cell-cell junctions can form[173]. The extruded cell is then released into the extracellular space. Whether a cell extrudes toward the apical or basal side depends on where the actomyosin belt is formed. Formation of the belt at the basal surface causes the neighboring cells to pinch in and squeeze the extruded cell out from the apical side, whereas formation of the belt at the apical surface results in basal cell extrusion. The direction of cell extrusion is not important for apoptotic extrusion; however, directionality is of great concern for live cell extrusion. In normal tissue, when a cell is extruded apically into the lumen, it usually dies via anoikis, or loss of survival cues from the cell matrix[74,75]. Basally extruded cells are released into the tissue that the epithelia encases and will usually undergo anoikis as well. In cancerous tissues that have increased survival signals, extruded cells could survive and travel to other sites (after apical extrusion) or become established in the underlying tissue (basal extrusion) where they could establish new tumors[74].

Therefore, understanding the mechanisms that regulate cell extrusion are crucial to further our understanding of basic epithelial biology and for understanding tumorigenesis and metastasis.

An important feature of epithelial tissue homeostasis is the ability of the tissue to maintain appropriate tension. Tension is important for the barrier function of the tissue. If tension becomes too great, the cell-cell junctions can break apart, and if there is not enough tension, the tissue is weak and cannot uphold barrier function. Epithelial tension is a dynamically regulated process due to the continuous cycling of cell death, cell growth, and cell division that occurs within a healthy epithelium. Therefore, a variety of mechanisms exist to control tension in response to the changing demands of the tissue. One such mechanism is cell extrusion.

There are two main signaling pathways that control cell extrusion – the apoptosis-induced pathway and the cell crowding, or tension-mediated pathway[175]. Apoptosis-induced cell extrusion is controlled via signaling through Sphingosin-1-phosphate, a signaling sphingolipid, which is produced in the dying cell and secreted. Sphingosin-1-phosphate will then bind cell-surface receptors in neighboring cells which leads to activation of the RhoA signaling pathway[174,176]. The cell crowding pathway is controlled by a stress-activated channel protein, Piezo, which when under non-homeostatic tension, will active Sphingosin-1-phosphate. When Sphingosin-1-phosphate is active, it is secreted and binds to cell-surface receptors on neighboring cells to activate RhoA signaling[177]. Both cell extrusion pathways rely on the activation and cycling of the small GTPase RhoA which signals downstream to promote actin polymerization and myosin II activation and subsequent formation of the contractile extrusion belt[173]. Therefore, cell extrusion events represent another cellular process that requires the

formation of a RhoA-regulated transient contractile array, and is thus governed by the RhoA

regulators, GEFs and GAPs. Indeed it has been shown that the RhoA GEF, p115RhoGEF, is

required for RhoA activation in both apoptotic and crowding induced extrusion[174], but the GAP

that regulates RhoA signaling in these contexts has not yet been identified.

While conducting experiments for the projects described in Chapters 1 and 2 of this

dissertation, I observed cell extrusion events when MgcRacGAP's (Mgc's) GAP activity was

perturbed either by knockdown or by knockdown and replacement with point mutants that

disrupt GAP activity (e.g. MgcS386E). My preliminary data suggests that perturbation of Mgc's

GAP activity causes a significant increase in cell extrusion events; these events were not

observed in control embryos or Mgc MO+MgcWT embryos (Appendix 1, Figure 1). Using live

confocal microscopy, I found that cells from Mgc MO+MgcS386E embryos would frequently

shrink rapidly to a fraction of their original size with concomitant accumulation of RhoA-GTP

and F-actin at the cortex, then undergo extrusion from the epithelial tissue (Appendix 1, Figure

2).

I next tried to determine whether the cells extruded apically or basally. Both apical and

basal extrusion events occurred in Mgc MO+MgcS386E embryos. I observed several examples

of live cell apical extrusion events where the extruded cell could be seen moving across the

apical surface of the epithelium post extrusion (Appendix 1, Figures 3 A, A', C). By co-injecting

embryos with a probe for active RhoA (GFP-rGBD) and F-actin (mChe-UtrCH), I confirmed that a

basal band of active RhoA and F-actin formed around the neighboring cells of an apically

extruded cell (Appendix 1, Figures 3 B – C).

Based on this preliminary data, I wanted to investigate the functional role that Mgc may play in regulating epithelial cell extrusion events. *I hypothesized that when Mgc's GAP activity is perturbed, epithelial tension homeostasis is disrupted resulting in apical extrusion via the Piezo pathway.* To test the hypothesis that Mgc's GAP activity negatively regulates epithelial cell extrusion, the following experiments are suggested.

I. Experiments to investigate MgcRacGAP's role in epithelial extrusion:

1. Verify that the observed extrusion events are carried out via the known extrusion biochemical/mechanochemical signaling pathways.

   - Examine levels of sphingosin-1-phosphate (S1P) using fixed staining in embryos where Mgc's GAP activity has been perturbed via knockdown and/or knockdown and replacement with a GAP dead mutant. Will need to identify an S1P antibody with reactivity in *Xenopus* and optimize staining conditions.

   - Control: Artificially induce apoptosis to confirm that an increase in S1P can be detected.

2. Expand the current preliminary data set of live confocal imaging in *Xenopus* embryos where endogenous Mgc has been knocked down and replaced with a GAP dead point mutant, and quantify the rates of extrusion, apical vs. basal extrusion, and the dynamics of RhoA, F-actin, and myosin II during these events.

3. Perform fixed staining of embryos where cell extrusion has been induced either artificially or with Mgc MO+MgcGAP dead, to determine whether Mgc co-localizes with

RhoA-GTP, F-actin, and phospho-myosin at the contractile ring of extruding cells.

4. Determine the biochemical/mechanochemical signaling pathway that regulates cell extrusion in Mgc GAP dead embryos. It is important to determine whether Mgc functions in the apoptosis-induced or cell tension-induced pathway.

- Co-inject embryos with Mgc MO+MgcGAP dead and a lineage tracer, fix and stain for cleaved caspase-3 (apoptosis-induced path) or the stretch-activated channel Piezo (tension-induced path), respectively. We would expect to observe increased cleaved caspase-3 staining associated with apoptotic cells. Likewise, we would expect to see increased Piezo staining around cell-cell junctions undergoing tension changes. A cleaved caspase-3 antibody with reactivity in *Xenopus* has been identified and optimized (see results section). Will need to identify a Piezo antibody with reactivity in *Xenopus* and optimize staining conditions.

- Control: To artificially induce apoptosis, co-inject embryos with a lineage tracer and BAD, a Bcl-2 family member that is pro-apoptotic. To artificially induce Piezo signaling, tension across the epithelia must be perturbed. This could be done by a variety of mechanisms; laser ablation of several neighboring cell-cell junctions, application of exogenous ATP, or using *Xenopus* epithelial explants in an artificial cell stretcher.

5. If the results from the above experiments indicate that Mgc may function in an extrusion signaling pathway, it will be important to test whether Mgc is directly or

indirectly involved in extrusion. Next, since Mgc can regulate both RhoA and Rac1, dominant negative mutant versions of RhoA and Rac1 can be utilized to test which GTPase regulates cell extrusion and which GTPase Mgc's GAP activity is specific for in this pathway. See Breznau et al., 2015[28] for optimized dominant negative GTPase concentrations in gastrula stage embryos.

II. Reagent preparation and optimization for future experiments.

1. <u>Cleaved Caspase-3 immunostaining to detect apoptosis.</u>

Method: Embryos were injected with GFP-farnesyl alone or Mgc MO+GFP-farnesyl. Prior to fixation, DMSO was applied to embryos in fertilization petri dishes as described below. Embryos were fixed via the TCA fixation protocol and immunostained as follows: primary rabbit anti-cleaved caspase-3 antibody (BD Pharmingen) 1:200, mouse anti-GFP 1:200; Alexa-conjugated secondary antibodies at 1:200; blocking buffer contained 2% TX-100. Referenced Gu and Rosenblatt, JCB 2011[176] for methods. The following DMSO treatments to induce apoptosis were tried:

- 0.5% and 1% DMSO, incubated on ice for 20 minutes.

- 1.5% DMSO incubated at room temperature, shaking for 25 minutes.

Results (Appendix 1, Figures 4 A and B): The 1.5% DMSO treatment at room temperature with shaking worked in the GFP-farnesyl injected embryos; 25% of treated embryos showed cells that appeared to be undergoing apoptosis with distinct cleaved caspase-3 staining. The 0.5% and 1% DMSO treatments did not show cell extrusion or apoptotic cells, but they did exhibit rosette formation which can be a result of cell extrusion. Rosette formation frequency was dose

dependent.

2. <u>Immunostaining for phospho-myosin and Mgc at extrusion contractile ring.</u>

Method: Performed fixed immunostaining on uninjected embryos to test mouse anti-phospho-myosin light chain 2 (mAb Cell Signaling, #3675, Ser19) staining of extruding cells. Cells were fixed via the TCA staining protocol and immunostained as follows: primary mouse anti-phospho-myosin 1:200, rabbit anti-β-catenin 1:200; Alexa conjugated secondary antibodies at 1:200; blocking buffer contained 1% TX-100.

Results (Appendix 1, Figure 4C): The embryos show weak phospho-myosin signal at cell-cell junctions with high background cytoplasmic signal. There was faint accumulation of phospho-myosin at the contractile ring of a dividing cell. These results did not show staining that was robust enough for a co-localization analysis at extruding cells. Further reagent optimization was conducted to try to identify the proper experimental conditions, but unfortunately were not successful. Below is a list of experimental conditions that have been tried:

1. Primary antibody phospho-myosin concentrations: 1:200, 1:600, 1:800. Tried both Cell Signaling mouse anti-phospho-myosin (#3675) and rabbit anti-phospho-myosin (#3671).

2. Fixation method: both PFA and TCA protocols tried, neither worked.

3. Fixation using either 1xTBS or 1xPBS buffers did not change results.

4. Variations on detergent concentration: TX-100 concentrations of 0.5, 1.0, 1.5, and 2%. The lower percentages seemed to work better.

3. <u>Pro-apoptotic Bcl-2 family members, to promote apoptosis.</u>

- Mouse BAD in the pCMV vector was obtained from Cell Signaling (pCMV vector, Kan

resistant). Sub-cloning was performed to move mBAD into our mRNA expression vector pCS2+: pCMV-mBAD was digested with BstB1 and Xho1 restriction enzymes. The mBAD excised band of ~ 600 bp was ligated into pCS2+ that was digested with BstB1 and Xho1 and treated with Shrimp Alkaline Phosphatase. Positive clones were sequence verified. pCS2+-mBAD (Amp resistant) is clone #402 in the Miller Lab Strain Collection.

- The *Xenopus* pro-apoptotic Bcl-2 and Bcl-xl genes were obtained from Dr. Revin Stein's Lab Tel Aviv University, Israel[178]. pGEM-HJ-Bcl-2 and pGEM-HJ-Bcl-xl (Amp resistant) are in the Miler Lab Strain Collection, clone #'s 418 and 419, respectively.

Appendix 1, Figure A1.1
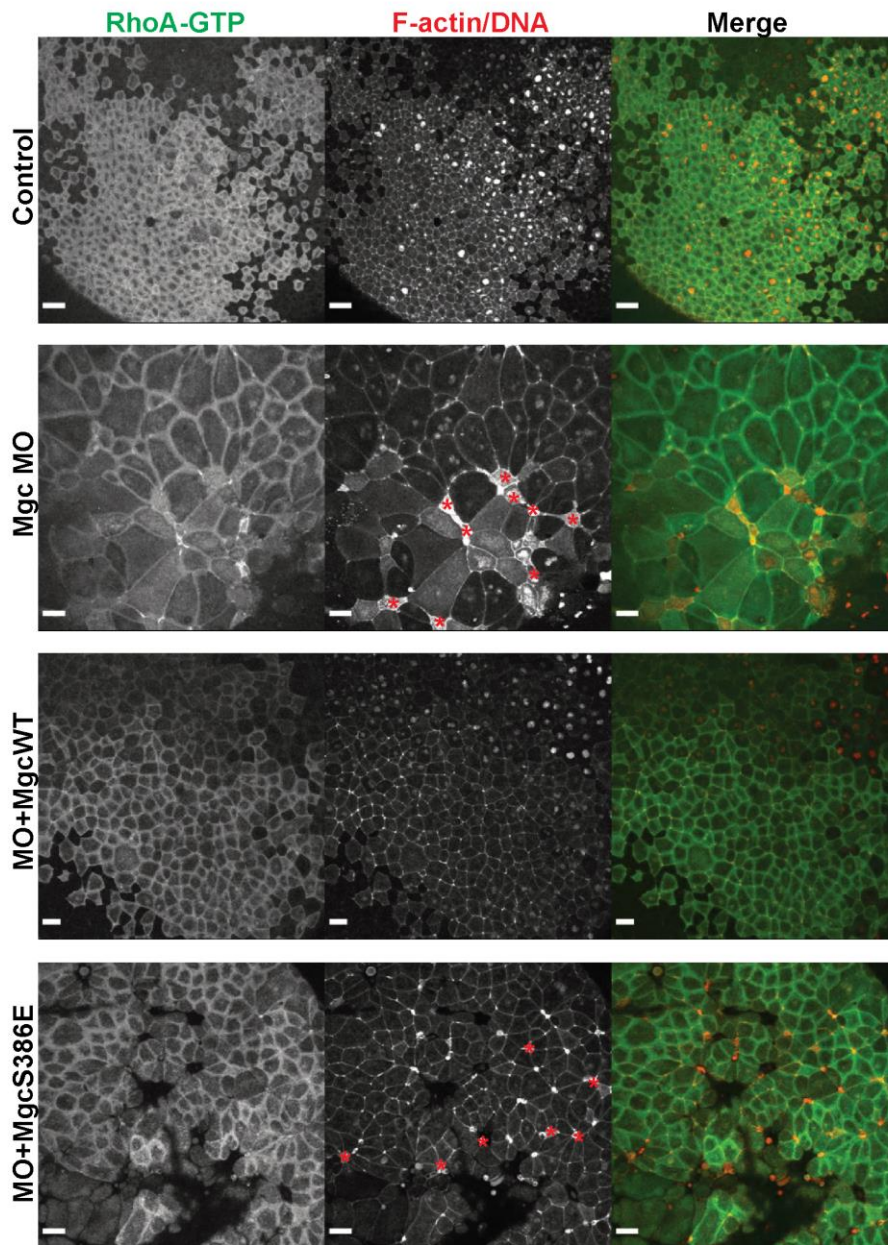
Figure A1.1 Disruption of Mgc's GAP activity causes wide scale epithelial extrusion events.
Still images from live movies of *Xenopus* embryos that were co-injected with MO plus indicated replacement construct where specified, along with probes for active Rho (GFP-rGBD, green); F-actin (mChe-UtrCH, red); and DNA (mChe-H2B, red). Control embryos were injected with probes only. Embryos were allowed to develop to gastrula stage (NF stage 10.5), then live cell imaging was carried out using a 20x objective. Cell extrusion events are marked with red astericks. Scale bars = 20µm.

Appendix 1, Figure A1.2
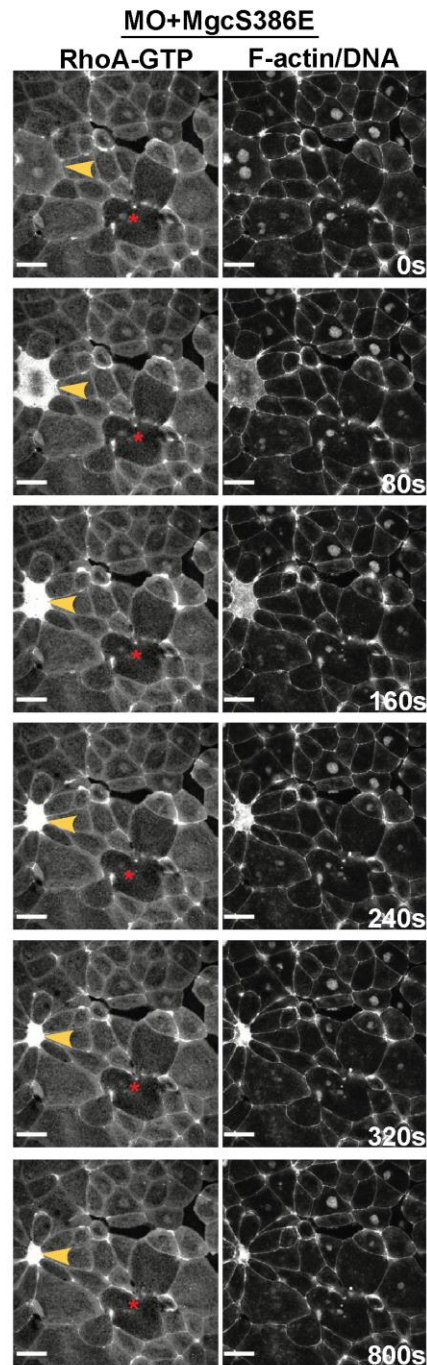
Figure A1.2 Cell extrusion events in Mgc GAP defective embryos are preceded by a rapid reduction in cell size and accumulation of RhoA and F-actin.

Still images from live movies of *Xenopus* embryos co-injected with MO+MgcS386E (GAP-dead mutant of Mgc) along with probes for RhoA-GTP (GFP-rGBD), F-actin (mChe-UtrCH) and DNA (mChe-H2B). Embryos were allowed to develop to gastrula stage (NF stage 10.5) then live cell imaging was carried out using a 60x objective. The site of a cell extrusion event, where the cell exhibits rapid cell size reduction is shown (yellow arrow). A defective cell division is shown in a neighboring cell (red astericks). Scale bars = 20µm.

Appendix 1, Figure A1.3
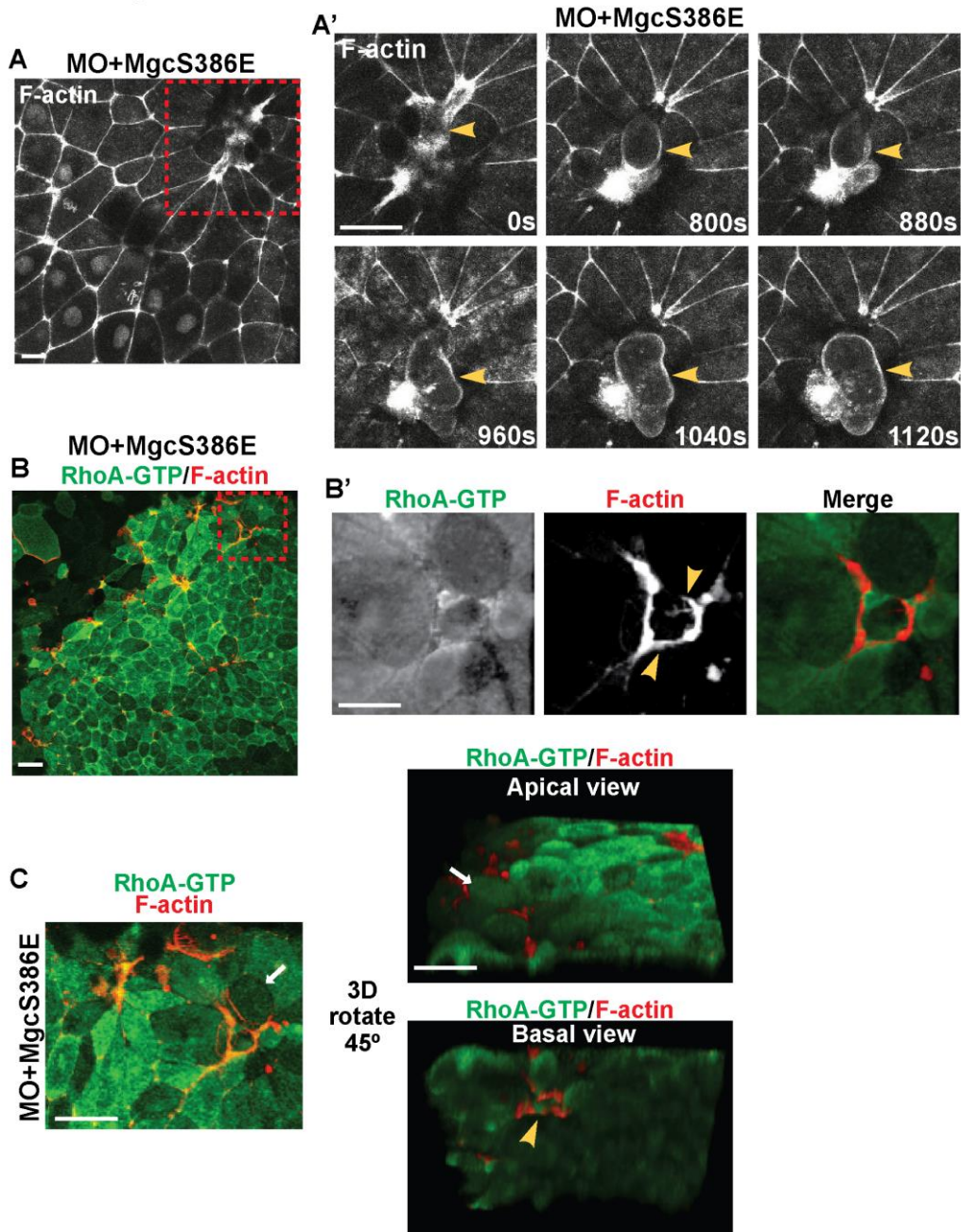
Figure A1.3 Live apical cell extrusion events in Mgc GAP defective embryos.
Still images from live movies of *Xenopus* embryos co-injected with MO+MgcS386E, along with probes for active Rho (GFP-rGBD, green); F-actin (mChe-UtrCH, red). Embryos were incubated at 15° C overnight, then live cell imaging was carried out using a 60x objective. A) An example of an apical cell extrusion event in MO+MgcS386E embryo (red box). Scale bar = 20 µm. A') Time series images of the apical extrusion event from the red box in (A).The extruding cell is marked with a yellow arrowhead. Scale bar = 20µm. B) Another example of an apical extrusion event in a MO+MgcS386E embryo (Red box). Scale bar = 20µm. B') Basal view of the red boxed region from (B) showing formation of an F-actin rich contractile ring. Scale bar = 20 µm. C) The image from (B') zoomed out and 3D rotated 45º to show the apical and basal planes of the cell extrusion event. Live apically extruded cell (white arrow) and basal F-actin contractile ring (yellow arrowhead). Scale bar = 30 µm.

Appendix 1, Figure A1.4
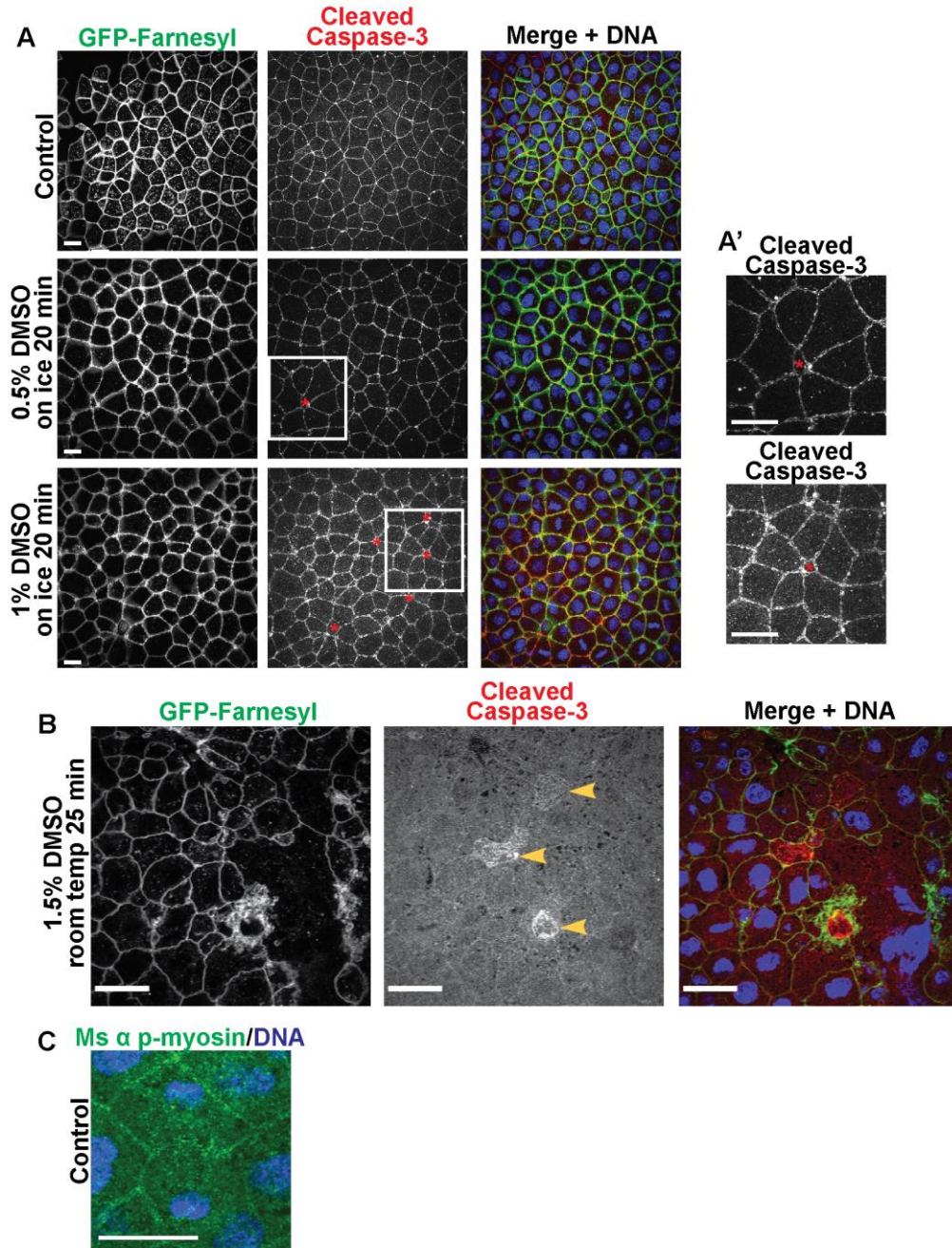
Figure A1.4 Preliminary experiments to optimize extrusion project reagents and methods.
Fixed images from *Xenopus* embryos injected with GFP-farnesyl. Embryos were allowed to develop to gastrula stage (NF stage 10.5), TCA fixed, then incubated with the indicated primary antibodies. A) Fixed images of DMSO optimization experiment. DMSO concenetrations and incubation conditions are indicated. Embryos were incubated with anti-GFP (green) and anti-cleaved caspase 3 (red) antibodies and stained with DAPI. White box represents inset shown in (A'). Red astericks indicate rosette formation which is indicative of cell extrusion. A') Inset shows a magnified view of cleaved caspase-3 staining from the white boxed region in (A), to illustrate rosette formation. B) Experiment described in (A) where the DMSO treatment induced apoptosis. Yellow arrowheads indicate positive cleaved caspase 3 staining. (C) A fixed image of a control embryo incubated with a mouse anti phospho-myosin antibody (green) and stained with DAPI. There is weak p-myosin staining at the contractile ring and along cell-cell junctions. Scale bars = 20μm.

Appendix 2: Preparation of *Xenopus* egg extracts for use as a biochemically tractable experimental system.

Xenopus extracts are ideal for *in vitro* reconstitution of cellular events because the concentrated cytoplasm is not under cell cycle regulation, but maintains many properties of intact cytoplasm and can be easily biochemically manipulated[179–181]. *Xenopus* egg extracts are arrested in metaphase of meiosis II by the activity of cytostatic factor (CSF), a product of the proto-oncogene c-Mos. A calcium spike is triggered by fertilization and destroys the CSF arrest, thereby allowing the egg to exit from metaphase[182]. Egg extracts can be driven into anaphase by the addition of calcium, or can maintain metaphase arrest by addition of a calcium chelating agent to the media[183]. This system is beneficial to the study of cytokinesis because we can obtain cytoplasm that is enriched in anaphase proteins and maintains endogenous signaling factors, but is free from the complexities of the *in vivo* cellular environment. Additionally, the extracts are open to biochemical manipulations and can recapitulate many cellular processes.

Xenopus laevis egg extracts have been used as a model system to study events surrounding cell division for almost 30 years[180,181,183–185]. Dr. Rebecca Heald is a leader in using *Xenopus* egg extracts as a model system. The Heald lab has made significant contributions to the field of cell biology through discoveries in spindle assembly, MT dynamics, and spindle and organelle size scaling[60,186,187]. I had the opportunity to meet Dr. Heald during the fall of 2012

and she generously offered to teach me the techniques for making *Xenopus* egg extracts and carrying out experiments with them.

In May 2013, I traveled to Dr. Heald's lab of the University of California Berkeley. I was awarded an internationally competitive travel fellowship from the *Journal of Cell Science* to fund this trip. In Dr. Heald's lab, I learned many different techniques and experimental methods for collecting and carrying out experiments with *Xenopus* egg extracts. During my visit, I became proficient in the proper technique for the preparation of *Xenopus* egg extract and a clarified extract, in which all residual lipid and glycogen have been removed. Second, I gained experience in biochemical manipulations of the extract such as immunodepletion of endogenous protein and *in vitro* spindle assays. The training I received provided me with the expertise necessary to carry out *in vitro* experiments with *Xenopus* extracts here at Michigan and to teach my lab the protocols so that they too, can use this system. I had planned to use extracts for two different experiments described briefly below. Forward progress was made on both experiments, but ultimately they were not carried to completion, as the work described in Chapters 1 and 2 of this dissertation took priority.

I. Preparation of *Xenopus* extract for *in vitro* microtubule assays.

The first experiment we planned to use *Xenopus* egg extracts for was an alternative approach to test whether Mgc's SxIP motif mediated binding to EB1, related to the work described in Chapter 2 of this dissertation. Briefly, we wanted to visualize localization of MgcWT-3xGFP and MgcSxNN-3xGFP on MTs in monopolar spindles generated *in vitro* in *Xenopus* egg extract. The advantage of this system is that there would be no overlapping central spindle MTs to complicate our analysis. Additionally, the *in vitro* system will allow us to

carry out biochemical perturbations such as depletion of EB1 to test the dependency of Mgc localization on EB1. The planned approach was to add purified centrosomes and fluorescently-tagged EB1 protein to extracts to nucleate MTs and to enhance MT plus end visualization, respectively[180]. The extracts would be immunodepleted of endogenous Mgc, then purified MgcWT-3xGFP or MgcSxNN-3xGFP would be added back. Additionally, extracts could be supplemented with fluorescent tubulin for visualization of MTs. The monopolar spindles would be imaged by time-lapse fluorescence microscopy, and we would quantify the colocalization of MgcWT with EB1 vs. MgcSxNN with EB1. Progress on this project is outlined below:

1) I successfully prepared *Xenopus* egg extracts and high speed clarified extracts in Dr. Heald's lab that were capable of cycling through M-phase (Appendix 2, Figure 1 A-C). I repeated the procedure in our lab then performed Western blots to test whether Mgc was present in the extracts.

> **Methods:** *Xenopus* extracts were prepared following published protocols[180]. Western blots were performed as described in Breznau et al., 2015[28].
>
> **Results (Appendix 2, Figure 1 A-D):** *Xenopus* egg extracts were prepared successfully as measured by the ability of the extract to produce robust *in vitro* spindles that cycled as expected with addition of Ca^{2+}. I found that Mgc was present in the extracts as shown by the presence of a strong band at the correct size for Mgc detected with an anti-*Xenopus* Mgc antibody.

2) In Dr. Heald's lab I successfully performed experiments to nucleate MTs using de-membranated sperm nuclei in *Xenopus* extract, and observed MT plus end dynamics with the addition of GFP-tagged EB1 (Appendix 2, Figure 1E).

147

3) Bacterial expression conditions of WT-Mgc-GFP and MgcSxNN-GFP were determined for

protein purification via a collaboration with the University of Michigan's Center for Structural

Biology.

> **Results (Appendix 2, Figure 1F)**: It was determined that proper bacterial expression
>
> conditions for MgcWT and MgcSxNN for protein purification would require a weak
>
> promoter (SL1) and addition of trimethylamine-N-oxide (TMAO) as a chemical
>
> chaperone to assist with protein folding. Size exclusion chromatography would also be
>
> used when the purification was scaled up to remove the smaller molecular weight
>
> contaminating bands.

II. Development of an *in vitro* Rho GTPase assay

The second experiment we planned to use *Xenopus* egg extract for was to develop a Rho

GTPase activity assay that reconstitutes the *in vivo* Rho GTPase regulatory machinery but is

biochemically tractable. *Xenopus* egg extracts can be manipulated biochemically by

immunodepleting proteins, adding back purified recombinant proteins, or introducing small

molecule inhibitors. This assay would be useful because the current *in vitro* approaches to study

Rho GTPase activity do not account for the multiple mechanisms that regulate Rho GTPases *in*

vivo including Rho GTPase prenylation (required for membrane insertion), the lipid bilayer

itself, Rho Guanine Nucleotide Dissociation Inhibitors (GDIs), GAPs and GEFs, or adaptive

compensation from other Rho GTPases[107,110].

We wanted to develop an *in vitro* reconstitution Rho GTPase assay with *Xenopus* egg

extracts as a source of concentrated cytoplasm that is not under gene or cell cycle regulation,

but does include the endogenous regulatory factors described above. The extracts could be

applied to spherical supported lipid bilayers (Appendix 2, Figure 2 A-B) of known lipid composition, to mimic the cell membrane and allow for insertion of the Rho GTPase's prenyl group. The readout for GTPase activity would be fluorescence intensity of a probe for active RhoA, GFP-rGBD (RhoA binding domain of Rhotekin fused to GFP)[90]. Known concentrations of purified GFP-rGBD would be added to the extracts, and fluorescence intensity of GFP-rGBD on lipid coated beads would be monitored by fluorescence confocal microscopy and quantified. For proof of principle experiments, we would compare the unperturbed level of RhoA-GTP with the following perturbations to the extract; addition of GTPγS (non-hydrolyzable GTP analog to activate all RhoA), addition of a prenyl transferase inhibitor, immunodepletion of RhoA modulators (Appendix 2, Figure 2 C). Progress on the development of this assay was made as outlined below:

1) In collaboration with the University of Michigan's Center for Structural Biology, I purified protein probes that report active populations of RhoA (GFP-rGBD, 2.12 mg/ml) and Rac1 (GFP-pGBD, 4.23 mg/ml). The purified proteins remain in -80° C storage in the Miller Lab (Appendix 2, Figure 2 D).

2) To ensure that the purified proteins were correctly folded and functional, I tested the purified GTPase activity probes in live *Xenopus* embryos undergoing cytokinesis. In this context, we should see a strong accumulation of GFP-rGBD at the contractile ring, and a weaker accumulation for GFP-pGBD.

> **Method:** I co-injected each purified GTPase activity probe with a probe for F-actin (mChe-UtrCH). The embryos were left at room temperature for 2-3 hours, then imaged by confocal microscopy at Nieuwkoop and Faber stage 5-6 using the 20x objective.

149

Result (Appendix 2, Figure 2 E and E'): The purified RhoA probe (GFP-rGBD) did accumulate along the equatorial cortex of a dividing cell and co-localized with the F-actin contractile ring. However, the GFP-rGBD signal was slightly weaker than the accumulation we see upon injection of GFP-rGBD mRNA into blastomeres. Similar results were obtained with the GFP-pGBD probe (data not shown). Nonetheless, the experimental result did provide evidence to suggest that the purified protein probes do localize correctly in the cell and do report the active populations of RhoA and Rac1.

3) I learned how to make supported lipid bilayers of specific lipid composition and to apply them to silica beads, with training from Dr. Allen Liu's Lab at the University of Michigan. The advantage of using lipid coated beads is that the bead spatially confines where the Rho GTPase regulation is happening and makes it possible to use quantitative fluorescent microscopy as a readout. I performed pilot experiments with the supported lipid bilayer beads to determine if I could detect active GTPase on the bead.

Method: Supported lipid bilayers were made of phosphatidylcholine, phosphatidylserine, cholesterol, and rhodamine-labeled phosphatidylethanolamine (as a fluorescent tracer). We also planned in future experiments to carry out the assay in the presence or absence of PIP$_2$, because PIP$_2$ accumulates at the cleavage furrow and active prenylated RhoA preferentially inserts into PIP$_2$-rich lipids. The *Xenopus* egg extract and support lipid bilayer beads were premixed (see below). 10 µl of extract/lipid bead mixture was placed into a single well of a glass bottom 96 well plate. Just before imaging, 1-2 µl of purified GFP-rGBD or GFP-pGBD was added to the well. Imaging was

carried out using the 60X objective (488 laser power ranged from 15-25%, 568 laser

power ranged from 20-30%).

900 µl Extract
10 µl lipid beads
0.9 µl LPC (protease inhibitors)
1.8 µl cytochalasin-D (10 ug/ml)
18 µl Energy mix

Result (Appendix 2, Figure 2 F-G): GFP-rGBD and GFP-pGBD fluorescence signal were

detected on some of the beads (yellow arrowheads). Further optimization and analysis

would be required to determine whether the proposed proof-of-principle experiments

show quantifiable changes in signal as predicted and to determine the proper conditions

for using this assay to test how various Rho regulators modulate Rho GTPase activity.

Appendix 2, Figure A2.1
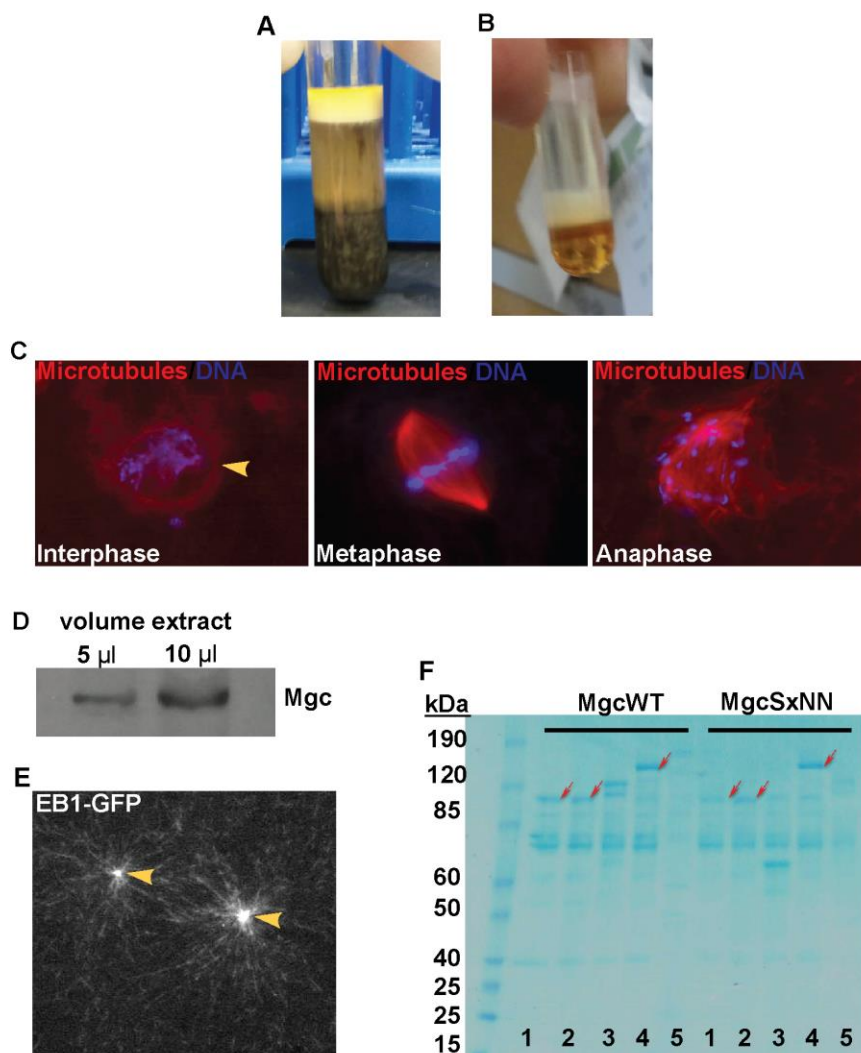
Figure A2.1 *Xenopus* egg extract preparation and experimentation.
A) *Xenopus* extacts were prepared following the methods of Hannak and Heald, 2006. Extracts separate into yolk, cytoplasm and lipid layers post centrifugation of packed eggs. B) High speed clarified extract. C) Spindles formed *in vitro* with extract and addition of sperm nuclei. The extracts were cycled with addition of exogenous Ca^{2+}. Cycled spindles are shown: interphase, the nuclear membrane (yellow arrowhead) surrounding the DNA (blue); metaphase, the MTs (red) connected to the kinetochores on the DNA (blue); anaphase, DNA (blue) separating along the MTs (red). D) Western blot showing Mgc protein levels in *Xenopus* egg extract. E) Asters (yellow arrowheads) nucleated *in vitro* by addition of sperm nuclei to extract. Purified EB1-GFP (grey) was added to extract to visualize microtubule dynamics. F) Small scale protein purification to determine optimal bacterial expression conditions for MgcWT and MgcSxNN (red arrows). Proteins were purified in the presence of trimethylamine-N-oxide (TMAO), as a chemical chaperone. Lane 1 = His-tag,Trc promoter; lane 2 = His-tag, SL promoter; lane 3 = MBP-tag, Trc promoter, lane 4= MBP-tag, SL promoter, lane 5 = SC promoter. Lane 1 provided optimal expression conditions and the His-tagged construct was used for our first scaled up protein purification attempt.

Appendix 2, Figure A2.2
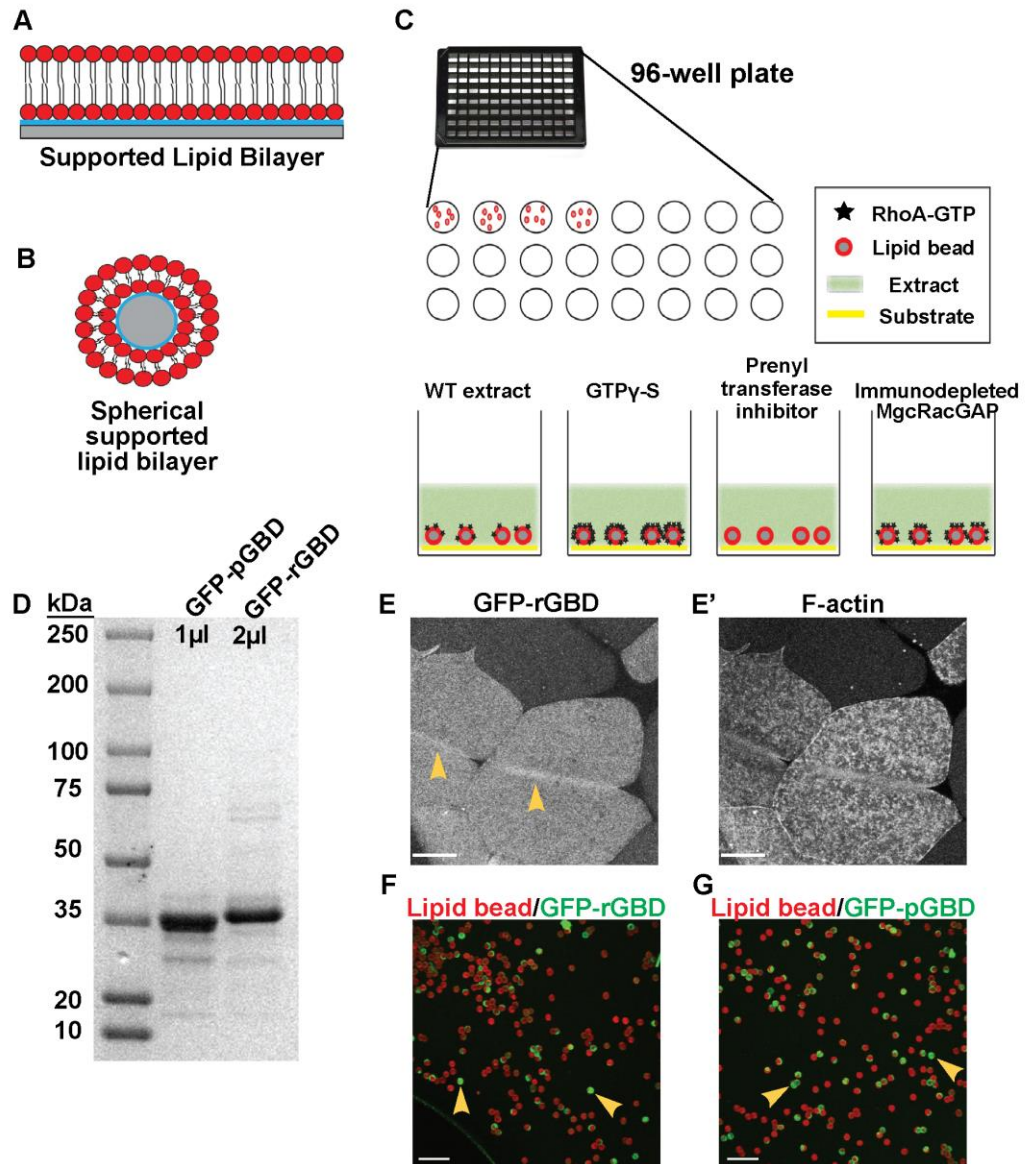
Figure A2.2 Development of an *in vitro* Rho GTPase assay using *Xenopus* extracts.
A and B) Illustration of different forms of supported lipid bilayer. C) Illustration of how the GTPase assay will be carried out in 96 well format. Supported lipid bilayer will be applied to beads (red) that rest on a polyethylene glycol substrate (yellow). Extract (green) supplemented with an energy mix will be deposited in the well. Various chemical inhibitors or other perturnbations will be applied as indicated. D) SDS-PAGE coomassie stained gel showing results of purified GFP-pGBD and GFP-rGBD proteins. E) Still image from a time lapse movie of a stage 5 *Xenopus* embryo expressing purified GFP-rGBD. The image shows a representative example of GFP-rGBD localization to the contractile ring of a dividing cell (yellow arrowhead). Scale = 40 µm. E') Same as described in (E) but showing a probe for F-actin (mChe-UtrCH). Scale = 40 µm. F and G) Fluorescence confocal image of supported lipid bilayer on beads. The beads (red) are resting in 1xPBS buffer with GFP-rGBD (F) and GFP-pGBD (G). Yellow arrowheads point to examples of beads where active GTPase signal is detected (green). Scale = 20 µm.

References

1.   Fujiwara, T. *et al.* Cytokinesis failure generating tetraploids promotes tumorigenesis in p53-null cells. *Nature* **437,** 1043–7 (2005).

2.   Lacroix, B. & Maddox, A. S. Cytokinesis, ploidy and aneuploidy. *J. Pathol.* **226,** 338–51 (2012).

3.   G. L. Kite and Robert Chambers. Vital Staining of Chromosomes and the Function and Structure of the Nucleus . *Science (80-.).* **36,** 639–641 (1912).

4.   Chambers, R. Structural and kinetic aspects of cell division. *J. Cell. Comp. Physiol.* **12,** 149–165 (1938).

5.   Swann, M. M. & Mitchison, J. M. Cleavage of Sea-Urchin Eggs in Colchicine. *J. Exp. Biol.* **30,** 506–514 (1953).

6.   Hiramoto, Y. Further studies on cell division without mitotic apparatus in Sea Urchin. *J. Cell Biol.* **25,** SUPPL:161–7 (1965).

7.   Rappaport, R. Experiments concerning the cleavage stimulus in sand dollar eggs. *J. Exp. Zool.* **148,** 81–89 (1961).

8.   Rappaport, Ray and Conrad, G. W. An experimental analysis of unilateral cleavage in invertebrate eggs. *J. Exp. Zool.* **153,** 99–112 (1963).

9.   Rappaport, R. Cell division: direct measurement of maximum tension exerted by furrow of echinoderm eggs. *Science* **156,** 1241–3 (1967).

10.   Rappaport, R. On the rate of movement of the cleavage stimulus in sand dollar eggs. *J. Exp. Zool.* **183,** 115–120 (1973).

11.   Schroeder, T. E. Actin in dividing cells: contractile ring filaments bind heavy meromyosin. *Proc. Natl. Acad. Sci. U. S. A.* **70,** 1688–92 (1973).

12.   Fujiwara, K. & Pollard, T. D. Fluorescent antibody localization of myosin in the cytoplasm, cleavage furrow, and mitotic spindle of human cells. *J. Cell Biol.* **71,** 848–75 (1976).

13.   Piekny, A., Werner, M. & Glotzer, M. Cytokinesis: welcome to the Rho zone. *Trends Cell Biol.* **15,** 651–8 (2005).

14.   Bement WM, Miller AL, von D. G. Rho GTPase activity zones and transient contractile arrays. . *BioEssays* 983–993 (2006).

15.   Miller, A. L. & Bement, W. M. Regulation of cytokinesis by Rho GTPase flux. **11,** 71–77 (2009).

16.   Piekny A, Werner M, G. M. Cytokinesis: Welcome to the Rho zone. *Trends Cell Biol.* **15,** 651–658 (2005).

17.   Matsumura F, Yamakita Y, Y. S. Myosin light chain kinases and phosphatase in mitosis and cytokinesis. *Arch. Biochem. Biophys.* 76–82 (2011).

18. Jantsch-Plunger, V. *et al.* CYK-4: A Rho family gtpase activating protein (GAP) required for central spindle formation and cytokinesis. *J. Cell Biol.* **149,** 1391–404 (2000).

19. Mishima, M., Kaitna, S. & Glotzer, M. Central spindle assembly and cytokinesis require a kinesin-like protein/RhoGAP complex with microtubule bundling activity. *Dev. Cell* **2,** 41–54 (2002).

20. Mishima, M., Pavicic, V. & Gru, U. Cell cycle regulation of central spindle assembly. **430,** 0–5 (2004).

21. Somers, W. G. & Saint, R. A RhoGEF and Rho family GTPase-activating protein complex links the contractile ring to cortical microtubules at the onset of cytokinesis. *Dev. Cell* **4,** 29–39 (2003).

22. Yüce, O., Piekny, A. & Glotzer, M. An ECT2-centralspindlin complex regulates the localization and function of RhoA. *J. Cell Biol.* **170,** 571–82 (2005).

23. Nishimura, Y. & Yonemura, S. Centralspindlin regulates ECT2 and RhoA accumulation at the equatorial cortex during cytokinesis. *J. Cell Sci.* **119,** 104–14 (2006).

24. Lekomtsev, S. *et al.* Centralspindlin links the mitotic spindle to the plasma membrane during cytokinesis. *Nature* **492,** 276–9 (2012).

25. Canman, J. C. *et al.* Inhibition of Rac by the GAP activity of centralspindlin is essential for cytokinesis. *Science (80-.).* **322,** 1543–1546 (2008).

26. Bastos, R. N., Penate, X., Bates, M., Hammond, D. & Barr, F. a. CYK4 inhibits Rac1-dependent PAK1 and ARHGEF7 effector pathways during cytokinesis. *J. Cell Biol.* **198,** 865–80 (2012).

27. Minoshima, Y. *et al.* Phosphorylation by aurora B converts MgcRacGAP to a RhoGAP during cytokinesis. *Dev. Cell* **4,** 549–60 (2003).

28. Breznau, E. B., Semack, A. C., Higashi, T. & Miller, A. L. MgcRacGAP restricts active RhoA at the cytokinetic furrow and both RhoA and Rac1 at cell-cell junctions in epithelial cells. *Mol. Biol. Cell* **26,** 2439–55 (2015).

29. Lekomtsev, S. *et al.* Centralspindlin links the mitotic spindle to the plasma membrane during cytokinesis. *Nature* **492,** 276–9 (2012).

30. Valencia, A., Chardin, P., Wittinghofer, A. and Sander, C. The ras protein family: evolutionary tree and role of conserved amino acids. *Biochemistry* **30,** 4637–4648 (1991).

31. Jaffe, A. B. & Hall, A. Rho GTPases: biochemistry and biology. *Annu. Rev. Cell Dev. Biol.* **21,** 247–69 (2005).

32. Bishop, A. L. & Hall, A. Rho GTPases and their effector proteins. *Biochem. J.* **348 Pt 2,** 241–55 (2000).

33. Dvorsky, R. & Ahmadian, M. R. Always look on the bright site of Rho: structural implications for a conserved intermolecular interface. *EMBO Rep.* **5,** 1130–6 (2004).

34. Ridley A, H. A. The small GTP-binding protein rho regulates the assembly of focal adhesions and actin stress fibers in response to growth factors. . *Cell* **70,** 389–399 (1992).

35. Joyce, D. *et al.* Integration of Rac-dependent regulation of cyclin D1 transcription through a nuclear factor-kappaB-dependent pathway. *J. Biol. Chem.* **274,** 25245–9 (1999).

36. Welsh, C. F. *et al.* Timing of cyclin D1 expression within G1 phase is controlled by Rho. *Nat. Cell Biol.* **3,** 950–7 (2001).

37. Coso, O. A. *et al.* The small GTP-binding proteins Rac1 and Cdc42 regulate the activity of the JNK/SAPK signaling pathway. *Cell* **81,** 1137–46 (1995).

38. Minden, A., Lin, A., Claret, F. X., Abo, A. & Karin, M. Selective activation of the JNK signaling cascade and c-Jun transcriptional activity by the small GTPases Rac and Cdc42Hs. *Cell* **81,** 1147–57 (1995).

39. Miralles, F., Posern, G., Zaromytidou, A.-I. & Treisman, R. Actin dynamics control SRF activity by regulation of its coactivator MAL. *Cell* **113,** 329–42 (2003).

40. Jaffe, A. B., Hall, A. & Schmidt, A. Association of CNK1 with Rho guanine nucleotide exchange factors controls signaling specificity downstream of Rho. *Curr. Biol.* **15,** 405–12 (2005).

41. Izumi, Y. *et al.* An atypical PKC directly associates and colocalizes at the epithelial tight junction with ASIP, a mammalian homologue of Caenorhabditis elegans polarity protein PAR-3. *J. Cell Biol.* **143,** 95–106 (1998).

42. Gibson, M. C. & Perrimon, N. Apicobasal polarization: epithelial form and function. *Curr. Opin. Cell Biol.* **15,** 747–52 (2003).

43. Braga, V. M., Machesky, L. M., Hall, A. & Hotchin, N. A. The small GTPases Rho and Rac are required for the establishment of cadherin-dependent cell-cell contacts. *J. Cell Biol.* **137,** 1421–31 (1997).

44. Magie, C. R., Pinto-Santini, D. & Parkhurst, S. M. Rho1 interacts with p120ctn and alpha-catenin, and regulates cadherin-based adherens junction components in Drosophila. *Development* **129,** 3771–82 (2002).

45. Reyes, C. C. *et al.* Anillin regulates cell-cell junction integrity by organizing junctional accumulation of Rho-GTP and actomyosin. *Curr. Biol.* **24,** 1263–70 (2014).

46. Ratheesh, A. *et al.* Centralspindlin and α-catenin regulate Rho signalling at the epithelial zonula adherens. *Nat. Cell Biol.* **14,** 818–28 (2012).

47. Wheeler, A. P. & Ridley, A. J. Why three Rho proteins? RhoA, RhoB, RhoC, and cell motility. *Exp. Cell Res.* **301,** 43–9 (2004).

48. Vega, F. M. & Ridley, A. J. Rho GTPases in cancer cell biology. *FEBS Lett.* **582,** 2093–101 (2008).

49. Kraynov, V. S. *et al.* Localized Rac activation dynamics visualized in living cells. *Science* **290,** 333–7 (2000).

50. Nakagawa, M., Fukata, M., Yamaga, M., Itoh, N. & Kaibuchi, K. Recruitment and activation of Rac1 by the formation of E-cadherin-mediated cell-cell adhesion sites. *J. Cell Sci.* **114,** 1829–38 (2001).

51. DeMali, K. A., Sun, X. & Bui, G. A. Force Transmission at Cell–Cell and Cell–Matrix Adhesions. *Biochemistry* **53,** 7706–7717 (2014).

52. Touré, a *et al.* MgcRacGAP, a new human GTPase-activating protein for Rac and Cdc42 similar to Drosophila rotundRacGAP gene product, is expressed in male germ cells. *J. Biol. Chem.* **273,** 6019–23 (1998).

53. Hallen, M. A., Liang, Z.-Y. & Endow, S. A. Ncd motor binding and transport in the spindle. *J. Cell Sci.* **121,** 3834–41 (2008).

54. Douglas, M. E., Davies, T., Joseph, N. & Mishima, M. Europe PMC Funders Group Aurora B and

14-3-3 Coordinately Regulate Clustering of Centralspindlin during Cytokinesis. **20,** 927–933 (2012).

55. Hutterer, A., Glotzer, M. & Mishima, M. Clustering of centralspindlin is essential for its accumulation to the central spindle and the midbody. *Curr. Biol.* **19,** 2043–9 (2009).

56. Kumar, P. & Wittmann, T. +TIPs: SxIPping along microtubule ends. *Trends Cell Biol.* **22,** 418–28 (2012).

57. Honnappa, S. *et al.* An EB1-binding motif acts as a microtubule tip localization signal. *Cell* **138,** 366–76 (2009).

58. Komarova, Y. *et al.* Mammalian end binding proteins control persistent microtubule growth. *J. Cell Biol.* **184,** 691–706 (2009).

59. Jiang, K. & Akhmanova, A. Microtubule tip-interacting proteins: a view from both ends. *Curr. Opin. Cell Biol.* **23,** 94–101 (2011).

60. Patel, K., Nogales, E. & Heald, R. Multiple domains of human CLASP contribute to microtubule dynamics and organization in vitro and in Xenopus egg extracts. *Cytoskeleton (Hoboken).* **69,** 155–65 (2012).

61. Honnappa, S., John, C. M., Kostrewa, D., Winkler, F. K. & Steinmetz, M. O. Structural insights into the EB1-APC interaction. *EMBO J.* **24,** 261–9 (2005).

62. Kim, J.-E., Billadeau, D. D. & Chen, J. The tandem BRCT domains of Ect2 are required for both negative and positive regulation of Ect2 in cytokinesis. *J. Biol. Chem.* **280,** 5733–9 (2005).

63. Kim, H., Guo, F., Brahma, S., Xing, Y. & Burkard, M. E. Centralspindlin assembly and 2 phosphorylations on MgcRacGAP by Polo-like kinase 1 initiate Ect2 binding in early cytokinesis. *Cell Cycle* **13,** 2952–61 (2014).

64. Wolfe, B. a, Takaki, T., Petronczki, M. & Glotzer, M. Polo-like kinase 1 directs assembly of the HsCyk-4 RhoGAP/Ect2 RhoGEF complex to initiate cleavage furrow formation. *PLoS Biol.* **7,** e1000110 (2009).

65. Petronczki, M., Glotzer, M., Kraut, N. & Peters, J.-M. Polo-like kinase 1 triggers the initiation of cytokinesis in human cells by promoting recruitment of the RhoGEF Ect2 to the central spindle. *Dev. Cell* **12,** 713–25 (2007).

66. Rappaport, R. Experiments concerning the cleavage stimulus in sand dollar eggs. *J. Exp. Zool.* **148,** 81–9 (1961).

67. Bement, W. M., Benink, H. A. & von Dassow, G. A microtubule-dependent zone of active RhoA during cleavage plane specification. *J. Cell Biol.* **170,** 91–101 (2005).

68. Bement, W. M., Miller, A. L. & von Dassow, G. Rho GTPase activity zones and transient contractile arrays. *Bioessays* **28,** 983–93 (2006).

69. Loria, A., Longhini, K. M. & Glotzer, M. The RhoGAP domain of CYK-4 has an essential role in RhoA activation. *Curr. Biol.* **22,** 213–9 (2012).

70. Canman, J. C. *et al.* Inhibition of Rac by the GAP activity of centralspindlin is essential for cytokinesis. *Science* **322,** 1543–6 (2008).

71. Ratheesh, A., Priya, R. & Yap, A. S. Coordinating Rho and Rac: the regulation of Rho GTPase signaling and cadherin junctions. *Prog. Mol. Biol. Transl. Sci.* **116,** 49–68 (2013).

72. Guillemot, L. *et al.* MgcRacGAP interacts with cingulin and paracingulin to regulate Rac1 activation and development of the tight junction barrier during epithelial junction assembly. *Mol. Biol. Cell* **25,** 1995–2005 (2014).

73. TERASIMA, T. & TOLMACH, L. J. Growth and nucleic acid synthesis in synchronously dividing populations of HeLa cells. *Exp. Cell Res.* **30,** 344–62 (1963).

74. Gu, Y. & Rosenblatt, J. New emerging roles for epithelial cell extrusion. *Curr. Opin. Cell Biol.* **24,** 865–70 (2012).

75. Eisenhoffer, G. T. & Rosenblatt, J. Bringing balance by force: live cell extrusion controls epithelial cell numbers. *Trends Cell Biol.* **23,** 185–92 (2013).

76. Doki, N. *et al.* Constitutive phosphorylation of a Rac GAP MgcRacGAP is implicated in v-Src-induced transformation of NIH3T3 cells. *Cancer Sci.* **100,** 1675–9 (2009).

77. Lu, K. H. *et al.* Selection of potential markers for epithelial ovarian cancer with gene expression arrays and recursive descent partition analysis. *Clin. Cancer Res.* **10,** 3291–300 (2004).

78. Godinho, S. A. *et al.* Oncogene-like induction of cellular invasion from centrosome amplification. *Nature* **510,** 167–71 (2014).

79. Green, R. a, Paluch, E. & Oegema, K. Cytokinesis in animal cells. *Annu. Rev. Cell Dev. Biol.* **28,** 29–58 (2012).

80. Hirose, K., Kawashima, T., Iwamoto, I., Nosaka, T. & Kitamura, T. MgcRacGAP is involved in cytokinesis through associating with mitotic spindle and midbody. *J. Biol. Chem.* **276,** 5821–8 (2001).

81. Goldstein, A. Y. N., Jan, Y.-N. & Luo, L. Function and regulation of Tumbleweed (RacGAP50C) in neuroblast proliferation and neuronal morphogenesis. *Proc. Natl. Acad. Sci. U. S. A.* **102,** 3834–9 (2005).

82. Yamada, S. & Nelson, W. J. Localized zones of Rho and Rac activities drive initiation and expansion of epithelial cell-cell adhesion. *J. Cell Biol.* **178,** 517–27 (2007).

83. Braga, V. M., Del Maschio, A., Machesky, L. & Dejana, E. Regulation of cadherin function by Rho and Rac: modulation by junction maturation and cellular context. *Mol. Biol. Cell* **10,** 9–22 (1999).

84. Jou, T. S., Schneeberger, E. E. & Nelson, W. J. Structural and functional regulation of tight junctions by RhoA and Rac1 small GTPases. *J. Cell Biol.* **142,** 101–15 (1998).

85. Terry, S., Nie, M., Matter, K. & Balda, M. S. Rho signaling and tight junction functions. *Physiology (Bethesda).* **25,** 16–26 (2010).

86. Matsuura, A. & Lee, H. H. Crystal structure of GTPase-activating domain from human MgcRacGAP. *Biochem. Biophys. Res. Commun.* **435,** 367–72 (2013).

87. Burkel, B. M., von Dassow, G. & Bement, W. M. Versatile fluorescent probes for actin filaments based on the actin-binding domain of utrophin. *Cell Motil. Cytoskeleton* **64,** 822–32 (2007).

88. Su, K.-C., Takaki, T. & Petronczki, M. Targeting of the RhoGEF Ect2 to the equatorial membrane controls cleavage furrow formation during cytokinesis. *Dev. Cell* **21,** 1104–15 (2011).

89. Carvalho, A., Desai, A. & Oegema, K. Structural memory in the contractile ring makes the duration of cytokinesis independent of cell size. *Cell* **137,** 926–37 (2009).

90. Benink, H. A. & Bement, W. M. Concentric zones of active RhoA and Cdc42 around single cell

wounds. *J. Cell Biol.* **168,** 429–39 (2005).

91.   Rittinger, K. *et al.* Crystal structure of a small G protein in complex with the GTPase-activating protein rhoGAP. *Nature* **388,** 693–7 (1997).

92.   Miura, K. *et al.* ARAP1: a point of convergence for Arf and Rho signaling. *Mol. Cell* **9,** 109–19 (2002).

93.   Lavelin, I. & Geiger, B. Characterization of a novel GTPase-activating protein associated with focal adhesions and the actin cytoskeleton. *J. Biol. Chem.* **280,** 7178–85 (2005).

94.   Shang, X., Moon, S. Y. & Zheng, Y. p200 RhoGAP promotes cell proliferation by mediating cross-talk between Ras and Rho signaling pathways. *J. Biol. Chem.* **282,** 8801–11 (2007).

95.   D'Avino, P. P., Savoian, M. S. & Glover, D. M. Mutations in sticky lead to defective organization of the contractile ring during cytokinesis and are enhanced by Rho and suppressed by Rac. *J. Cell Biol.* **166,** 61–71 (2004).

96.   Li, Z., Aizenman, C. D. & Cline, H. T. Regulation of rho GTPases by crosstalk and neuronal activity in vivo. *Neuron* **33,** 741–50 (2002).

97.   Danilchik, M. V & Brown, E. E. Membrane dynamics of cleavage furrow closure in Xenopus laevis. *Dev. Dyn.* **237,** 565–79 (2008).

98.   Herszterg, S., Leibfried, A., Bosveld, F., Martin, C. & Bellaiche, Y. Interplay between the dividing cell and its neighbors regulates adherens junction formation during cytokinesis in epithelial tissue. *Dev. Cell* **24,** 256–70 (2013).

99.   Machacek, M. *et al.* Coordination of Rho GTPase activities during cell protrusion. *Nature* **461,** 99–103 (2009).

100.   Priya, R., Yap, A. S. & Gomez, G. a. E-cadherin supports steady-state Rho signaling at the epithelial zonula adherens. *Differentiation.* **86,** 133–40 (2013).

101.   Doe, C. *et al.* Novel Rho kinase inhibitors with anti-inflammatory and vasodilatory activities. *J. Pharmacol. Exp. Ther.* **320,** 89–98 (2007).

102.   Rittinger, K., Walker, P. A., Eccleston, J. F., Smerdon, S. J. & Gamblin, S. J. Structure at 1.65 A of RhoA and its GTPase-activating protein in complex with a transition-state analogue. *Nature* **389,** 758–62 (1997).

103.   Davies, T. & Canman, J. C. Stuck in the middle: Rac, adhesion, and cytokinesis. *J. Cell Biol.* **198,** 769–71 (2012).

104.   O'Connell, C. B., Wheatley, S. P., Ahmed, S. & Wang, Y. L. The small GTP-binding protein rho regulates cortical activities in cultured cells during division. *J. Cell Biol.* **144,** 305–13 (1999).

105.   Yoshizaki, H. *et al.* Activity of Rho-family GTPases during cell division as visualized with FRET-based probes. *J. Cell Biol.* **162,** 223–32 (2003).

106.   Yoshizaki, H. *et al.* Cell type-specific regulation of RhoA activity during cytokinesis. *J. Biol. Chem.* **279,** 44756–62 (2004).

107.   Boulter, E. *et al.* Regulation of Rho GTPase crosstalk, degradation and activity by RhoGDI1. *Nat. Cell Biol.* **12,** 477–83 (2010).

108.   Brill, J. A., Wong, R. & Wilde, A. Phosphoinositide function in cytokinesis. *Curr. Biol.* **21,** R930–4 (2011).

109. Canagarajah, B. *et al.* Structural mechanism for lipid activation of the Rac-specific GAP, beta2-chimaerin. *Cell* **119,** 407–18 (2004).

110. Tnimov, Z. *et al.* Quantitative analysis of prenylated RhoA interaction with its chaperone, RhoGDI. *J. Biol. Chem.* **287,** 26549–62 (2012).

111. Lévay, M., Bartos, B. & Ligeti, E. p190RhoGAP has cellular RacGAP activity regulated by a polybasic region. *Cell. Signal.* **25,** 1388–94 (2013).

112. Burridge, K. Crosstalk between Rac and Rho. *Science* **283,** 2028–9 (1999).

113. Manukyan, A., Ludwig, K., Sanchez-Manchinelly, S., Parsons, S. J. & Stukenberg, P. T. A complex of p190RhoGAP-A and anillin modulates RhoA-GTP and the cytokinetic furrow in human cells. *J. Cell Sci.* **128,** 50–60 (2015).

114. Su, L., Agati, J. M. & Parsons, S. J. p190RhoGAP is cell cycle regulated and affects cytokinesis. *J. Cell Biol.* **163,** 571–82 (2003).

115. Zanin, E. *et al.* A conserved RhoGAP limits M phase contractility and coordinates with microtubule asters to confine RhoA during cytokinesis. *Dev. Cell* **26,** 496–510 (2013).

116. von Dassow, G., Verbrugghe, K. J. C., Miller, A. L., Sider, J. R. & Bement, W. M. Action at a distance during cytokinesis. *J. Cell Biol.* **187,** 831–45 (2009).

117. Woolner, S., Miller, A. L. & Bement, W. M. Imaging the cytoskeleton in live Xenopus laevis embryos. *Methods Mol. Biol.* **586,** 23–39 (2009).

118. Le Page, Y., Chartrain, I., Badouel, C. & Tassan, J.-P. A functional analysis of MELK in cell division reveals a transition in the mode of cytokinesis during Xenopus development. *J. Cell Sci.* **124,** 958–68 (2011).

119. Canman, J. C. *et al.* Determining the position of the cell division plane. *Nature* **424,** 1074–8 (2003).

120. Foe, V. E. & von Dassow, G. Stable and dynamic microtubules coordinately shape the myosin activation zone during cytokinetic furrow formation. *J. Cell Biol.* **183,** 457–70 (2008).

121. Shannon, K. B., Canman, J. C., Ben Moree, C., Tirnauer, J. S. & Salmon, E. D. Taxol-stabilized microtubules can position the cytokinetic furrow in mammalian cells. *Mol. Biol. Cell* **16,** 4423–36 (2005).

122. Montenegro Gouveia, S. *et al.* In vitro reconstitution of the functional interplay between MCAK and EB3 at microtubule plus ends. *Curr. Biol.* **20,** 1717–22 (2010).

123. Strickland, L. I., Wen, Y., Gundersen, G. G. & Burgess, D. R. Interaction between EB1 and p150glued is required for anaphase astral microtubule elongation and stimulation of cytokinesis. *Curr. Biol.* **15,** 2249–55 (2005).

124. Vale, R. D., Spudich, J. A. & Griffis, E. R. Dynamics of myosin, microtubules, and Kinesin-6 at the cortex during cytokinesis in Drosophila S2 cells. *J. Cell Biol.* **186,** 727–38 (2009).

125. Douglas, M.E. Davies, T. J. N. M. M. Aurora B and 114-3-3 coordinately regulate clustering of centralspindlin during cytokinesis. *Curr. Biol.* **20,** 927–933 (2010).

126. Kumar, P. *et al.* Multisite phosphorylation disrupts arginine-glutamate salt bridge networks required for binding of cytoplasmic linker-associated protein 2 (CLASP2) to end-binding protein 1 (EB1). *J. Biol. Chem.* **287,** 17050–64 (2012).

127. Duellberg, C. *et al.* Reconstitution of a hierarchical +TIP interaction network controlling microtubule end tracking of dynein. *Nat. Cell Biol.* **16,** 804–11 (2014).

128. Watanabe, T. *et al.* TTBK2 with EB1/3 regulates microtubule dynamics in migrating cells through KIF2A phosphorylation. *J. Cell Biol.* **210,** 737–51 (2015).

129. Gumy, L. F. *et al.* The kinesin-2 family member KIF3C regulates microtubule dynamics and is required for axon growth and regeneration. *J. Neurosci.* **33,** 11329–45 (2013).

130. Blake-Hodek, K. A., Cassimeris, L. & Huffaker, T. C. Regulation of microtubule dynamics by Bim1 and Bik1, the budding yeast members of the EB1 and CLIP-170 families of plus-end tracking proteins. *Mol. Biol. Cell* **21,** 2013–23 (2010).

131. Akhmanova, A. & Steinmetz, M. O. Tracking the ends: a dynamic protein network controls the fate of microtubule tips. *Nat. Rev. Mol. Cell Biol.* **9,** 309–22 (2008).

132. D'Avino, P. P. *et al.* Interaction between Anillin and RacGAP50C connects the actomyosin contractile ring with spindle microtubules at the cell division site. *J. Cell Sci.* **121,** 1151–8 (2008).

133. Gregory, S. L. *et al.* Cell division requires a direct link between microtubule-bound RacGAP and Anillin in the contractile ring. *Curr. Biol.* **18,** 25–9 (2008).

134. Frenette, P. *et al.* An anillin-Ect2 complex stabilizes central spindle microtubules at the cortex during cytokinesis. *PLoS One* **7,** e34888 (2012).

135. White, E. a & Glotzer, M. Centralspindlin: at the heart of cytokinesis. *Cytoskeleton (Hoboken).* **69,** 882–92 (2012).

136. Cai, D., McEwen, D. P., Martens, J. R., Meyhofer, E. & Verhey, K. J. Single molecule imaging reveals differences in microtubule track selection between Kinesin motors. *PLoS Biol.* **7,** e1000216 (2009).

137. Dovas, A. & Couchman, J. R. RhoGDI: multiple functions in the regulation of Rho family GTPase activities. *Biochem. J.* **390,** 1–9 (2005).

138. Groysman, M., Hornstein, I., Alcover, A. & Katzav, S. Vav1 and Ly-GDI two regulators of Rho GTPases, function cooperatively as signal transducers in T cell antigen receptor-induced pathways. *J. Biol. Chem.* **277,** 50121–30 (2002).

139. Olofsson, B. Rho guanine dissociation inhibitors: pivotal molecules in cellular signalling. *Cell. Signal.* **11,** 545–54 (1999).

140. Platko, J. V *et al.* A single residue can modify target-binding affinity and activity of the functional domain of the Rho-subfamily GDP dissociation inhibitors. *Proc. Natl. Acad. Sci. U. S. A.* **92,** 2974–8 (1995).

141. Michaelson, D. *et al.* Differential localization of Rho GTPases in live cells: regulation by hypervariable regions and RhoGDI binding. *J. Cell Biol.* **152,** 111–26 (2001).

142. Vaughan, E. M. *et al.* Lipid domain-dependent regulation of single-cell wound repair. *Mol. Biol. Cell* **25,** 1867–76 (2014).

143. Field, S. J. *et al.* PtdIns(4,5)P2 functions at the cleavage furrow during cytokinesis. *Curr. Biol.* **15,** 1407–12 (2005).

144. Tolias, K. F., Couvillon, A. D., Cantley, L. C. & Carpenter, C. L. Characterization of a Rac1- and RhoGDI-Associated Lipid Kinase Signaling Complex. *Mol. Cell. Biol.* **18,** 762–770 (1998).

145. Tse, Y. C. *et al.* RhoA activation during polarization and cytokinesis of the early Caenorhabditis elegans embryo is differentially dependent on NOP-1 and CYK-4. *Mol. Biol. Cell* **23,** 4020–31 (2012).

146. Burridge, K. & Wittchen, E. S. The tension mounts: stress fibers as force-generating mechanotransducers. *J. Cell Biol.* **200,** 9–19 (2013).

147. Mammoto, T., Mammoto, A. & Ingber, D. E. Mechanobiology and developmental control. *Annu. Rev. Cell Dev. Biol.* **29,** 27–61 (2013).

148. D.R. Cook, P.A. Solski, S.J. Bultman, G. Kauselmann, M. Schoor, R. Kuehn, L.S. Friedman, D.O. Cowley, D.T. Van, J.J. Yeh, L. Johnson, C. J. Der. The Ect2 Rho Guanine Nucleotide Exchange Factor Is Essential for Early Mouse Development and Normal Cell Cytokinesis and Migration. *Genes Cancer* **2,** 932–942

149. T. Tatsumoto, X. Xie, R. Blumenthal, I. Okamoto, T. M. Human ECT2 is an exchange factor for Rho GTPases, phosphorylated in G2/M phases, and involved in cytokinesis. *J. Cell Biol.* **147,** 921–927 (1999).

150. D'Avino, P. P., Savoian, M. S. & Glover, D. M. Cleavage furrow formation and ingression during animal cytokinesis: a microtubule legacy. *J. Cell Sci.* **118,** 1549–58 (2005).

151. Murthy, K. & Wadsworth, P. Dual role for microtubules in regulating cortical contractility during cytokinesis. *J. Cell Sci.* **121,** 2350–9 (2008).

152. Settleman, J., Narasimhan, V., Foster, L. C. & Weinberg, R. A. Molecular cloning of cDNAs encoding the GAP-associated protein p190: Implications for a signaling pathway from ras to the nucleus. *Cell* **69,** 539–549 (1992).

153. Su, L., Pertz, O., Mikawa, M., Hahn, K. & Parsons, S. J. p190RhoGAP negatively regulates Rho activity at the cleavage furrow of mitotic cells. *Exp. Cell Res.* **315,** 1347–59 (2009).

154. Wildenberg, G. A. *et al.* p120-catenin and p190RhoGAP regulate cell-cell adhesion by coordinating antagonism between Rac and Rho. *Cell* **127,** 1027–39 (2006).

155. Noren, N. K., Arthur, W. T. & Burridge, K. Cadherin engagement inhibits RhoA via p190RhoGAP. *J. Biol. Chem.* **278,** 13615–8 (2003).

156. Akhmanova, A. & Hoogenraad, C. C. Microtubule plus-end-tracking proteins: mechanisms and functions. *Curr. Opin. Cell Biol.* **17,** 47–54 (2005).

157. Pellman, D. Cancer. A CINtillating new job for the APC tumor suppressor. *Science* **291,** 2555–6 (2001).

158. Slep, K. C. Structure of the human discs large 1 PDZ2- adenomatous polyposis coli cytoskeletal polarity complex: insight into peptide engagement and PDZ clustering. *PLoS One* **7,** e50097 (2012).

159. Fodde, R. *et al.* Mutations in the APC tumour suppressor gene cause chromosomal instability. *Nat. Cell Biol.* **3,** 433–8 (2001).

160. Lagana, A. *et al.* A small GTPase molecular switch regulates epigenetic centromere maintenance by stabilizing newly incorporated CENP-A. *Nat. Cell Biol.* **12,** 1186–93 (2010).

161. Kawashima, T. *et al.* A Rac GTPase-activating protein, MgcRacGAP, is a nuclear localizing signal-containing nuclear chaperone in the activation of STAT transcription factors. *Mol. Cell. Biol.* **29,** 1796–813 (2009).

162. Yasuda, S. *et al.* Cdc42 and mDia3 regulate microtubule attachment to kinetochores. *Nature* **428,** 767–71 (2004).

163. Hall, A. Rho GTPases and the actin cytoskeleton. *Science* **279,** 509–14 (1998).

164. Van Aelst, L. & D'Souza-Schorey, C. Rho GTPases and signaling networks. *Genes Dev.* **11,** 2295–322 (1997).

165. Murphy, G. A. *et al.* Cellular functions of TC10, a Rho family GTPase: regulation of morphology, signal transduction and cell growth. *Oncogene* **18,** 3831–45 (1999).

166. Marinissen, M. J., Chiariello, M. & Gutkind, J. S. Regulation of gene expression by the small GTPase Rho through the ERK6 (p38 gamma) MAP kinase pathway. *Genes Dev.* **15,** 535–53 (2001).

167. Zuo, Y., Oh, W. & Frost, J. A. Controlling the switches: Rho GTPase regulation during animal cell mitosis. *Cell. Signal.* **26,** 2998–3006 (2014).

168. Wang, S. M., Ooi, L. L. P. J. & Hui, K. M. Upregulation of Rac GTPase-activating protein 1 is significantly associated with the early recurrence of human hepatocellular carcinoma. *Clin. Cancer Res.* **17,** 6040–51 (2011).

169. Parri, M. & Chiarugi, P. Rac and Rho GTPases in cancer cell motility control. *Cell Commun. Signal.* **8,** 23 (2010).

170. Loirand, G., Guérin, P. & Pacaud, P. Rho kinases in cardiovascular physiology and pathophysiology. *Circ. Res.* **98,** 322–34 (2006).

171. Ikenoya, M. *et al.* Inhibition of rho-kinase-induced myristoylated alanine-rich C kinase substrate (MARCKS) phosphorylation in human neuronal cells by H-1152, a novel and specific Rho-kinase inhibitor. *J. Neurochem.* **81,** 9–16 (2002).

172. Martin, T. A., Ye, L., Sanders, A. J., Lane, J. & Jiang, W. G. Cancer Invasion and Metastasis: Molecular and Cellular Perspective. (2013).

173. Rosenblatt, J., Raff, M. C. & Cramer, L. P. An epithelial cell destined for apoptosis signals its neighbors to extrude it by an actin- and myosin-dependent mechanism. *Curr. Biol.* **11,** 1847–57 (2001).

174. Slattum, G., McGee, K. M. & Rosenblatt, J. P115 RhoGEF and microtubules decide the direction apoptotic cells extrude from an epithelium. *J. Cell Biol.* **186,** 693–702 (2009).

175. Marinari, E. *et al.* Live-cell delamination counterbalances epithelial growth to limit tissue overcrowding. *Nature* **484,** 542–5 (2012).

176. Gu, Y., Forostyan, T., Sabbadini, R. & Rosenblatt, J. Epithelial cell extrusion requires the sphingosine-1-phosphate receptor 2 pathway. *J. Cell Biol.* **193,** 667–76 (2011).

177. Eisenhoffer, G. T. *et al.* Crowding induces live cell extrusion to maintain homeostatic cell numbers in epithelia. *Nature* **484,** 546–9 (2012).

178. Braun, T. *et al.* Expression of Bcl-x(S) in Xenopus oocytes induces BH3-dependent and caspase-dependent cytochrome c release and apoptosis. *Mol. Cancer Res.* **1,** 186–94 (2003).

179. Guse, A., Fuller, C. J. & Straight, A. F. A cell-free system for functional centromere and kinetochore assembly. *Nat. Protoc.* **7,** 1847–69 (2012).

180. Hannak, E. & Heald, R. Investigating mitotic spindle assembly and function in vitro using Xenopus laevis egg extracts. *Nat. Protoc.* **1,** 2305–14 (2006).

181.   Lohka, M. J. & Masui, Y. Formation in vitro of sperm pronuclei and mitotic chromosomes induced by amphibian ooplasmic components. *Science* **220,** 719–21 (1983).

182.   Sagata, N., Watanabe, N., Vande Woude, G. F. & Ikawa, Y. The c-mos proto-oncogene product is a cytostatic factor responsible for meiotic arrest in vertebrate eggs. *Nature* **342,** 512–8 (1989).

183.   Wignall, S. M. & Heald, R. Methods for the study of centrosome-independent spindle assembly in Xenopus extracts. *Methods Cell Biol.* **67,** 241–56 (2001).

184.   Lohka, M. J. & Masui, Y. Effects of Ca2+ ions on the formation of metaphase chromosomes and sperm pronuclei in cell-free preparations from unactivated Rana pipiens eggs. *Dev. Biol.* **103,** 434–42 (1984).

185.   Brown, K. S. *et al.* Xenopus tropicalis egg extracts provide insight into scaling of the mitotic spindle. *J. Cell Biol.* **176,** 765–70 (2007).

186.   Levy, D. L. & Heald, R. Mechanisms of intracellular scaling. *Annu. Rev. Cell Dev. Biol.* **28,** 113–35 (2012).

187.   Loughlin, R., Wilbur, J. D., McNally, F. J., Nédélec, F. J. & Heald, R. Katanin contributes to interspecies spindle length scaling in Xenopus. *Cell* **147,** 1397–407 (2011).

188.   Jordan, S. N. & Canman, J. C. Rho GTPases in animal cell cytokinesis: an occupation by the one percent. *Cytoskeleton (Hoboken).* **69,** 919–30 (2012).